

INFORMATION TO USERS

This manuscript has been reproduced from the microfilm master. UMI films the text directly from the original or copy submitted. Thus, some thesis and dissertation copies are in typewriter face, while others may be from any type of computer printer.

The quality of this reproduction is dependent upon the quality of the copy submitted. Broken or indistinct print, colored or poor quality illustrations and photographs, print bleedthrough, substandard margins, and improper alignment can adversely affect reproduction.

In the unlikely event that the author did not send UMI a complete manuscript and there are missing pages, these will be noted. Also, if unauthorized copyright material had to be removed, a note will indicate the deletion.

Oversize materials (e.g., maps, drawings, charts) are reproduced by sectioning the original, beginning at the upper left-hand corner and continuing from left to right in equal sections with small overlaps. Each original is also photographed in one exposure and is included in reduced form at the back of the book.

Photographs included in the original manuscript have been reproduced xerographically in this copy. Higher quality 6" x 9" black and white photographic prints are available for any photographs or illustrations appearing in this copy for an additional charge. Contact UMI directly to order.

UMI

A Bell & Howell Information Company
300 North Zeeb Road, Ann Arbor MI 48106-1346 USA
313/761-4700 800/521-0600



SOIL EROSION PROCESSES AND SEDIMENT ENRICHMENT
IN A WELL-AGGREGATED, UNIFORMLY-TEXTURED OXISOL

A DISSERTATION SUBMITTED TO THE GRADUATE DIVISION OF THE
UNIVERSITY OF HAWAII IN PARTIAL FULFILLMENT OF THE
REQUIREMENTS FOR THE DEGREE OF

DOCTOR OF PHILOSOPHY

IN

AGRONOMY AND SOIL SCIENCE

MAY 1996

By

Yongshan Wan

Dissertation Committee:

Samir A. El-Swaify, Chairperson
Carl I. Evensen
Richard E. Green
James A. Silva
Ross A. Sutherland

UMI Number: 9629861

UMI Microform 9629861
Copyright 1996, by UMI Company. All rights reserved.

**This microform edition is protected against unauthorized
copying under Title 17, United States Code.**

UMI
300 North Zeeb Road
Ann Arbor, MI 48103

ACKNOWLEDGMENTS

This dissertation research was supported by a project funded by the U.S. Department of Agriculture Section 406, Food for Peace Act, Cooperative State Research Service Special Grant Agreement No. 91-34135-6177, managed by the Pacific Basin Administrative Group. Their support is gratefully acknowledged.

My deepest gratitude are also due to my advisor Dr. Samir A. El-Swaify for his guidance and supervision, to my outside committee member Dr. Ross A. Sutherland for his invaluable input into this dissertation research, and to my other committee members: Dr. Richard E. Green, Dr. James A. Silva, and Dr. Carl I. Evensen, for their assistance with refinement of this research.

The field rainfall simulation experiment was a team activity. The rainfall simulator was kindly provided by the USDA-ARS, National Soil Erosion Laboratory. My good friend, Stanley Oshita, helped with installation and calibration of the rainfall simulator. Tom Burke, Jinbo Zhang, and Adly Mirza were involved with field sampling. Their assistance is gratefully acknowledged.

I also wish to thank Dr. G Uehara, Dr. R. Fox, Dr. N.V. Hue, Dr. R. Yost, Dr. R. Jones, and Ms. Randi Schneider. They had been helpful with many of my questions and problems I encountered through out the period of this study.

Finally, I would like to dedicate this dissertation to my parents, whom I know have terribly missed their son during the past four years but have always been encouraging and supportive, to my wife for her understanding, love, and help, and to my newborn son, Christopher, who kept me wonderful accompany through many late nights during the writing stage of this research.

ABSTRACT

The basic primary and secondary processes of soil erosion by water are not well understood for Hawaii's soils despite substantial research and empirical information on overall factors. A series of laboratory and field rainfall simulation experiments were conducted to study the mechanisms and processes of soil erosion and sediment enrichment from a well-aggregated, uniformly-textured Oxisol from the island of Oahu, Hawaii. Interrill splash and wash were partitioned with a specially-designed laboratory device under varying rainfall intensities and slope gradients. Results indicated that both splash and wash can be predominant erosion processes, depending on slope and runoff conditions. The power function, $E = aI^b$, where E is the erosion rate and I is the rainfall intensity, well described rainfall intensity effects on all the splash and wash components. However, b values for splash were close to 1 while these for wash were above 2. Slope controls on interrill splash and wash dynamics were modeled with linear or near-linear slope functions, showing a monotonic increase of erosion with increasing slope angle. Rill erosion was evaluated in a ridge-and-furrow system using a series of simulated storms and overland inflows. Results indicated that flow detachment in rills responded to the average flow shear stress differently under laminar and turbulent flow regimes but the relationship can be modeled with a linear function for both.

The quality of detached sediment was determined in association with the above interrill splash and wash and rill erosion processes. With splash, sediment sizes varied with directional components and were generally coarser than with wash. Enrichment of the <0.063 mm fraction was observed in both splash and wash sediments. Sediment transported by rill flow became coarser as flow shear stress increased. Soil erosion did not

display selective transport of primary clay particles from this "clay" textured soil. However, soil organic carbon (OC) and extractable phosphorus (Ext-P) were enriched due to selective transport of fine aggregates which were richer in OC and Ext-P than coarser one. This chemical enrichment was partially associated with the reduced accessibility of sorption sites inside large aggregates.

TABLE OF CONTENTS

ACKNOWLEDGMENTS	iii
ABSTRACT	iv
LIST OF TABLES	viii
LIST OF FIGURES	x
CHAPTER 1 INTRODUCTION	1
CHAPTER 2 PARTITIONING INTERRILL SPLASH AND WASH DYNAMICS WITH A NOVEL LABORATORY APPROACH	7
2.1 Introduction	8
2.2 Materials and Methods	10
2.2.1 The soil	10
2.2.2 The rainfall simulator	11
2.2.3 The soil tray and splash collectors	11
2.2.4 Experimental procedures	15
2.3 Results and Discussion	16
2.3.1 Partitioning total splash into directional components	16
2.3.2 Partitioning downslope transport into wash and splash components	22
2.3.3 Slope controls on wash and splash transport	27
2.4 Conclusions	30
CHAPTER 3 MODELING RAINFALL INTENSITY AND SLOPE EFFECTS ON INTERRILL SPLASH AND WASH DYNAMICS	32
3.1 Introduction	33
3.2 Materials and Methods	36
3.3 Results and Discussion	37
3.3.1 Effects of rainfall intensity	39
3.3.2 Effects of slope steepness	48
3.3.3 Interrill erodibility: Splashability and washability	51
3.4 Conclusions	56
CHAPTER 4 INFLUENCE OF PLASTIC MULCH AND FLOW HYDRAULIC REGIMES ON RUNOFF GENERATION AND RILL EROSION	59
4.1 Introduction	60
4.2 Flow Hydraulic Regimes and Resistance	62
4.3 Materials and Methods	64
4.4 Results and Discussion	67
4.4.1 Runoff generation and runoff rate	67
4.4.2 Soil loss and sediment concentration	71
4.4.3 Flow hydraulic regimes and rill detachment	74
4.5 Conclusions	79

CHAPTER 5	SIZE CHARACTERISTICS OF INTERRILL SPLASH AND WASH SEDIMENTS OVER A RANGE OF RAINFALL INTENSITIES AND SLOPE ANGLES	81
5.1	Introduction	82
5.2	Materials and Methods	83
5.3	Results and Discussion	86
5.3.1	Overall splash and wash GMD and ER	86
5.3.2	Effect of rainfall intensity and slope gradient	89
5.3.3	Interrill sediment delivery	97
5.4	Conclusions	99
CHAPTER 6	SEDIMENT ENRICHMENT DURING FLOW TRANSPORT FROM A WELL-AGGREGATED AND UNIFORMLY-TEXTURED OXISOL	100
6.1	Introduction	101
6.2	Materials and Methods	103
6.3	Results and Discussion	106
6.3.1	Flow hydraulics and sediment concentration	106
6.3.2	Aggregate size distribution	110
6.3.3	Primary particle size distribution	113
6.3.4	Organic carbon and extractable phosphorus	117
6.4	Conclusions	122
CHAPTER 7	SEDIMENT ENRICHMENT BY SOIL ORGANIC CARBON AND PHOSPHORUS: IMPLICATIONS OF FERTILIZATION, AGGREGATE BREAKDOWN BY RAINFALL, AND SELECTIVE TRANSPORT OF FINE AGGREGATES	123
7.1	Introduction	124
7.2	Materials and Methods	126
7.2.1	Dry sieving experiment	126
7.2.2	Aggregate breakdown experiment	128
7.2.3	Interrill erosion experiment	129
7.3	Results and Discussion	130
7.3.1	Dry sieving experiment	130
7.3.2	Aggregate breakdown experiment	133
7.3.3	Interrill erosion experiment	137
7.4	Conclusions	144
CHAPTER 8	OVERALL SUMMARY AND CONCLUSIONS	147
REFERENCES	152

LIST OF TABLES

<u>Table</u>	<u>Page</u>
2.1 Physical and chemical properties of the Wahiawa Oxisol	10
2.2 Hydraulic parameters of interrill overland flow at steady state	25
3.1 F values of ANOVA for rainfall intensity and slope effects on splash and wash components	38
3.2 Parameter estimates from regression analysis of splash components fitted for a power function model and a linear function model	40
3.3 Parameter estimates from regression analysis of wash and interrill sediment delivery based on log-transformed data	43
3.4 Parameter estimates from regression analysis of slope controls on splash and wash fitted for a linear function and a power function	49
4.1 Time to runoff initiation in simulated storms	68
4.2 Treatment effects on steady state runoff rate and runoff coefficient	70
4.3 Treatment effects on steady state sediment concentrations and soil loss rates	71
5.1 Wet-sieved aggregate size fractions (%) and geometric mean diameter (mm) for the in-situ soil	85
5.2 Splash and wash sediment geometric mean diameters	86
5.3 Mean enrichment ratios for splash and wash sediments	88
5.4 P values of ANOVA for rainfall intensity and slope effects on geometric mean diameters of splash and wash sediments	89
5.6 Comparison of geometric mean diameter means by slope and rainfall intensity for splash	91
5.6 Comparison of geometric mean diameter means by slope and rainfall intensity for wash	94
6.1 Selected soil properties of the in-situ soil	106
6.2 Flow properties at steady state for the four rainfall events	107

<u>Table</u>	<u>Page</u>
6.3 Primary particle size distributions and clay enrichment ratios of sediment from the four events	115
6.4 Primary particle size distributions and clay aggregate enrichment ratios for aggregates of varying size fractions	116
6.5 Comparison of time-averaged enrichment ratios for organic carbon and extractable phosphorus	117
6.6 Organic carbon and extractable phosphorus concentrations and aggregate enrichment ratio for aggregates of varying size fractions	121
7.1 Selected soil properties of the Wahiawa soil receiving different fertilization treatments.....	128
7.2 Contents of organic carbon in dry-sieved aggregates of varying size	131
7.3 Extractable phosphorus concentrations in dry-sieved aggregates of varying size	132
7.4 Organic carbon contents in aggregates produced by a 20-min rainfall from dry-sieved aggregates	136
7.5 Extractable phosphorus concentrations in aggregates produced by a 20-min rainfall from dry-sieved aggregates	136

LIST OF FIGURES

<u>Figure</u>		<u>Page</u>
2.1	Experimental configurations of soil tray and splash collectors	12
2.2	Dimensions (in meters) of soil tray and splash collectors	13
2.3	Effect of slope on total splash flux	18
2.4	Effect of slope on directional splash rate	19
2.5	Illustration of slope effect on directional splash	21
2.6	Effect of slope on transport flux of wash and downslope splash	23
2.7	Comparison between measured interrill erosion rates and predicted values using the WEPP interrill erosion model	29
3.1	Interrill splash and wash flux for different slopes as a power function of rainfall intensity	41
3.2	Comparison of downslope splash and wash as affected by slope under four rainfall intensities	45
3.3	Comparison of measured sediment flux with predicted flux	55
4.1	Plot set-up for the plastic-crown treatment and rainfall simulator	66
4.2	Change of runoff rate with time during the dry run	69
4.3	Change in sediment concentration with time during rainfall simulation	73
4.4	Darcy-Weisbach roughness coefficient versus Reynolds number	75
4.5	Flow detachment capacity versus Reynolds number	76
4.6	Flow detachment capacity versus shear stress	78
5.1	Change of enrichment ratios of <0.063 mm and 1-2 mm fractions with slope and rainfall intensity for downslope and upslope splash sediment	93
5.2	Change of enrichment ratios of <0.063 mm fraction in wash sediment with slope and rainfall intensity	95

<u>Figure</u>	<u>Page</u>
5.3 Aggregate size distribution of splash and wash and total interrill sediment for splash and wash dominated transport regimes	98
6.1 Temporal variation in sediment concentration during the four events	109
6.2 Temporal variation in concentrations of aggregate size fractions during the four events	111
6.3 Aggregate size distributions of sediment from the four events and the in-situ soil	114
6.4 Temporal variation in organic carbon enrichment ratios during the four events	118
6.5 Temporal variation in extractable phosphorus enrichment ratios during the four events	120
7.1 Water stable aggregate size distribution of selected dry-sieved fractions under rainfall impact	135
7.2 Changes of sediment concentration and runoff rate with time	138
7.3 Changes of sediment aggregate size composition and enrichment ratios with time.....	140
7.4 Aggregate size distribution of eroded surface and the in-situ soil	141
7.5 Changes of extractable phosphorus concentration and organic carbon content in sediment aggregates of varying size with time	143
7.6 Changes of sediment enrichment ratio of extractable phosphorus and organic carbon with time	145

CHAPTER 1

INTRODUCTION

Accelerated soil erosion by water has long been recognized as one of the major factors contributing to worldwide soil degradation (El-Swaify, 1993; Rose, 1993). The subsequent transport of erosional sediments to water bodies has also received substantial attention since sediment and associated chemicals contribute to nonpoint source pollution (Menzel, 1980; Sharpley, 1985; El-Swaify, 1994). These environmental concerns are particularly serious in tropical areas where erosion rates are generally higher than in temperate regions (El-Swaify, 1993 & 1994).

Traditional soil erosion research on sediment quantity and its controlling factors have commonly employed the empirical "black-box" approach. This is exhibited by the enormous effort expended on the development of empirical soil erosion models such as the USLE (Universal Soil Loss Equation) model and its revised versions (e.g. Wischmeier and Smith, 1978; Cooley and Williams, 1985; Renard et al., 1992). These models have served as important tools for estimating sediment output from agricultural areas. However, their limitations have been widely recognized in addressing event-based predictions or transferability to regions where site-specific runoff-plot data are not available for model validation (e.g. Foster, 1990; Rose, 1993). To address this concern, the U. S. Department of Agriculture initiated the development of a process-based model, i.e., Water Erosion Prediction Project (WEPP) to replace the USLE model (Lane and Nearing, 1989). Similar process-based models have also been developed in Australia by Rose (1985, 1993) and in Europe by Morgan et al. (1992). These models are intended to describe soil erosion processes of detachment, transport, and deposition according to the basic physical theories

involved. For example, the WEPP model divides soil erosion processes into "rill erosion" and "interrill erosion". These two processes are conceptualized with distinct physical and hydrological meanings: i.e., interrill erosion is associated with thin and unconcentrated overland flow and is driven by rainfall impact while rill erosion is associated with concentrated overland flow and is driven by flow shear stress. More basic erosion processes including (i) detachment by rain drops, (ii) entrainment or detachment by overland flow, (iii) transport by rain drops, (iv) transport by overland flow, and (v) deposition by gravity, are either explicitly contained or implicitly lumped in the interrill and rill components of the WEPP model. The delicate interaction between these processes is complex and requires additional study. Presently, a significant amount of effort has been made to estimate soil erodibility parameters for temperate soil based on quantitative representations of interrill and rill erosion in the WEPP model (Laflen et al., 1987; Liebenow et al., 1990). Such information is, however, lacking in the tropics where little research has been conducted to quantify individual processes or to relate theoretical to empirical information (e.g., Lo et al., 1988). Quantitative understanding of erosion processes and their controlling factors is important for predictive model development and for designing the most appropriate soil and water conservation practices.

While most of the research effort on soil erosion has focused on sediment quantity issues, sediment quality concerns are also of critical importance. "Selectivity" is another basic process of soil erosion with the sediment being enriched with fine particles. Subsequently, organic matter, nutrients, pesticides and other chemicals are also enriched in comparison with the in-situ soil (Massey and Jackson, 1952; Stoltenberg and White, 1953; Bhatt, 1977; Alberts and Moldenhauer, 1981; Alberts et al., 1983; Sharpley, 1985; McIsaac et al., 1991). The impact of accelerated soil erosion, therefore, should be

understood in terms of both sediment quantity and sediment quality. To address this concern, certain water quality and soil erosion models such as CREAMS (Chemicals, Runoff, and Erosion from Agricultural Management Systems, Menzel, 1980), GLEAMS (Groundwater Loading Effects of Agricultural Management Systems, Leonard et al., 1987), and WEPP (Lane and Nearing, 1989) have incorporated a sediment quality factor, known as enrichment ratio for use in estimating the on-site and off-site environmental impacts of soil erosion. The enrichment ratio (ER) is defined as the ratio of a specific constituent (e.g., nutrients) concentration in sediment to that of the same constituent in the in-situ soil. Thus, in the case of nutrients:

$$ER = \frac{\text{Nutrient concentration in sediment}}{\text{Nutrient concentration in-situ soil}} \quad [1.1]$$

The ER concept for sediment may relate to nutrient or pesticide concentration, soil organic matter content, soil particle or aggregate size distributions and various other chemical and physical properties. However, by only comparing the two concentrations in Eq. [1.1], information about processes involved with sediment enrichment is not readily available. Studies with temperate soils have attributed the enrichment of nutrients in sediment to the selective erosion of fine soil particles and/or organic matter (Stoltenberg and White, 1953; Menzel, 1980; Avenimelech and McHenry, 1984; Flanagan and Foster, 1989). However, processes responsible for preferential removal of chemically enriched fines and organic matter and their contribution to sediment enrichment are poorly defined. As noted by El-Swaify and Fownes (1992), "this phenomenon is little understood or utilized in process modeling; available data and models for its occurrence

remain descriptive and empirical at best." Limited process-based studies (e.g., Palis et al., 1990a&b; Ghadiri and Rose, 1991a&b) indicate that sediment enrichment varies with erosion processes, flow hydraulics, and soil type. Information on the relationship between the selectivity of erosion processes and sediment enrichment by chemicals is, however, lacking for highly weathered tropical soils. This information is essential for adding sediment enrichment computations to existing erosion and water quality models and for understanding the linkages between erosion, nonpoint source pollution, and long-term changes in soil productivity and sustainability in tropical areas. It also has practical significance in the development of alternative conservation measures for soil erosion and nonpoint source pollution control.

The overall objective of this dissertation study was to advance the present state of our knowledge concerning the basic processes and mechanisms responsible for soil erosion and sediment enrichment in tropical settings. A well-aggregated and uniformly-textured Oxisol was selected to represent the highly weathered soils of the tropics. The following specific objectives were addressed:

Objective 1

To quantitatively partition sediment fluxes (mass of sediment produced by a erosional process from per unit land area per unit time) from the two sub-processes of interrill erosion, namely detachment and transport by rainfall impact (splash) and transport by interrill overland flow (wash) under varying slope angles and rainfall intensities. The research will test the following hypotheses: (i) the relative importance of splash and wash in interrill sediment transport depends on slope steepness and rainfall intensity; and (ii) sediment transport by splash and wash are associated with distinct physical mechanisms and can be modeled accordingly.

Objective 2

To assess the relationship between runoff generation, hydraulics of concentrated overland flow, and rill erosion in an agriculturally managed ridge-and-furrow system. The research will test the following hypotheses: (i) runoff generation in the system is enhanced by plastic mulch in the ridge area; and (ii) flow detachment in rills depends on flow hydraulic regimes, i.e., laminar or turbulent.

Objective 3

To investigate the selectivity of splash and wash in interrill erosion and that of concentrated overland flow in an interrill-rill erosion system as reflected by sediment aggregate (grain) size distributions. The research will test the following hypotheses: (i) wash is selective and splash is non-selective; and (ii) interrill sediment delivery into concentrated overland flow results in sediment which is finer than that without interrill sediment contributions.

Objective 4

To determine the relationship between chemical enrichment of organic carbon and phosphorus in sediment and physical enrichment of clay particles and fine aggregates. The research will test the following hypotheses: (i) the eroded sediment from this well-aggregated and uniformly-textured Oxisol is enriched with nutrients, phosphorus in particular; and (ii) this enrichment is associated with selective erosion of fine aggregates instead of primary clay particles.

Objective 5

To elucidate the mechanisms of sediment enrichment as influenced by fertilization, aggregate breakdown by rainfall, and selective transport of fine aggregates from this Oxisol. The research will test the following hypotheses: (i) the fine aggregates

existing in the in-situ soil before rainfall impact will possess a greater enrichment for nutrients than larger aggregates; (ii) the fine aggregates produced by rainfall impact will possess a greater enrichment for nutrients than larger aggregates; and (iii) fertilization practices influences the pattern of sediment enrichment .

These objectives are addressed and hypotheses tested , with Objective 1 in Chapters 2 and 3, Objective 2 in Chapter 4, Objective 3 in Chapters 5 and 6, and Objectives 4 and 5 in Chapters 6 and 7. This sequence allows a logical presentation of the primary erosion processes, i.e, the interrill and rill erosion, and the secondary processes which control selectivity and sediment enrichment. The first set of processes determine the quantitative aspects of soil erosion by water while the second set determine the quality attribute of eroded sediment.

CHAPTER 2
PARTITIONING INTERRILL SPLASH AND WASH DYNAMICS
WITH A NOVEL LABORATORY APPROACH

Abstract

An innovative experimental device was designed for simultaneous measurement of interrill splash and wash associated with soil erosion on an Oxisol. The method was used to partition these processes at 4, 9, 18, 27, and 36% slopes under a constant rainfall intensity of 65 mm h⁻¹ in a laboratory setting. The runoff and sediment collection system allowed partitioning total splash into directional components (upslope, downslope, and lateral) and interrill sediment transport into wash and splash components. Results show that downslope and lateral splash components increased with slope steepness while the upslope component decreased. Overall there was a linear increase of total splash from the 0.18 m² plot with increasing slope angle. A transport-limited regime prevailed in all studied slopes. The wash process dominated sediment transport at low slopes (<9%) and was linearly related to slope with a steady state flux ranging from 0.65 g m⁻² min⁻¹ at 4% slope to 3.15 g m⁻² min⁻¹ at 36% slope. Downslope splash transport was dominant at high slopes (>9%) and was best described with a power function model (exponent=1.3) with a flux ranging from 0.33 g m⁻² min⁻¹ at 4% slope to 5.31 g m⁻² min⁻¹ at 36% slope. The WEPP interrill erosion algorithm was inadequate for describing total interrill sediment delivery from this Oxisol. The practical implication of this finding is that splash can be an important process of sediment transport in interrill erosion. Failure to include splashed sediment in interrill erosion measurements using the common "runoff-trough" approach may underestimate total soil loss or interrill sediment delivery to rills.

2.1 Introduction

Soil erosion occurring in interrill areas with thin and unconcentrated flow (interrill erosion, previously known as sheet erosion) has been identified as one of the major processes contributing to soil and water quality degradation. At the process level interrill erosion is commonly understood to be a combination of two sub-processes: detachment and transport by raindrop impact (splash) and transport by thin unconcentrated flow (wash) (Meyer, 1981; Foster, 1990), hereafter referring to interrill splash and wash dynamics. Successful modeling of interrill erosion and its environmental impact depends on a full understanding of the basic processes involved.

A significant amount of research has been conducted on interrill erosion. However, most studies have only considered wash transport, or failed to partition sediment transported by wash and by splash (e.g., Meyer, 1981; Watson and Laflen, 1986; Meyer and Harmon, 1989). These two distinct sub-processes are also implicitly lumped together in the recently developed process-based WEPP model (Nearing et al., 1990). There are at least two reasons which account for this current approach to studying interrill erosion.

First, it is generally accepted that interrill flow (wash) is the primary process by which sediment is transported. Splash, though important in detaching sediment, is considered to be of limited significance in sediment transport (Meyer, 1981; Elliot et al., 1991). Limited information from studies with long and shallow slopes supported this statement (Moss and Green, 1983). However, experimental data from short and steep slopes, particularly with well-aggregated tropical soils, are lacking in the literature.

Second, experimental separation of sediment transported by splash and wash, particularly in the field, is difficult. This has been recognized by a number of researchers

(Bryan, 1979; Meyer, 1981). In a controlled laboratory setting, however, isolation of these two processes is possible. Previous attempts at partitioning splash and wash commonly used a "double-pan" approach (Bryan, 1979; Luk, 1979; Garnier, 1988). In these studies splash sediment was collected in an outside pan while wash sediment was collected by an "open" runoff slot at the downslope end of an inner soil pan. There are three limitations of this approach. Firstly, the splash sediment collected as such is sediment transported in all directions. Downslope splash transport cannot be obtained directly. Secondly, simultaneous measurement of splash and wash sediment in a temporal manner during an event is difficult, if not impossible, due to the inherent setup of the outside pan. Thirdly, since the simulated rainfall is always applied to an area which is generally larger than the size of the inner soil-containing pan, splash sediment may not be collected easily due to the comparatively large amount of water collected in the outside pan.

In this Chapter, an experimental setup which allows partitioning total splash into directional components and sediment transport into splash and wash components under a laboratory setting is presented. Sediment transported by interrill overland flow (wash) is collected in a runoff collector. Sediment detached or transported by splash is collected by a series of specially designed splash collectors. With this approach, Sutherland et al. (1996) investigated the temporal variations in sediment transport by wash and splash. The objective of this study was to determine the effect of slope steepness (hereafter shortened as "slope") on the dynamics of directional splash and wash from a highly weathered, well-aggregated tropical soil.

2.2 Materials and Methods

2.2.1 The soil

The soil used in this study was the Wahiawa silty clay, a Rhodic Eutruxox, collected from the Poamoho Experimental Station on the island of Oahu, Hawaii. Annual rainfall in the area is about 1100 mm, with an 1-h storm of 60-70 mm for a 10-y return interval. This soil was selected since it covers 5-6% of the surface area of the island (Foote et al., 1972) and is widely used for intensive cultivation of pineapple, sugarcane and other crops. Erosion of this soil has been linked to off-site water quality problems (El-Swaify and Cooley, 1980; El-Swaify, 1992). The Wahiawa soil, developed from residual basic igneous rock, contains about 90% clay ($< 2 \mu\text{m}$) and is well aggregated (El-Swaify, 1980). Selected properties of this soil are shown in Table 2.1. Soil samples collected from the surface 0.1 m were air-dried and sieved through a sieve with 6-mm openings.

Table 2.1 Physical and chemical properties of the Wahiawa Oxisol

Soil Property	Soil Depth (m)	Value(s)
pH (soil water ratio = 1:1)	0-0.1	4.90-5.90
Organic carbon (%)	0-0.1	1.30-2.21
Field bulk density (Mg m^{-3})	0-0.1	0.97-1.10
	0.3-0.5	1.25-1.35
Dispersed Particle size distribution (%)		
Sand ($> 53 \mu\text{m}$)	0-0.1	1.33-2.56
Silt ($2 - 53 \mu\text{m}$)	0-0.1	8.17-9.60
Clay ($< 2 \mu\text{m}$)	0-0.1	88.2-89.7
Water stable aggregates ($>0.25 \text{ mm}$) (%)	0-0.1	67.8-78.1
Steady state infiltration rate (mm h^{-1}) [†]	whole profile	19.2-25.4

[†] Dangler et al. (1976)

2.2.2 The rainfall simulator

A laboratory drip-type rainfall simulator based on the design of Munn and Huntington (1976) was used. The principal component of the rainfall simulator is a rainfall chamber with 841 extended drop forming tubing tips to provide simulated rainfall covering an area of 0.76 by 0.76 m. The drop former consisted of 22 mm sections cut from 23-gauge hyperdermic needles which were fit into 20 mm tubes cut from 0.58 mm inside diameter and 0.97 mm outside diameter polyethylene tubing. These tubes produced uniform raindrops with a diameter of 3.2 mm and prevented drop breaking and deformation. The rainfall unit was supported by an iron frame with a maximum fall height of 2.3 m, producing a kinetic energy flux of $16 \text{ J m}^{-2} \text{ mm}^{-1}$ of rain. Estimated equivalence to natural rain, in terms of anergy delivery, ranged from 43-72% in the literature (Munn and Huntington, 1976; Sutherland et al., 1996). Domestic water supply with a temperature of 22 °C was used. Rainfall intensity was controlled by a pressure regulator and monitored by a pressure gauge. Two opposing oscillating fans were used to prevent drops falling repeatedly in the same location.

2.2.3 The soil tray and splash collectors

The soil tray and splash collectors (Figure 2.1) made from galvanized sheet metal were housed within a 0.85 (length) by 0.85 (width) by 0.55 (depth) m water-resistant plywood box, which was elevated 0.25 m above the ground to allow for runoff sampling. The soil tray had dimensions of 0.60 (length) by 0.30 (width) by 0.10 (depth) m, simulating a slope length representative of a typical ridge-furrow management system. A rectangular 0.30 by 0.04 m apron was mounted to connect the lower edge of the tray and a 0.04 (length) by 0.30 (width) by 0.05 (depth) m trough which acted as the runoff collector. A longitudinal cross-sectional view of the soil tray is shown in Figure 2.2a. The apron surface

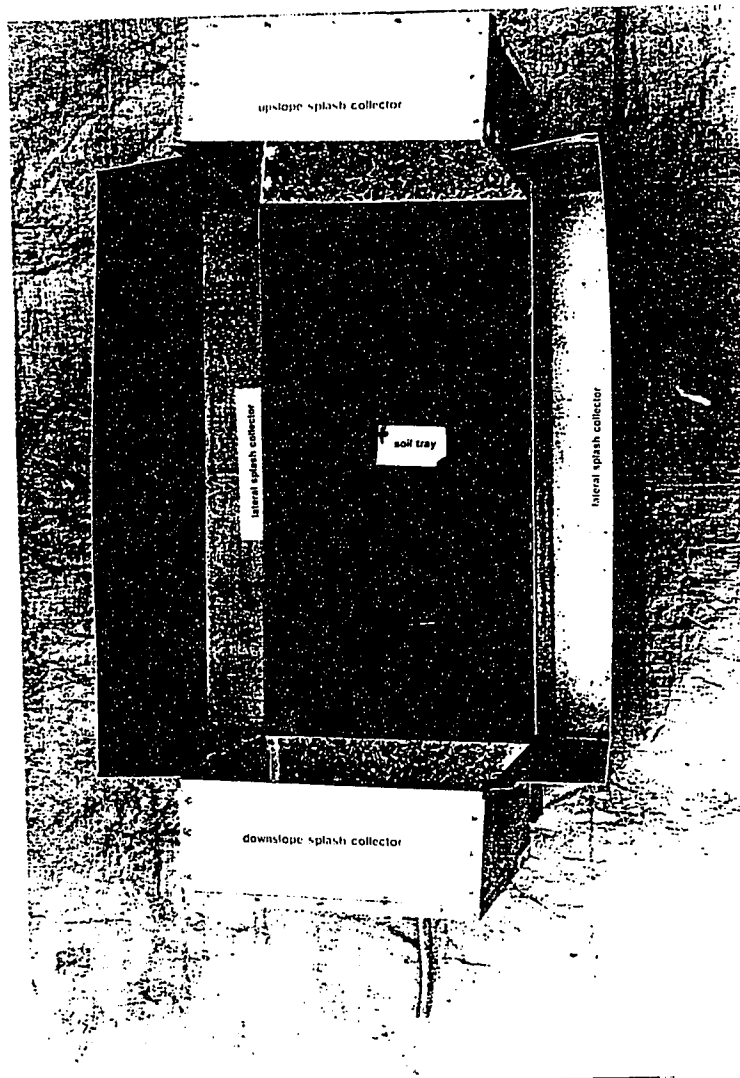


Figure 2.1 Experimental configurations of soil tray and splash collectors.

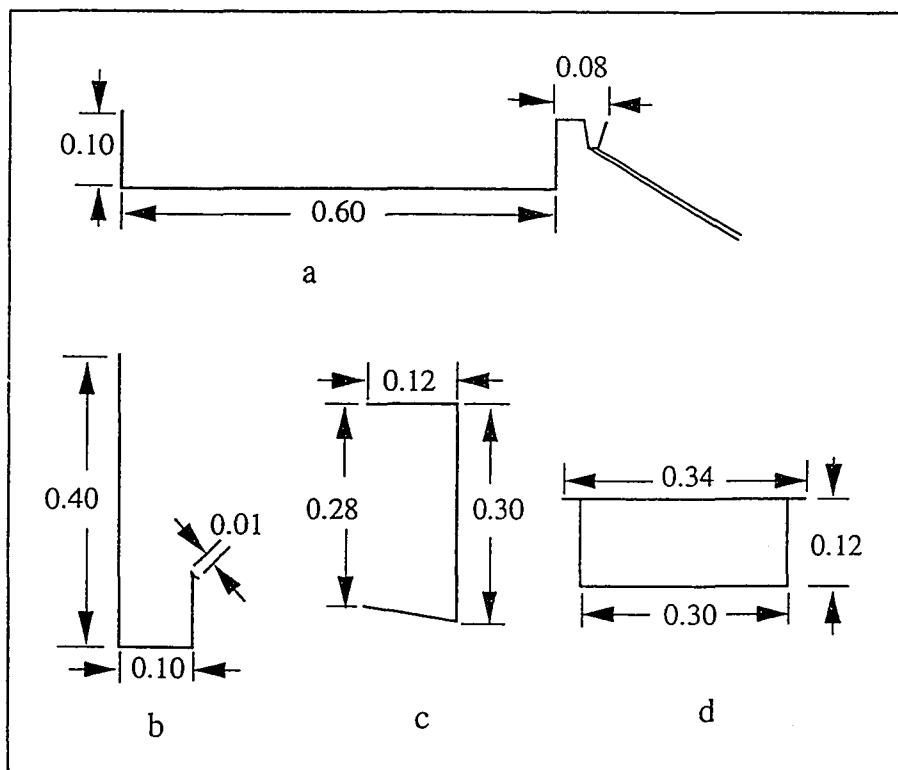


Figure 2.2 Dimensions (in meters) of soil tray and splash collectors: a. longitudinal cross-sectional view of soil tray; b. horizontal cross-sectional view of lateral splash collector; c. longitudinal cross-sectional view of downslope splash collector; and d. plan view of downslope splash collector.

was 5 mm lower than the trough edge so that runoff was directed into the trough. This apron was used to avoid direct sediment dislodgement into the trough. Runoff was funneled into the trough bottom through tygon tubing and into a collecting vessel outside the wooden box. At the base of the soil tray a percolation outlet was used for infiltration measurements. The slope of the soil tray can be adjusted from 0 to 100% using a specially designed mounting device.

Two easily detachable lateral splash collectors were attached, one to each side of the soil tray. The lateral splash collectors had dimensions of 0.60 (length) by 0.10 (width) by 0.10 (depth) m with additional 0.30 m extended sidewalls to retain sediment splashed laterally. A horizontal cross-sectional view of the lateral splash collector is shown in Figure 2.2b. A 0.01 m lip along the collector side was used to attach the collector to the soil tray. The level of the soil surface was below this lip so that there was no possibility of washover into the lateral collectors. The downslope splash collector was laid on top of the apron and trough and supported by the front wall of the wooden box. Detailed dimensions are shown in Figure 2.2 c&d. The slight angle in the bottom as shown in Figure 2.2c was designed to retain splashed water so that overflow would not occur. The 0.02 m extended splash guard at both sides as shown in Figure 2.2d allowed the downslope splash collector to stand on the lips of the two lateral splash collectors leaving an opening of 5-8 mm above the soil surface for free passage of runoff. The upslope splash collector was identical to the front splash collector, and rested on the upper edge of the soil tray and the back wall of the wooden box. To ensure accurate collection of upslope and downslope splash sediment, it was critical that the upslope and downslope splash collectors be set perpendicular to the floor level so that there were no rain drops falling directly onto the collector bottom. For this

purpose, additional wooden plates were placed between the splash collectors and the wooden box walls whenever necessary during slope adjustment.

The interrill sediment collection system described above provides an effective means of partitioning sediment transported by interrill splash and wash processes in a laboratory setting. The splash collector system further allows for directional partitioning of total splash into downslope, upslope, and lateral components. Additionally, the splash collectors are easily detachable, thus providing a means of quantifying temporal variations in interrill splash and wash transport.

2.2.4 Experimental procedures

A glass bead layer of about 20 mm was evenly placed at the bottom of the soil tray to provide free drainage. A metal screen with an attached layer of cheesecloth separated the glass beads and a 20-mm pre-wet soil layer (water content about 35 Mg Mg⁻¹). This soil layer was compacted to a bulk density of approximately 1.3 Mg m⁻³ to simulate a subsoil horizon found in the field (Table 2.1). Subsequently, air-dried soil was packed uniformly in the soil tray to produce a soil bed of 60 mm depth with a level surface. The dry bulk density of the surface layer was about 1 Mg m⁻³, similar to that found in the field (Table 2.1). Preliminary trials indicated that this soil layering had a steady state infiltration rate of about 25 mm h⁻¹, which was similar to that measured in the field with rainfall simulation (Dangler et al., 1976). The soil bed was wetted to near saturation from the bottom percolation outlet prior to slope adjustments. Slopes studied were 4, 9, 18, 27, and 36 %, and it is assumed that this range of interrill slopes would simulate a gradual transition from a transport-limited regime to a detachment-limited regime as defined by Foster (1990). After slope adjustment, the soil tray was subjected to a simulated rainfall with a constant intensity of 65±1.1 mm h⁻¹

(± 1 standard deviation). Runoff and percolate were volumetrically measured every 5 min. After achieving a steady runoff state which took about 20-25 min for all slopes, the splash collectors were attached for a 20-min period. During this period runoff was sampled and measured in a 2-L beaker. Directionally splashed sediment was transferred to a set of three beakers with sediment from the two lateral splash collectors combined. Visual observations of the soil surface and sediment transport patterns were made both during and after rainfall simulation. Particular attention was paid to surface morphological features formed during rainfall. Rainfall simulation for each of the slopes was replicated three times and new soil was used for each replicate. The collected wash and splash sediment was fractionated by wet sieving through a nest of sieves with openings of 4, 2, 1, 0.5, 0.25, 0.125, and 0.063 mm (See Chapter 5). Wet-sieved aggregates were oven dried for 16 hours at 105 °C and mass determinations were made. The total mass of sediment transported was obtained by the summation of all aggregate size fractions. The mean of the three replicates was reported, but all data were used for statistical analysis. Sediment transport flux rates were corrected with areal projection area of the plot for all the slopes.

2.3 Results and Discussion

2.3.1 Partitioning total splash into directional components

A considerable number of studies have been conducted to address the relationship between splash and slope (e.g. Morgan, 1978; Bryan, 1979; Quansah, 1981; Garnier, 1988). Three types of splash-slope relationship have been observed: (i) splash rate increased with slope following linear or power functions (e.g. Quansah, 1981); (ii) splash rate increased with slope and then decreased after a peak splash rate was reached as

described by polynomial functions (e.g. Bryan, 1979); and (iii) splash rate was not affected by slope (e.g. Morgan, 1978). Comparison of results between studies is complex due to different experimental procedures and rainfall characteristics involved. The data from the present study showed that the total splash output (combining upslope, downslope and lateral) from the studied 0.18 m² plot increased linearly with slope (Figure 2.3). The best-fit regression equation (significant at P<0.001 with a standard error of the estimate: SEE of 1.096 g m⁻² min⁻¹) between total splash flux and slope was:

$$F_{ts} = 0.334 S + 2.964 \quad n = 15, \text{Adj. } r^2 = 0.932 \quad [2.1]$$

where F_{ts} = total splash flux (g m⁻² min⁻¹), and S = slope gradient (%). The positive intercept represented splash flux when slope was zero. This result can be compared with the power function relationship for splash and slope suggested by Quansah (1981). The slope exponents of Quansah's power function model ranged from 0.13 to 0.27 for three soil types studied, showing a weaker dependence of total splash flux on slope.

While most splash studies measured only non-directional splash, the directionally partitioned splash data (Figure 2.4) exhibited some interesting patterns. Note that the directional splash rates were expressed as mass of sediment splashed across a 1 m soil boundary per unit time (g m⁻¹ min⁻¹) instead of g m⁻² min⁻¹. This unit was used to eliminate the plot geometry effect on directional splash so that the directional splash rates can be compared directly. It was observed that as slope increased the upslope splash rate decreased while the downslope splash rate increased. This supports the observations of Ghadiri and Payne (1988) on splash droplet distributions as affected by slope. It is interesting to note that the lateral splash rate, a measure of sediment redistribution, also

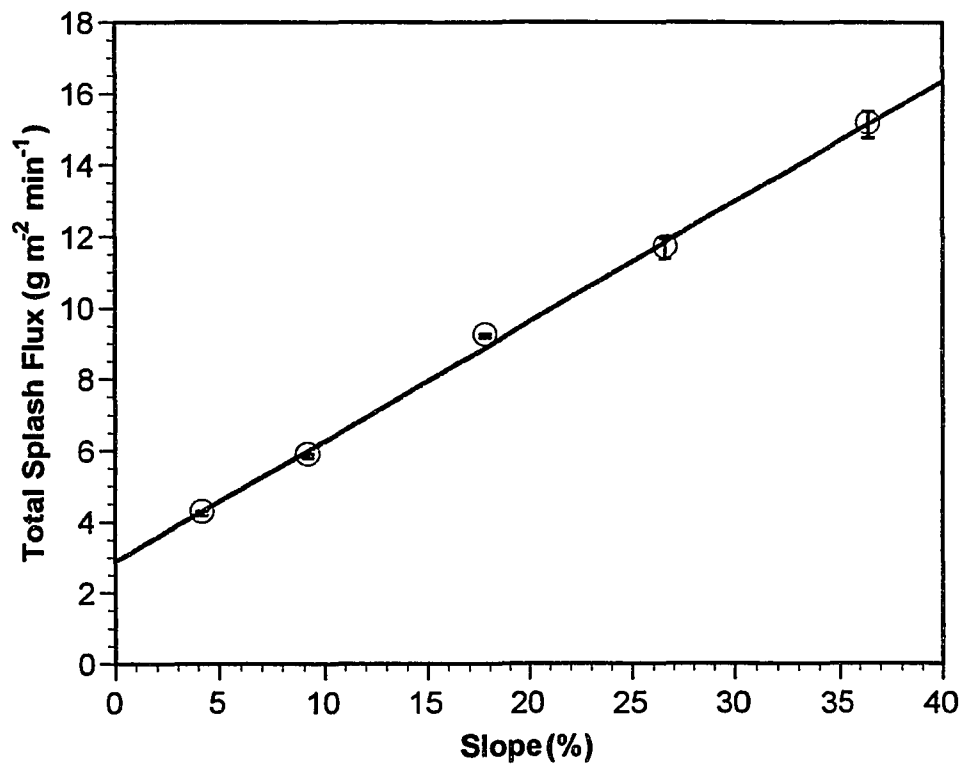


Figure 2.3 Effect of slope on total splash flux. Error bars are standard errors for the mean of three replicates.

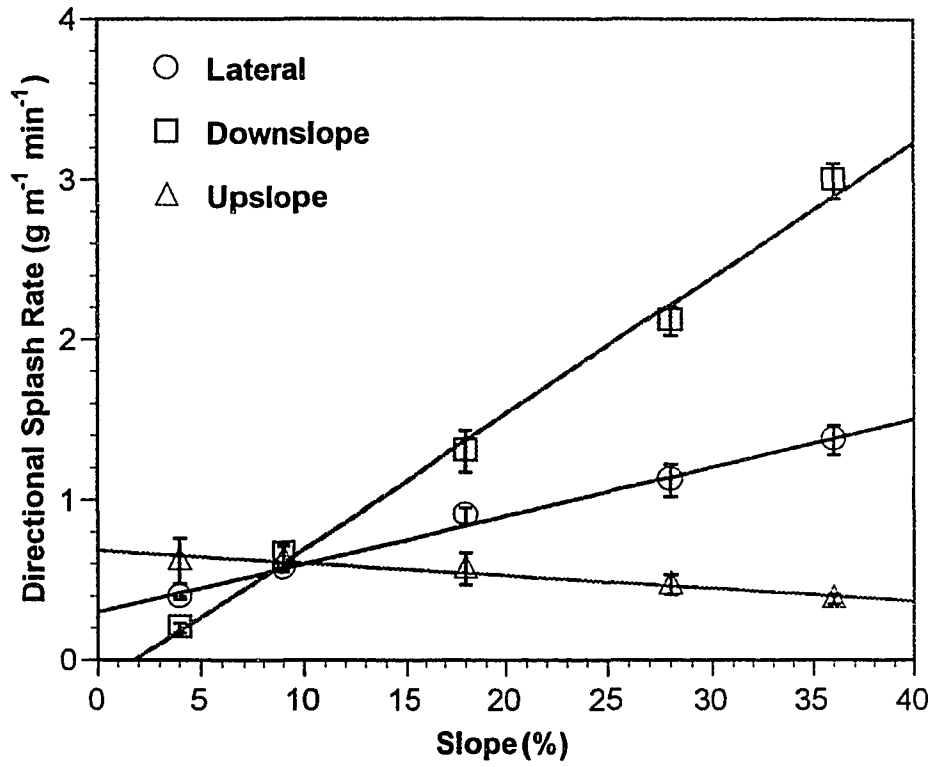


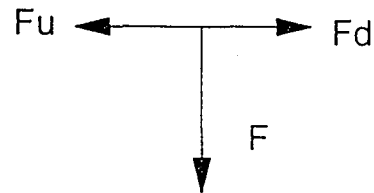
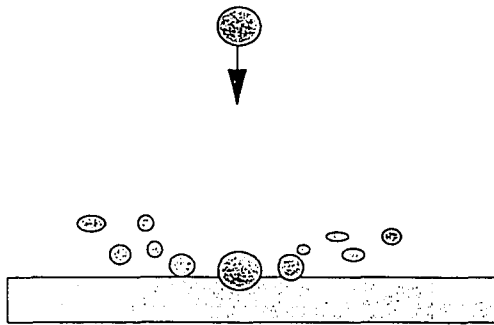
Figure 2.4 Effect of slope on directional splash rate. Error bars are standard errors for the mean of three replicates.

increased with slope though not as significantly as that of the downslope splash component. The increase of lateral splash and downslope splash was consistent with the total splash increase indicating that the decrease of upslope splash had little effect on the change of total splash output.

The change of directional splash rates with slope as discussed previously can be understood from the standpoint of mechanics. Raindrop impacts create a series of forces which can be idealized as two components: normal forces perpendicular to the soil surface and shear forces parallel to the soil surface. The shear forces can be further idealized as directional components. These forces interact with one another, causing random sediment movement. When the slope gradient is zero the normal forces will be at maximum and the directional shear forces will be equivalent to one another. As slope increases both the normal forces and the shear forces in the upslope direction decrease and the shear forces in the downslope direction increase, resulting in decreased upslope splash rates and increased downslope splash rates. The interaction between the lateral shear forces and the increased downslope shear forces also increases the lateral splash rate. It was visually observed that more splashed sediment was intercepted in the downslope area in the lateral splash collectors as slope increased. The effect of slope steepness on directional splash associated with the variation of shear forces is schematically represented in Figure 2.5.

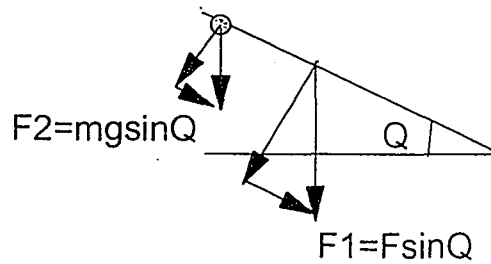
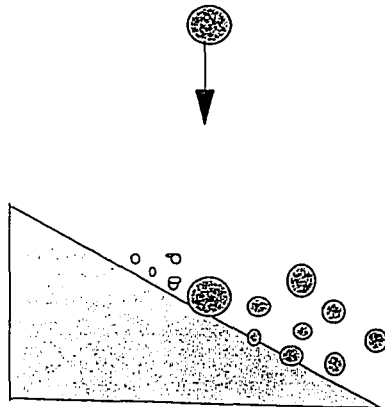
Theoretically, it is expected that splash rates for the three directional components equal one another when the slope is zero, and net downslope movement of splashed sediment occurs immediately when slope is greater than zero. However, as indicated in Figure 2.4 the following sequence of splash rates were observed for the 4% slope: upslope > lateral > downslope. Visual observations indicated that significant ponding of sheet flow was present in the downslope area of the 4% slope. This water layer probably had a

a. level surface



$$F_d = F_u$$

b. inclined surface



$$F_d' > F_d + F_2 + F_1 > F_u > F_u'$$

Figure 2.5 Illustration of the slope effect on directional splash at a level surface (a) and an inclined surface with a slope angle of Q (b). For the level surface: F = the normal component of raindrop impact force; F_d , F_u = shear components. For the inclined surface: F_1 = downslope shear force derived from F ; F_2 = downslope shear force derived from particle gravitational force (mg); F_d' = total downslope shear force; and F_u' = total upslope shear force

cushioning effect and shielded soil from splash, as documented by Moss and Green (1983) and Proffitt and Rose (1991a). Splash in the upslope areas was not influenced by water layer development and was thus more vigorous than downslope splash. Ponding still occurred near the outlet at 9% slope though the water layer depth was reduced, resulting in a roughly equal splash rate for the three components. It should be noted that the measured upslope and downslope splash rates in this study were merely at the two arbitrary plot edges. The magnitude of the upslope and downslope splash rates across any boundaries along the slope are partly dependent on the significance of the cushioning effect of the water layer on soil surface. Therefore, a splashed sediment balance performed by subtracting the upslope splash rate from downslope splash rate should be interpreted carefully if ponding is not uniform over the plot. When slopes were larger than 9%, Figure 2.4 showed a net downslope sediment movement caused by splash and the magnitude of the net sediment movement significantly increased with slope ($P < 0.001$). This trend supports a net downslope splash model initially proposed by Poesen and Savat (1981).

2.3.2 Partitioning downslope transport into wash and splash components

A comparison between wash flux and downslope splash flux (Figure 2.6) showed a gradual transition from a wash-dominated transport regime at low slopes (<9%) to a splash-dominated transport regime at high slopes (>9%). With slopes less than 9% the wash process dominated sediment transport. Wash flux from the 4% slope was $0.65 \text{ g m}^{-2} \text{ min}^{-1}$, which was double the downslope splash flux. The dominance of wash transport at low slopes was primarily due to, as mentioned previously, the development of a water layer which impeded downslope splash. The change of flow depth and velocity with slope was

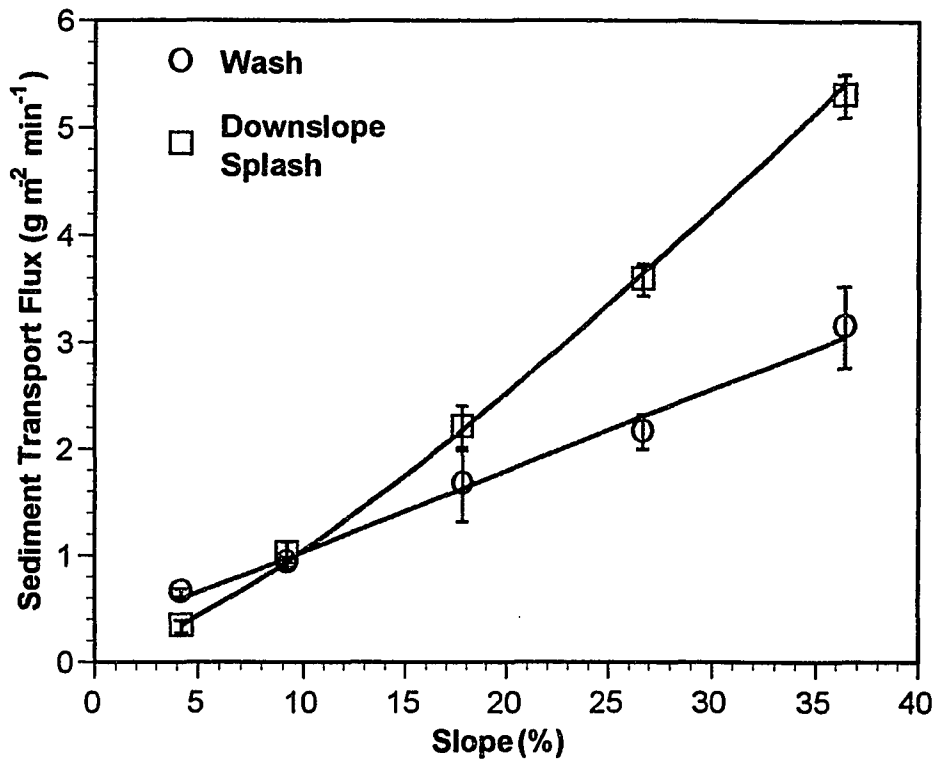


Figure 2.6 Effect of slope on transport flux of wash and downslope splash. Error bars are standard errors for the mean of three replicates.

approximated from the Chezy-Manning's equation for uniform flow and rectangular channels with width much larger than depth (Lindeburg, 1990):

$$D = (nQ/ws^{0.5})^{3/5} \quad [2.2]$$

where D = flow depth (m), n = Manning roughness coefficient (0.018 is assumed for this soil and flow condition), Q = flow discharge rate ($\text{m}^3 \text{s}^{-1}$), w = channel width (m), and s = slope (m m^{-1}). The results are shown in Table 2.2. A similar approach was also employed by Bryan (1979). It should be noted that this estimation procedure was only approximate since the water layer developed at downslope areas of 4 and 9% slopes was visually observed to be larger than that in upslope areas. Nevertheless, it was indicated that as slope increases water layer depth decreases and interrill flow velocity increases. As a result, the interaction between raindrop effects and the thin flow enhanced sediment transport by both wash and splash. However, given such a short distance the increase of wash transport with slope was unlikely due to the critical flow shear stress or stream power, as is the case for rill erosion. Field rill erosion studies with the same soil (Chapter 4) indicated that the critical shear stress for flow detachment was about 1 Pa, which corresponded to a stream power of about 0.12 W m^{-2} . Estimates of flow stream power in this interrill study (Table 2.2) were one to two orders of magnitude smaller than this critical value. The estimated values of shear velocity of the thin flow ranged from 0.86 to 1.8 cm s^{-1} , which were smaller than the critical value (3.0-3.5 cm s^{-1}) for rill initiation found by Govers (1985) for loamy soils. Visual observation indicated that the raindrop impact tended to create local sediment detachment in the thin flow. The detached sediment, mainly sand-sized aggregates, moved downslope under the influence of gravity and the tractive force

of the thin flow. This process was the principal mode of wash transport. The transport efficiency of this process was, however, low due to active deposition processes and the limited power that the thin flow generated. Only the detached sediment close to the downslope edge was lost via wash transport. The downslope splash transport flux increased with slope more rapidly than wash transport, however. When the slope gradient was larger than 9%, splash transport eventually exceeded wash transport due to the reduction in the water layer cushioning effect and the increased shear forces inserted by rain drops. The downslope splash flux of the 36% slope was $5.31 \text{ g m}^{-2} \text{ min}^{-1}$ while the wash flux was only $3.15 \text{ g m}^{-2} \text{ min}^{-1}$.

Table 2.2. Hydraulic parameters of interrill overland flow at steady state

Slope (m m^{-1})	Flow rate [†] ($10^{-6} \text{ m}^3 \text{ s}^{-1}$)	Flow depth [‡] (mm)	Flow velocity [§] (10^{-2} m s^{-1})	Stream power [£] (10^{-3} W m^{-2})	Shear velocity [£] (cm s^{-1})
0.04	2.03	0.19	3.56	2.65	0.86
0.09	1.99	0.14	4.74	5.83	1.12
0.18	2.00	0.12	5.56	11.74	1.44
0.27	2.04	0.11	6.18	17.98	1.67
0.36	2.00	0.10	6.80	23.49	1.84

[†] Mean of three replicates.

[‡] Estimated from Eq. [2.2].

[§] Determined from $V = Q/A$ where A = cross-sectional area of flow (m^2), and Q is defined in Eq [2.2].

[£] Determined from $\omega = (\rho g Q S)/w$ where ω = stream power (W m^{-2}), ρ = density of water at a given temperature (kg m^{-3}), g = acceleration of gravity (9.807 m s^{-2}), Q , S , and w are defined in Eq. [2.2].

[£] Determined from $U_s = (gRS)^{0.5}$ where U_s = shear velocity (m s^{-1}), R = hydraulic radius (m), which equals D in this case, and g is defined above.

Recognizing the splash-dominated transport regime as discussed previously implies that downslope splash can be an important process of sediment transport in interrill erosion. This splash-dominated regime may occur typically in short and steep slope settings, which are typical of many interrill areas in agricultural fields. Therefore, caution should always be taken when a dominant interrill sediment transport process is claimed. Actually, the relative contribution of splash and wash to sediment transport in an interrill area may be influenced by several factors, notably slope length and gradient, soil erodibility, rainfall intensity, ponding depth, and the proportion of rainfall lost as infiltration. The dominant process that governs sediment transport depends on a delicate balance of these factors.

When splash dominates interrill sediment transport, it is critical that sediment transported downslope by splash be measured in addition to that transported by wash. To our knowledge, most of studies in the literature dealing with interrill erosion commonly used a "runoff-trough" approach to measure soil loss (e.g. Watson and Lafen, 1986; Meyer and Harmon, 1989; Huang and Bradford, 1993): High speed photography has shown that splash angles may range from 15 to $>40^\circ$ (Al-Durrah and Bradford, 1981). The distance of splash transport was also observed to be from a few centimeters to over half a meter (Poesen and Savat, 1981; Ghadiri and Payne, 1988). Thus a sequential range of splash along slope may create significant downslope transport. It is very unlikely that the runoff trough can intercept most of the splashed sediment. In addition, the "Gerlach" type runoff troughs, which are not open for splash measurements, are also used in field interrill erosion studies (e.g. Roels and Jonker, 1983). Evaluation of interrill soil erosion based on this measurement approach may therefore result in an underestimation of interrill soil loss or sediment delivery to rills. An effective measurement device will have to include a splash

guard mounted on the runoff trough to completely intercept sediment transported downslope by splash.

2.3.3 Slope controls on splash and wash transport

Little is known about the independent slope functions for wash and downslope splash processes. Regression analysis indicated that wash flux was linearly related to slope ($P < 0.001$) while downslope splash flux was best modeled by a power function ($P < 0.001$). The best-fit regression equations were:

$$F_{\text{wash}} = 0.076 S + 0.293 \quad n = 15, \text{Adj. } r^2 = 0.796, \text{SEE} = 0.463 \quad [2.3]$$

$$F_{\text{splash}} = 0.052 S^{1.288} \quad n = 15, \text{Adj. } r^2 = 0.956, \text{SEE} = 0.262 \quad [2.4]$$

where F_{wash} = wash flux ($\text{g m}^{-2} \text{min}^{-1}$), F_{splash} = downslope splash flux ($\text{g m}^{-2} \text{min}^{-1}$), and S = slope gradient (%). Similar linear or near-linear slope functions for interrill sediment transport were reported in the literature for slopes less than 20% (Evelt and Dutt, 1985; Huang and Bradford, 1993). For steeper slopes, however, a gradually diminishing slope effect on sediment transport was suggested (Watson and Laflen, 1986; Meyer and Harmon, 1989). Such a slope function is used in the WEPP model for interrill sediment transport (Liebenow et al., 1990):

$$D_i = K_i I^2 S_r \quad [2.5]$$

where D_i = interrill erosion rate ($\text{g m}^{-2} \text{min}^{-1}$), K_i = interrill erodibility (g min m^{-4}), I = rainfall intensity (m min^{-1}), and $S_r = 1.05 - 0.085 \exp(-\sin\theta)$ with θ the slope angle in degrees. This

slope function (S_r) ranges from 0.2 at zero slope to 1 at 100% slope, diminishing gradually when slope is larger than 30%. Two implicit assumptions underlying Eq. [2.5] are that (i) the slope function is valid for all soils; and (ii) K_i is independent of slope for a given soil. Based on these two assumptions, a least squares linear regression was conducted for the measured D_i in this study, which is the sum of the measured F_{wash} and F_{splash} in Eq. [2.3] and [2.4], against S_r . The best-fit equation is:

$$D_i = 7.664 S_r \quad n = 15, \text{ Adj. } r^2 = 0.700, \text{ SEE} = 1.539 \quad [2.6]$$

The regression equation was forced through the origin and was highly significant ($P < 0.001$). The measured D_i and predicted D_i using Eq. [2.6] were plotted against slope in Figure 2.7. It was noted that Eq. [2.6] overestimated D_i when slope was less than 27% and underestimated D_i when slope was larger than 27%. The discrepancy suggests that the slope function used in Eq. [2.5], which is developed with temperate United States soils, may not be applicable for well aggregated tropical soils.

Theoretical explanations about the diminishing slope effect in Eq. [2.5] are that interrill erosion is transport-limited at low slopes whereby not all detached sediment is transported while sediment transport becomes detachment-limited at high slopes meaning that all detached sediment is transported (Foster, 1990; Nearing et al., 1990). A comparison between the total splash flux in Figure 2.3 and downslope transport flux D_i (combining wash and downslope splash) in Figure 2.6 indicates that the total splash flux was consistently larger than downslope sediment transport flux at all studied slopes. In the literature total splash flux has been generally used as a surrogate of total raindrop detachment flux (Al-Durrah and Bradford, 1981; Bradford and Huang, 1993; Parsons et al., 1994). In this study,

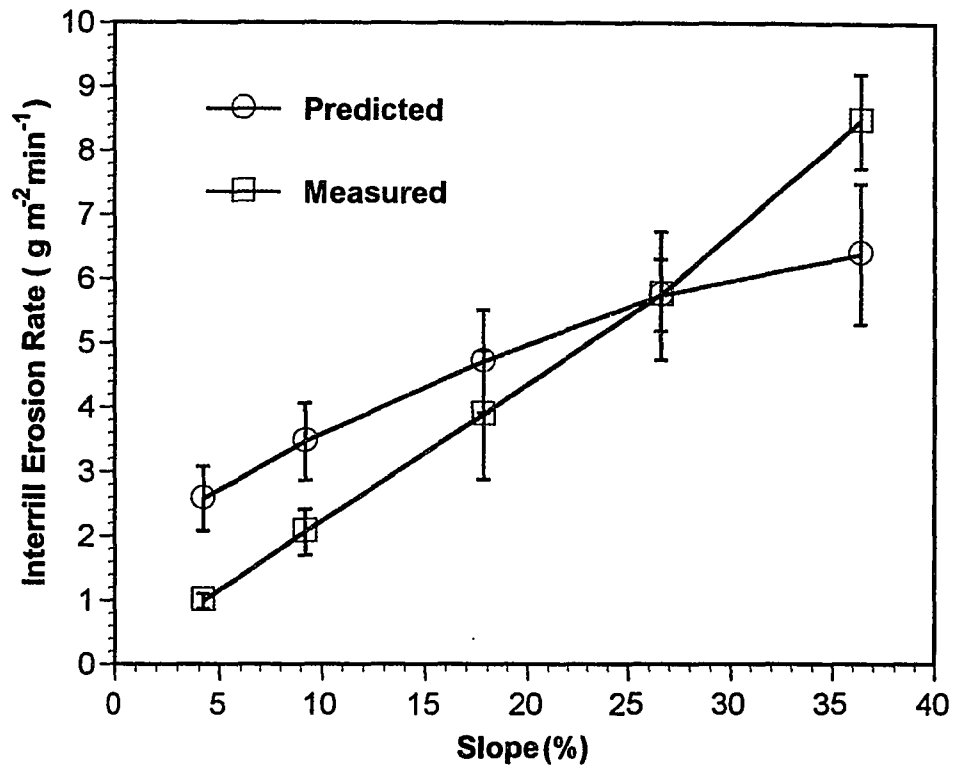


Figure 2.7 Comparison between measured interrill erosion rates and predicted values using the WEPP interrill erosion model (see Eq. [2.5]&[2.6]). Error bars are 95% confidence intervals.

it is not appropriate to equate the measured total splash flux with total raindrop detachment flux. The actual flux of total rainfall detachment should be much larger than the measured total splash flux due to instantaneous deposition processes occurring within the plot area (Proffitt and Rose, 1991a). It must also be noted that the amount of detached soil for transport under the studied experimental conditions would be less than that in the field since the sediment splashed into the lateral splash collectors would be balanced by reciprocal input from surrounding soils. The net implication of the above discussion is that, even with the lateral splash loss sediment transport was still in a transport-limited regime for all the studied slopes. This transport-limited regime was due partly to the plot size and experimental set-up, and partly to the unique soil aggregation characteristics of the Oxisol which was studied. Sand-sized aggregates, which represent a high percentage in the soil (Table 2.1), can be detached by raindrop impacts, but require further splash and more powerful runoff for complete transport. Such transport-limited conditions were also observed by Kinnell (1990). The inability of Eq. [2.5] to account for the sediment transport and slope relationship as described by Eq. [2.3] and [2.4] suggests that further research is required to calibrate the WEPP interrill erosion model when applied in well-aggregated tropical soils.

2.4 Conclusions

The method devised for this study succeeded in partitioning total splash into directional components and interrill sediment transport into wash and splash components. The data showed that slope steepness has a significant effect on all these components. Downslope and lateral splash increased with slope angle while the upslope component

decreased, reflecting changes in raindrop impacting forces and surface water ponding depth with slope. Overall there was a linear increase of total splash with increasing slope.

The results also showed that wash dominated interrill sediment transport at low slopes (<9%) and was linearly correlated with slope angle. Downslope splash transport was dominant at high slopes (>9%) and was best described by a power function predictive model. The fixed slope function in the WEPP interrill erosion model was inadequate for describing this sediment transport and slope relationship .

The practical implication of this finding is that splash is an important process of sediment transport in interrill erosion under steep and short slope settings. Failure to include splashed sediment in interrill erosion measurements using the common "runoff-trough" approach may underestimate total soil loss or interrill sediment delivery to rills.

These conclusions are, however, obtained from experiments with a single rainfall intensity and slope length. The influence of rainfall intensity and its interaction with slope angle on sediment transport and selectivity of interrill splash and wash dynamics were investigated using this approach and are presented in Chapter 3 and 5, respectively. In the field situation, interrill erosion acts mainly as a process of sediment delivery into rills which are typically spaced between 1 to 2 m in an agriculturally managed system such as the ridge-and-furrow configuration. The research on the rill erosion process and the interaction effect of interrill erosion and rill erosion on sediment transport and sediment quality are presented in Chapters 3 and 6.

CHAPTER 3
MODELING RAINFALL INTENSITY AND SLOPE STEEPNESS EFFECTS ON
INTERRILL SPLASH AND WASH DYNAMICS

Abstract

Simultaneous measurements of interrill directional splash and wash from an Oxisol at 4, 9, 18, 27, and 36% slopes were made using simulated rainfall with intensities of 45, 65, 90, and 135 mm h⁻¹. The effects of rainfall intensity, slope steepness, and their interaction on interrill splash and wash were quantitatively determined. Results indicated that a power function, $E = aI^b$, where E is the erosion rate, I is the rainfall intensity, and a and b are fitted parameters, modeled the relationship between rainfall intensity and all splash and wash components reasonably well. However, b -values for splash were close to 1 (range 0.5-1.4) while those for wash were greater than 2 (range 2.1- 4.2), indicating basic dynamic differences between the two processes. It was also observed that b -values increased with increasing slope indicating that rainfall intensity effects were dependent on slope steepness. Slope controls on interrill splash and wash were well described by either linear function or power functions, both showing a monotonic increase in erosion with increasing slope. The additive or lumped effect of wash and splash on interrill sediment delivery was also studied. It was concluded that the commonly measured interrill erodibility was a dynamic combination of splashability and washability, representing the erodibility factors for splash and wash, respectively. Runoff flux and slope gradient largely determined the relative contribution of these two components to interrill erodibility, implying that measured interrill erodibilities depend, in part, on the processes, i.e., splash or wash, controlling interrill sediment delivery.

3.1 Introduction

Studies of the influence of rainfall intensity on interrill soil erosion have been an important research area for a number of years. Researchers have commonly related the interrill erosion rate with rainfall intensity through a power function model:

$$E = aI^b \quad [3.1]$$

where E = interrill erosion rate ($M L^{-2} T^{-1}$), I = rainfall intensity ($L T^{-1}$), and a and b = fitted constants. It has been recognized that the coefficient 'a' is a soil and slope dependent parameter. Various values for exponent b are reported in the literature, with the pioneering work of Neal (1938) and Ekern (1954) reporting b -values of 2.2 and 1.5, respectively. Meyer (1981), using field rainfall simulation, found that b decreased slightly from 2.3 for soils with low clay content (<20%) to 1.6 for soils with about 50% clay content. He, therefore, proposed a b -value of 2 for low-clay soils, and this exponent value has been used in the interrill erosion algorithm in the WEPP model (Nearing et al., 1990). Watson and Lafien (1986), using three types of soil with similar texture, found that values of b ranged from 1.5 to 2.5. A recent study by Truman and Bradford (1993) further indicated that temporal variation in b -values during a rainfall event ranged from 0.66 to 3.85. As Sharma et al. (1993) noted, the reasons for the difference between b -values reported in the literature are not yet fully understood.

Another equally important line of research is the effect of slope steepness (hereafter shortened as "slope") on interrill erosion. When the slope effect is considered, Eq. [3.1] becomes:

$$E = K_i I^b S_f \quad [3.2]$$

where K_i = interrill erodibility factor (dimensions depend on the value of b , commonly expressed in the WEPP model as kg s m^{-4}), S_f = dimensionless slope factor; and E , I , b = defined as above. Several slope functions have been proposed in the literature. Some of the most common ones are: (i) the power function (e.g. Neal, 1938; Watson and Lafren, 1986), which is expressed as:

$$S_f = S^c \quad [3.3]$$

where S = slope gradient (m m^{-1}); and c = fitted exponent; (ii) the linear function (e.g. Foster et al., 1977; Huang and Bradford, 1993), which is expressed as:

$$S_f = dS + e \quad [3.4]$$

where S = slope gradient (m m^{-1}); and d and e = fitted constants; and (iii) the WEPP slope function (Liebenow et al., 1990), which is expressed as:

$$S_f = 1.05 - 0.085 \exp(-\sin\theta) \quad [3.5]$$

where θ = slope angle in degrees. The power function model has no intercept, and therefore, does not have physical meaning at zero slope since interrill erosion does occur even when $S = 0$. Values of exponent c ranged from 0.2 to 1.4 in the literature, and varied with the methods employed and soils studied (Qaunsah, 1981). The intercept term of the

linear function can be negative if interrill soil loss at low slopes is not linearly proportional to that at high slopes (Huang and Bradford, 1993), and thus may result in meaningless predictions at zero or near zero slopes. The WEPP slope function differs fundamentally from the other two in that it shows a gradual diminishing effect of slope on interrill erosion. The universality of the WEPP slope function, though based on several data sets with over 20 soils, has been questioned by Kinnell (1993a), Huang and Bradford (1993), and Wan et al. (1996). A universal slope function which is independent of soils and experimental conditions does not yet exist.

At the process level, interrill erosion is typically understood to be a combination of splash (detachment and transport by raindrop impacts) and wash (transport by unconcentrated overland flow) dynamics. One of the reasons for differences in the influences of rainfall intensity and slope on interrill erosion lies in the empirical basis of the above models. Therefore, they may have limitations when applied with different rainfall, slope, and soil conditions, depending on the source of the data from which they were developed. Furthermore, those equations were mostly derived from measurements which have only included wash transport, or failed to partition sediment transported by splash and wash (e.g. Meyer, 1981; Watson and Laflen, 1986). Successful modeling of interrill erosion requires an understanding both sub-processes. With the interrill splash and wash partitioning approach introduced previously, this Chapter reports the results of splash and wash sediment fluxes over a range of rainfall intensities and slope angles. The objective is to quantify the effects of rainfall intensity, slope angle, and their interaction on interrill splash and wash dynamics at a process level.

3.2 Materials and Methods

The soil, interrill splash and wash partitioning system, and experimental procedures were as described in Chapter 2. Briefly, the Wahiawa silty clay (a Rhodic Eutruxox) was collected from the surface 0.1 m in the Poamoho Experimental Station on the island of Oahu, Hawaii. Samples were air-dried and sieved through a square hole sieve with 6-mm openings. The splash and wash partitioning system consisted of a drip-type rainfall simulator based on the design of Munn and Huntington (1976), a soil tray with runoff collector, and four directional splash collectors. A glass bead layer of about 20 mm was evenly placed at the bottom of the soil tray to provide free drainage. A metal screen with an attached layer of cheesecloth separated the glass beads and a 20-mm pre-wet soil layer (soil moisture content \approx 35% mass). This "horizon" was compacted to a bulk density of approximately 1.3 Mg m^{-3} to simulate a subsoil layer found in the field (Table 2.1). Air-dried soil was packed uniformly in the soil tray to produce a soil bed of 60 mm in depth with a level surface. The dry bulk density was about 1 Mg m^{-3} , similar to that found in the field (Table 2.1). Preliminary trials indicated that this soil layering had a steady state infiltration rate of about 25 mm h^{-1} , which was close to that measured by rainfall simulation in the field (Dangler et al., 1976). The soil bed was wetted to near saturation through input water from the bottom percolation outlet prior to slope adjustment. Slopes studied were 4, 9, 18, 27, and 36 %, and it was assumed that this range of interrill slopes would simulate a gradual transition from a transport-limited regime to a detachment-limited regime as defined by Foster (1990). The rainfall intensities studied were 45 ± 2.1 , 65 ± 1.1 , 90 ± 4.2 , and $135 \pm 3.0 \text{ mm h}^{-1}$ (± 1 standard deviation). For each combination of slope and rainfall intensity, runoff and percolate were measured every 5 min after rainfall application. After achieving

steady state (\approx 20 to 30 min), splash collectors were attached for 20 min. After rainfall was stopped, runoff volume was measured and splashed sediment was separately collected with sediment from the two lateral splash collectors combined. Visual observations of the soil surface and sediment transport patterns were made both during and after rainfall simulation. Particular attention was paid to surface morphological features formed and water ponding during rainfall. Each combination of slope and rainfall intensity was replicated three times and a new soil sample was used for each replicate. The collected wash and splash sediments were oven dried and mass determinations were made. The mean of the three replicates was reported, but all the replicate data were used for statistical analysis (the least squares regression and analysis of variance). Splash and wash sediment fluxes were corrected for areal projection of the plot for all slopes.

3.3 Results and Discussion

Splash and wash fluxes ($\text{g m}^{-2} \text{h}^{-1}$) are reported separately for lateral splash, downslope splash, upslope splash, total splash (combination of the three directional components), wash, and interrill sediment delivery (combination of wash and downslope splash). Analysis of variance of these data (Table 3.1) showed that rainfall intensity and slope gradient significantly ($P < 0.001$) influenced the amount of sediment detached or transported by splash and wash. It is interesting to note that the interaction between rainfall intensity and slope also had a significant ($P < 0.001$) effect on interrill splash and wash except for the upslope splash component. This interaction indicates that the main effects of rainfall intensity and slope are not independent. Their mutual dependence is further examined in later sections.

Table 3.1 F values of ANOVA for rainfall intensity and slope effects on interrill splash and wash components: All F values are significant with $P < 0.001$ except where otherwise indicated.

Source of variance	df	Total splash	Upslope splash	Lateral splash	Downslope splash	Wash	Interrill sediment delivery
Rainfall intensity (I)	3	108.6	78.13	72.39	57.33	30.58	35.29
Slope (S)	4	98.25	9.65	54.95	271.8	12.04	18.71
I x S	12	6.73	0.97 [†]	5.41	10.52	9.08	10.15
Error	40						

[†] P = 0.49 not significant at $\alpha = 0.05$

3.3.1 Effects of rainfall intensity

To quantitatively determine the effect of rainfall intensity on interrill splash and wash dynamics, the data were subdivided into five groups according to slope. When slope was held constant rainfall intensity was the only variable that influenced interrill splash and wash. To test the adequacy of the power function model as described by Eq. [3.1], all splash and wash flux data and rainfall intensities were transformed to \log_{10} form prior to conducting the least squares linear regression analysis. Table 3.2 indicated that b-values for splash were generally less than 1 except for the upslope splash component. A closer examination of these values indicated that b-values generally increased with slope, a finding which was not previously reported in the reviewed literature. For example, b-values of total splash increased from 0.54 at 4% slope to 0.98 at 36% slope, and those of upslope splash increased from 0.89 at 4% slope to 1.36 at 36% slope. However, in contrast to the increased b-values as slope increased, the coefficient a in Eq. [3.1], however, tended to decrease with increasing slope. A graphic presentation of the power function for downslope splash is shown in Figure 3.1A.

Increased b-values imply that rainfall intensity has a more pronounced effect on splash as slope becomes steeper. Significant ponding of sheet flow was observed in the downslope areas of the 4% slope for all rainfall events. This water layer had a cushioning effect and shielded soil from splash, as documented by many researchers such as Moss and Green (1983) and Proffitt and Rose (1991a). The cushioning effect increased with rainfall intensity, resulting in smaller b-values at 4% than steeper slopes. The potential existence of ponded water is one of the reasons accounting for the lower level of explanation as measured by the coefficient of determination (r^2). The smaller r^2 values for the 4% slope indicate that splash models should be carefully constructed when a water

Table 3.2 Parameter estimates from linear regression analysis of splash components for the power function model $E = al^b$ (based on log-transformed data) and linear function model $E = al$ (intercept forced through origin) from data of sediment flux E ($g\ m^{-2}\ h^{-1}$) and l ($mm\ h^{-1}$): $n = 12$ for all cases[†]

E	Slope	$E = al^b$				$E = al$		
		a	b	r^2	SEE [‡]	a	r^2	SEE
Total splash	4%	27.99	0.54	0.56**	86.13	3.31	0.40*	89.27
	9%	15.96	0.76	0.77	87.33	5.53	0.83	79.72
	18%	20.61	0.79	0.87	101.9	7.93	0.78	116.5
	27%	14.79	0.90	0.90	106.6	9.27	0.85	116.8
	36%	13.15	0.98	0.89	126.1	11.9	0.91	127.0
Upslope splash	4%	1.600	0.89	0.57**	30.36	1.03	0.63	28.96
	9%	0.784	1.06	0.70	21.72	1.11	0.81	21.60
	18%	0.433	1.18	0.75	26.12	1.05	0.72	27.05
	27%	0.164	1.36	0.88	9.860	0.86	0.87	14.85
	36%	0.112	1.36	0.87	10.11	0.60	0.82	12.69
Lateral splash	4%	38.02	0.37	0.34*	57.21	2.00	0.10	65.24
	9%	10.96	0.75	0.76	63.84	3.62	0.79	58.92
	18%	12.52	0.81	0.89	64.94	5.18	0.79	74.62
	27%	9.142	0.89	0.84	84.29	5.55	0.76	90.20
	36%	4.943	1.07	0.84	105.6	6.91	0.85	105.0
Downslope splash	4%	2.421	0.51	0.23 ^{ns}	12.37	0.28	0.26 ^{ns}	12.13
	9%	8.973	0.46	0.41*	19.56	0.79	0.23 ^{ns}	22.15
	18%	13.84	0.54	0.65	27.78	1.70	0.20 ^{ns}	39.49
	27%	7.532	0.79	0.92	25.37	2.86	0.80	36.67
	36%	10.91	0.80	0.90	41.55	4.36	0.85	50.75

[†] All r^2 values are significant with $P < 0.001$ except where otherwise indicated by ** ($P < 0.01$), * ($P < 0.05$), and ns (not significant at $\alpha = 0.05$)

[‡] SEE = Standard error of the estimate

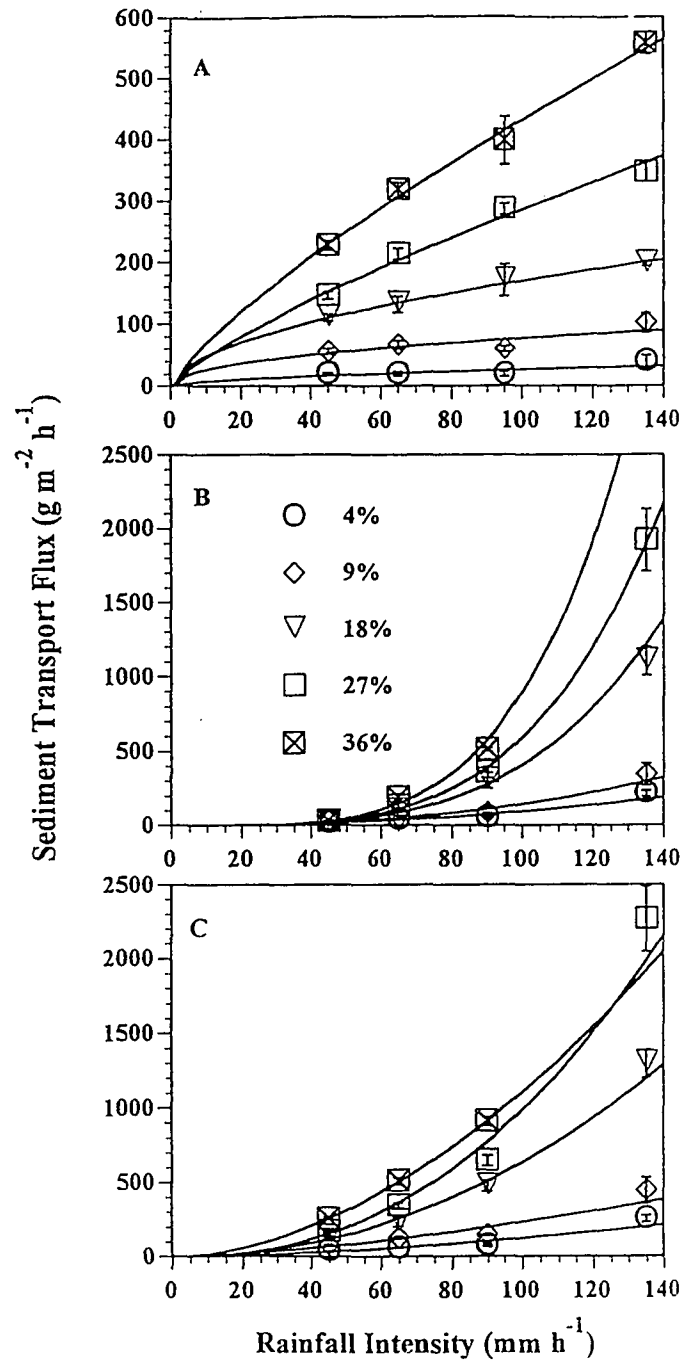


Figure 3.1. Interrill splash and wash flux for different slopes as a power function of rainfall intensity. A: downslope splash, B: wash, C: interrill sediment delivery. Data of 135 mm h⁻¹ at 36% for B (5334 ± 1201 g m⁻² h⁻¹; mean ± 1 standard error) and C (5891 ± 1186 g m⁻² h⁻¹) are not shown for clarity and the regression lines are not supported by these data. Error bars are standard errors for the mean of three replicates.

layer of significant depth exists at the soil surface. Presently available soil erosion models such as EUROSEM (Morgan et al., 1992) include a water layer depth factor in their rainfall detachment algorithms. The water depth factor used in EUROSEM is expressed as $\exp(-bh)$, where h is the water layer depth and b is an exponent that is a function of soil texture. Apparently, h is a function of slope and soil surface conditions, but these are not clearly specified in the model.

Early research by Rose (1961) and Mazurak and Mosher (1970) indicated that total splash was linearly related to rainfall intensity. Proffitt et al., (1991) further assumed a b -value of 1.0 in their power function model. The literature also supports a linear relationship between splash and rainfall kinetic energy (Al-Durrah and Bradford, 1982; Morgan et al., 1992; Sharma et al., 1993; 1995). Since raindrop size was uniform in this study, rainfall kinetic energy per unit area per unit time was linearly related with rainfall intensity (Munn and Huntington, 1976), and thus rainfall intensity and rainfall kinetic energy can be used interchangeably in the following discussion whenever " I " (rainfall intensity) is endowed with the physical meaning of raindrop impacts. Therefore, a linear regression analysis with the intercept forced through the origin was conducted. The results are shown in Table 3.2 for comparison with the power function model. An examination of r^2 and the standard error of the estimate (SEE) of both models indicated that the linear model generally described the splash and rainfall intensity relationship as well as the power function model. This is particularly true for high slopes when b -values were close to 1. For downslope splash, however, the power function model provided a marginally better fit for the data.

The regression equations between wash flux and rainfall intensity were highly significant ($P < 0.001$) with all r^2 values larger than 0.92 (Table 3.3 and Figure 3.1B). The

Table 3.3 Parameter estimates from regression analysis for wash and interrill sediment delivery based on log-transformed data of sediment flux E ($\text{g m}^{-2} \text{h}^{-1}$) and I (mm h^{-1}), Q (mm h^{-1}), and IQ ($\text{mm}^2 \text{h}^{-2}$) as independent variables: $n = 12$ for all cases except where otherwise indicated †

E	Slope	$E = aI^b$			$E = aQ^b$			$E = a(IQ)^b$		
		a	b	r^2	a	b	r^2	a	b	r^2
Wash	4%	0.006	2.10	0.92	0.21	1.42	0.91	0.049	0.85	0.92
	9%	0.003	2.37	0.93	0.11	1.66	0.92	0.024	0.98	0.93
	18%	2.4×10^{-5}	3.61	0.97	0.01	2.48	0.98	8.4×10^{-4}	1.47	0.98
	27%	1.2×10^{-5}	3.94	0.99	0.006	2.69	0.98	4.4×10^{-4}	1.58	0.99
	36%	7.8×10^{-7}	4.58	0.98	0.001	3.14	0.95	6.5×10^{-5}	1.87	0.97
	27% ‡	1.5×10^{-5}	3.79	0.97	0.015	2.40	0.99	0.001	1.47	0.99
	36% ‡	3.7×10^{-6}	4.19	0.96	0.008	2.66	0.94	3.9×10^{-4}	1.63	0.96
Interrill sediment delivery	4%	0.07	1.84	0.87	1.08	1.10	0.92	0.35	0.66	0.86
	9%	0.26	1.47	0.84	2.80	1.03	0.81	1.04	0.61	0.83
	18%	0.04	2.10	0.96	1.40	1.47	0.98	0.33	0.85	0.95
	27%	0.02	2.31	0.97	1.04	1.59	0.94	0.22	0.95	0.96
	36%	0.006	2.74	0.92	0.60	1.86	0.88	0.09	1.11	0.90
	27% ‡	0.12	1.91	0.98	4.07	1.20	0.98	1.03	0.74	0.98
	27% §	0.007	2.58	0.96	0.21	1.96	0.94	0.05	1.12	0.95
	36% ‡	0.24	1.83	0.98	0.68	1.17	0.98	1.79	0.72	0.99
36% §	3.9×10^{-4}	3.33	0.92	0.09	2.31	0.86	0.009	1.37	0.89	

† All r^2 values are significant with $P < 0.001$

‡ $n = 9$ with three data points at the rainfall intensity of 135 mm h^{-1} omitted

§ $n = 9$ with three data points at the rainfall intensity of 45 mm h^{-1} omitted

b-values ranged from 2.10 to 4.58, again increasing with slope. The a-values showed the same tendency to decrease with increasing slope as was the case for splash. However, the wash b-values were significantly larger than those for splash. This was evident from a comparison of Figure. 3.1A & B. These differences indicated a basic distinction between the two dynamic processes: splash is a process of expenditure of raindrop kinetic energy while wash is a process of dissipation of raindrop impacted flow energy. Two critical slopes associated with wash transport were identified from an examination of the magnitude of b-values. The first was from 9% to 18% where b-values increased from 2.37 to 3.61. This was associated with the rapid wash transport flux increase for the 90 and 135 mm h⁻¹ runs when slope was increased from 9 to 18% (Figure 3.2). The second was from 27% to 36% where b-values increased from 3.94 to 4.58. This coincided with rilling, which was visually observed during the 36% and 135 mm h⁻¹ runs (Figure 3.2C).

Since wash is a surface flow transport process, and the thin and unconcentrated flow is impacted by raindrops (Moss and Green, 1983), it is therefore more fundamental to model this process with flow parameters. Regression analyses using log-transformed data were conducted to fit the following models:

$$E = a Q^b \quad [3.6]$$

$$E = a (IQ)^b \quad [3.7]$$

where Q = runoff flux (expressed as mm h⁻¹) and E, a, b, I = defined as above. The results are shown in Table 3.3 for comparison with rainfall intensity as the independent variable. It was found that the power function of Q and IQ both described the relationship as well as that of rainfall intensity. This resulted from the infiltration rate being nearly a constant in this

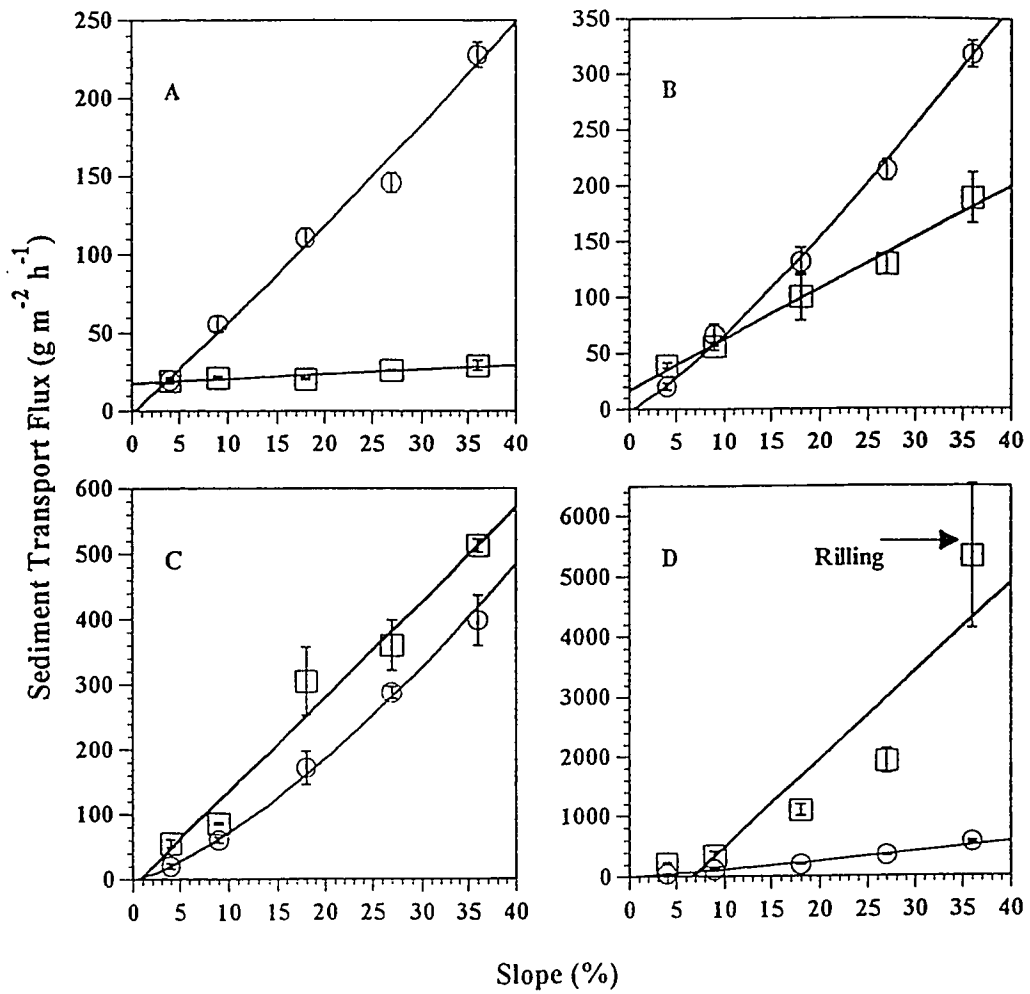


Figure 3.2. Comparison of downslope splash (O) and wash (□) as affected by slope under four rainfall intensities, A: 45 mm h⁻¹, B: 65 mm h⁻¹, C: 90 mm h⁻¹, and D: 135 mm h⁻¹. Downslope splash was fitted with a power function and wash with a linear function. Error bars are standard errors for the mean of three replicates.

study, and therefore Q was linearly related with I ($r^2 = 0.999$ results not shown). However, it is believed that IQ would generally be the most appropriate parameter describing interrill wash transport since it expresses the physical relationship between both raindrop impact (I) and flow flux (Q). A similar erosivity factor was proposed by Kinnell (1993b) to replace I^2 in the WEPP interrill erosion model. It should also be noted that b-values for runoff flux varied with slope, ranging from 1.42 to 3.14. This is larger than the unity linear effect of runoff flux on rill process transport, which is implicitly contained in the calculation of shear stress or stream power used in rill erosion models (Rose, 1985; Nearing et al., 1990).

For interrill sediment delivery, which combines wash and downslope splash, b-values ranged from 1.47 to 2.74 (Table 3.3 and Figure 3.1C). These values can be compared to the results from Truman and Bradford (1993) who indicated that b-values ranged from 0.66 to 3.85. The increase of b-values with increasing slope was again indicated in Table 3.3. Meyer and Harmon (1989), in a laboratory study, found the opposite, i.e., b-values decreased as slope increased. These apparently contradictory results may reflect soil texture and structure differences. The Oxisol used in this study was well-aggregated and had a relatively high infiltration capacity (Table 2.1). Sand-sized water stable aggregates can be detached by raindrop impacts, but require further splash and competent runoff for transport. Figure 3.1C indicates interrill sediment delivery is small when rainfall intensity is low (45 mm h^{-1}), and wash flux increases only slightly with increasing slope (Figure 3.2A). As rainfall intensity increases, interrill sediment delivery increases more rapidly with increasing slopes since raindrop energy and flow flux become more able to transport sand-sized aggregates. This nonlinear increase in interrill sediment delivery, mainly through the increase in wash transport, with increasing slope at high rainfall intensity accounts for the increased b-values in this study.

Since interrill sediment delivery is a combination of wash and downslope splash and these respond differently to changes in rainfall intensity, the relative contribution of these two processes to interrill sediment delivery determines the magnitude of b-values. Given the present experimental set-up, b-values of the interrill sediment delivery were less than those of wash alone and greater than those for downslope splash (Table 3.3). The lumped nature of interrill sediment delivery is illustrated in Figure 3.1. A comparison of the contribution of splash and wash to interrill sediment delivery (Figure 3.2) indicated that downslope splash dominated interrill sediment delivery under low magnitude rainfall intensities (45 mm h^{-1}) and wash dominated interrill sediment delivery under high magnitude events (135 mm h^{-1}). Regression analyses were performed with the data from 45 or 135 mm h^{-1} runs omitted. For comparison the results for 27 and 36% slopes are shown in Table 3.3. By omitting the 45 mm h^{-1} data b-values increased and the exclusion of the 135 mm h^{-1} data resulted in decreased b-values. A similar comparison was made for wash and the results (Table 3.3) indicate that omitting the 135 mm h^{-1} data tended to decrease b-values but not as significantly as those for interrill sediment delivery. This analysis confirmed the relative influence of splash and wash on changes in b-values in the power function model. Thus, it is not surprising that large variations in b-values are reported in the literature, considering the dynamic nature of splash and wash interactions under varying experimental conditions, notably different rainfall intensity, drop sizes, slope lengths and angles, soil properties, and sediment collection devices. The implication of these data is that a b-value close to 1 indicates the predominant role of raindrop impact in sediment detachment and transport. This may be either as splash or as an aiding agent for flow transport at fairly low slopes where sediment entrainment by flow shear stress is absent. On the other hand a

b-value close to or larger than 2 indicates the predominant role of a wash-driven process in sediment transport, which may be due to increased flow shear stress or "stream" power.

3.3.2 Effects of Slope Steepness

To isolate slope effects, data were subdivided into four groups according to rainfall intensity. Regression analyses were conducted assuming linear or power functions as suggested in the literature and shown by Eq. [3.3] and [3.4] (Table 3.4). Results of analyses with the WEPP slope function (Eq. [3.5]) were not included due to its lack of fit to these data (Chapter 2). Table 3.4 indicated that total splash, lateral splash, downslope splash, and wash were all positively related with slope while upslope splash decreased with increasing slope. Overall both linear and power functions were equally successful in describing slope controls on interrill splash and wash, though in a few instances one model provided a better fit than the other (Figure 3.2). McIsaac et al. (1987) also noted a similar relationship when they stated that, for slopes < 4 m in length, the slope factor was equally well described by either a linear function of percent slope, $\sin\theta$, or $\sin\theta^{0.8}$ (θ = slope angle in degree). It should be noted that these regression equations are incapable of providing physical meaning when slope is low. As indicated in Table 3.4, the intercept terms of the linear function, in some instances, were negative, and the power function essentially shows that there would be no splash and wash when slope is zero. Therefore, extrapolations to low slopes (<4%) are not encouraged. The cause of the negative intercept for downslope splash was mostly due to the cushioning effect of ponded water layers at low slopes (<9%), which resulted in a nonlinear increase in downslope splash flux as slope increased. The negative intercept for wash at 90 and 135 mm h⁻¹ intensities was caused by the rapid increase in wash transportability as slope exceeded 9% (Figure 3.2).

Table 3.4 Parameter estimates from regression analysis for slope controls on splash and wash flux E (g m⁻² h⁻¹) fitted by a linear function and a power function (obtained from log-transformed data): n = 15 for all cases except where otherwise indicated[†]

E	Rainfall Intensity (mm h ⁻¹)	Linear function E = aS + b				Power function E = aS ^b			
		a	b	r ²	SEE	a	b	r ²	SEE
Total	45	748.3	245.6	0.79	49.00	704.7	0.33	0.85	41.11
splash	65	2009	176.2	0.94	66.02	1565	0.59	0.95	68.17
	90	2351	206.2	0.82	137.3	2278	0.73	0.92	123.5
	135	3243	393.4	0.90	135.7	2660	0.56	0.88	128.7
Upslope	45	60.01	-110.8	0.53**	12.93	15.24	-0.43	0.50*	15.08
splash	65	76.77	-103.0	0.35*	17.79	32.79	-0.26	0.38*	17.10
	90	80.26	-79.78	0.24 ^{ns}	17.71	48.39	-0.13	0.12 ^{ns}	19.20
	135	178.3	-201.6	0.46**	27.48	93.88	-0.19	0.33*	31.01
Lateral	45	242.2	189.6	0.44**	34.59	337.9	0.20	0.61	29.37
splash	65	1204	119.9	0.89	52.68	966.1	0.59	0.94	49.63
	90	1227	165.0	0.70	101.9	1276	0.68	0.86	92.83
	135	1870	262.9	0.80	117.9	1642	0.56	0.80	107.3
Downslope	45	616.8	-4.192	0.97	13.98	695.0	1.11	0.97	13.42
splash	65	908.8	-20.54	0.96	19.35	1208	1.28	0.95	19.05
	90	1204	-39.23	0.93	40.33	1912	1.46	0.96	43.71
	135	1548	-47.77	0.96	37.90	1930	1.27	0.92	29.17
Wash	45	29.49	17.61	0.53**	3.463	31.17	0.16	0.46**	3.645
	65	457.2	17.20	0.81	27.75	349.9	0.72	0.87	28.11
	90	1448	-8.723	0.89	64.06	1622	1.12	0.93	63.79
	135	14835	-1003	0.68	1279	15488	1.46	0.90	1298
	135 [‡]	7850	-234.8	0.90	251.7	9134	1.26	0.89	254.6
Interrill	45	646.4	13.41	0.97	14.53	576.1	0.85	0.98	14.63
sediment	65	1366	-3.342	0.96	36.31	1314	0.99	0.97	35.38
delivery	90	2652	-47.94	0.97	61.29	3356	1.24	0.97	67.83
	135	16410	-1051	0.92	1287	17338	1.42	0.92	1287
	135 [‡]	9190	-256.7	0.92	261.6	10785	1.24	0.92	257.0

[†] All r² values are significant with P < 0.001 except where otherwise indicated by ** (P < 0.01), * (P < 0.05), and ns (not significant at α = 0.05).

[‡] n = 12 with the three data points associated with rilling at 36% slope omitted

It is interesting to note that the b -values of the power function for total splash ranged from 0.33 to 0.73 while those for downslope splash ranged from 1.11 to 1.46 (Table 3.4). This indicated that downslope splash was more sensitive to slope increase, supporting the finding of Quansah (1981) on slope effects on splash detachment and transport. Values of b for lateral splash were similar to those of total splash since lateral splash accounts for over 80% of total splash. It should be remembered that, in reality, lateral splash would be balanced from the surrounding area in the field and thus its net flux would be zero. The increase of b -values for splash with increasing rainfall intensity was not significant though b -values for 45 mm h⁻¹ events were consistently lower than those for the other intensities. For the wash component, however, b -values ranged from 0.16 for a rainfall intensity of 45 mm h⁻¹ to 1.46 for 135 mm h⁻¹. The different response of b -values for splash and wash with varying rainfall intensity indicates that slope effects on splash and wash are associated with different dynamics. For splash, the slope gradient determines the variation in depth of any ponded water, the magnitude of impacting forces, and the directional distribution of shear stress at the soil surface (Chang and Hills, 1993; Wan et al., 1996). For wash, the slope effect is related with flow shear stress or stream power, both of which are dependent on flow flux and thus on rainfall intensity. The increase in b -values for wash reflects the dependence of wash transport on the interaction of interrill flow flux and slope. At a rainfall intensity of 45 mm h⁻¹, the dependence of wash flux on slope is weak due to the limited transport capacity of overland flow. Similar observations were also reported by Sutherland et al. (1996) who found no significant difference in wash flux between slopes of 8.7% and 17.6%, using a rainfall intensity of 102 mm h⁻¹. However, the flow flux was only slightly larger than that resulting from the 45 mm h⁻¹ runs in this study. The implication of the weak response of wash to slope increase with low flow flux is that it is desirable to include a

critical flow flux in the modeling of interrill wash transport. The large b-values of the 135 mm h⁻¹ rainfall intensity reflects the effect of rill initiation at 36% slope. Exclusion of these data significantly improves the results of regression, particularly for the linear function.

The relative contribution of downslope splash and wash to interrill sediment delivery is shown in the regression equations in Table 3.4. The additive nature of the two components is apparent from the linear function. For the power function, this effect on b-values is similar to that of rainfall intensity. For instance, a comparison of b-values for downslope splash, wash, and interrill sediment delivery at 45 mm h⁻¹ rainfall intensity again indicated that downslope splash dominated interrill sediment delivery under this low flow condition (Figure 3.2).

3.3.3 Interrill erodibility: Splashability and washability

The erodibility factor in many erosion equations has been traditionally defined as a fitting parameter (Nearing et al., 1990). Previous analyses (Tables 3.2 and 3.3) indicated that values of a and b in Eq. [3.1] changed with slope in opposite directions. This complicated the task in defining a "universal" erodibility factor, though treating the coefficient 'a' as an erodibility factor using Eq. [3.1] exists in the literature (e.g. Rose, 1985). It is instructive to consider the interaction between rainfall intensity and slope as shown in Eq. [3.2]. The first attempt to examine this interaction was to conduct a regression analysis using the data obtained from all rainfall intensities and slopes (n = 60 for all splash components and n = 57 for wash and interrill sediment delivery, excluding the runs when rilling occurred) to fit the power function model for all the independent variables, i.e., I for splash, IQ for wash and interrill sediment delivery, and S for all components. The following regression equations were obtained for these components:

$$E_{ts} = 53.29 I^{0.78} S^{0.55} \quad r^2 = 0.90, \text{ SEE} = 110.93 \quad [3.8]$$

$$E_{ls} = 32.90 I^{0.76} S^{0.50} \quad r^2 = 0.83, \text{ SEE} = 85.62 \quad [3.9]$$

$$E_{us} = 0.24 I^{1.17} S^{-0.25} \quad r^2 = 0.73, \text{ SEE} = 24.70 \quad [3.10]$$

$$E_{ds} = 90.16 I^{0.61} S^{1.27} \quad r^2 = 0.95, \text{ SEE} = 30.83 \quad [3.11]$$

$$E_w = 0.02 (IQ)^{1.27} S^{0.75} \quad r^2 = 0.91, \text{ SEE} = 248.38 \quad [3.12]$$

$$E_i = 3.68 (IQ)^{0.76} S^{1.03} \quad r^2 = 0.94, \text{ SEE} = 242.26 \quad [3.13]$$

where E_{ts} , E_{ls} , E_{us} , E_{ds} , E_w , and E_i represent fluxes of total splash, lateral splash, upslope splash, downslope splash, wash, and interrill sediment delivery ($\text{g m}^{-2} \text{h}^{-1}$), respectively. These equations (all significant with $P < 0.001$) delineate the interactive controls of rainfall intensity and slope on sediment fluxes of various splash and wash components. However, a truly "inherent" erodibility factor is still not well defined by any of these relationships since the exponent for the erosivity term varied with erosional components. Therefore, a second attempt was made to standardize the erosivity term.

For splash components, using I as the erosivity term is justified by data in Table 3.2 and research presented in the literature (e.g. Proffitt et al., 1991; Sharma et al., 1993). Here only total splash and downslope splash were analyzed as examples. For total splash, a linear function of S (Table 3.4) was applied to provide physical meaning at zero slope, thus:

$$E_{ts} = 23.33 I (S + 0.14) \quad r^2 = 0.90, \text{ SEE} = 113.07 \quad [3.14]$$

Both the regression coefficient and the S intercept are significant with $P < 0.001$.

For downslope splash, the slope factor in Eq. [3.11] is considered to be appropriate and retained:

$$E_{ds} = 11.31 IS^{1.27} \quad r^2 = 0.95, \text{ SEE} = 33.94, P < 0.001 \quad [3.15]$$

Note that the fitted erodibility term in Eq. [8.14] is larger than that in Eq. [3.15]. This is more reasonable than what is shown in Eq. [3.8] and [3.11] since total splash is often considered as a surrogate of total raindrop detachment (Bradford and Huang, 1993; Parsons et al., 1994) while downslope splash is only a part of sediment transport.

For the wash component, a linear term of $I(Q - Q_{cr})S$, where Q_{cr} is the critical flow flux for significant response of wash transport with change of slope, is proposed to be the erosivity factor for rainfall impacted flow. The slope S is included in the erosivity term to show its influence on flow depth and velocity, and thus on flow shear stress or “stream” power. Regression analyses of these wash flux data resulted in:

$$E_w = 0.59 I(Q - 17.93)S \quad r^2 = 0.86, \text{ SEE} = 152.05, P < 0.001 \quad [3.16]$$

It is important to note that the erodibility factors in Eq. [3.15] and [3.16] are different in both quantity and dimensions. The fundamental difference was that downslope splash is driven by raindrop impact and wash is driven by the interaction of raindrop impact and the tractive force of the flow. The former is, therefore, defined as splashability, an intrinsic soil parameter describing soil resistance to splash by raindrop impact, and the later washability, an intrinsic soil parameter describing soil resistance to wash by raindrop impacted interrill

flow. These terms are useful descriptors and are helpful in understanding the basic processes involved in interrill erosion.

For interrill sediment delivery, IQ was used as the erosivity term to indicate the combined effects of raindrops and interrill flow on splash and wash transport. The best-fit regression equation is:

$$E_i = 0.63 (IQ) S^{1.15} \quad r^2 = 0.92, \text{ SEE} = 151.83, P < 0.001 \quad [3.17]$$

In this equation Q_{cr} was not necessary since the contribution from downslope splash correlates strongly with slope even when flow flux was low. The predicted values of total splash, downslope splash, wash and interrill sediment delivery fluxes using Eq. [3.14], [3.15], [3.16], and [3.17] were plotted against measured values in Figure 3.3. It was indicated that the measured sediment flux data fit Eq. [3.14] through [3.17] reasonably well. However, it is necessary to note that logarithmic scales were used in Figure 3.3C&D and thus variations at high slopes (>27%) and rainfall intensity (135 mm h⁻¹) were compressed.

It should be noted that the interrill erodibility term in Eq. [3.17] has the same dimensions as washability. However, it is essentially a dynamic combination of splashability and washability. Using K_s , K_w , and K_i to represent splashability, washability and interrill erodibility and combining Eq. [3.15], [3.16], and [3.17], thus:

$$K_i = \frac{K_s S^{0.12}}{Q} + \frac{K_w (1 - Q_{cr}/Q)}{S^{0.15}} \quad [3.18]$$

It is clearly shown that the relative contribution of K_s and K_w to K_i depends on S and Q. When S was held constant, the contribution of K_s to K_i decreased with increasing Q and

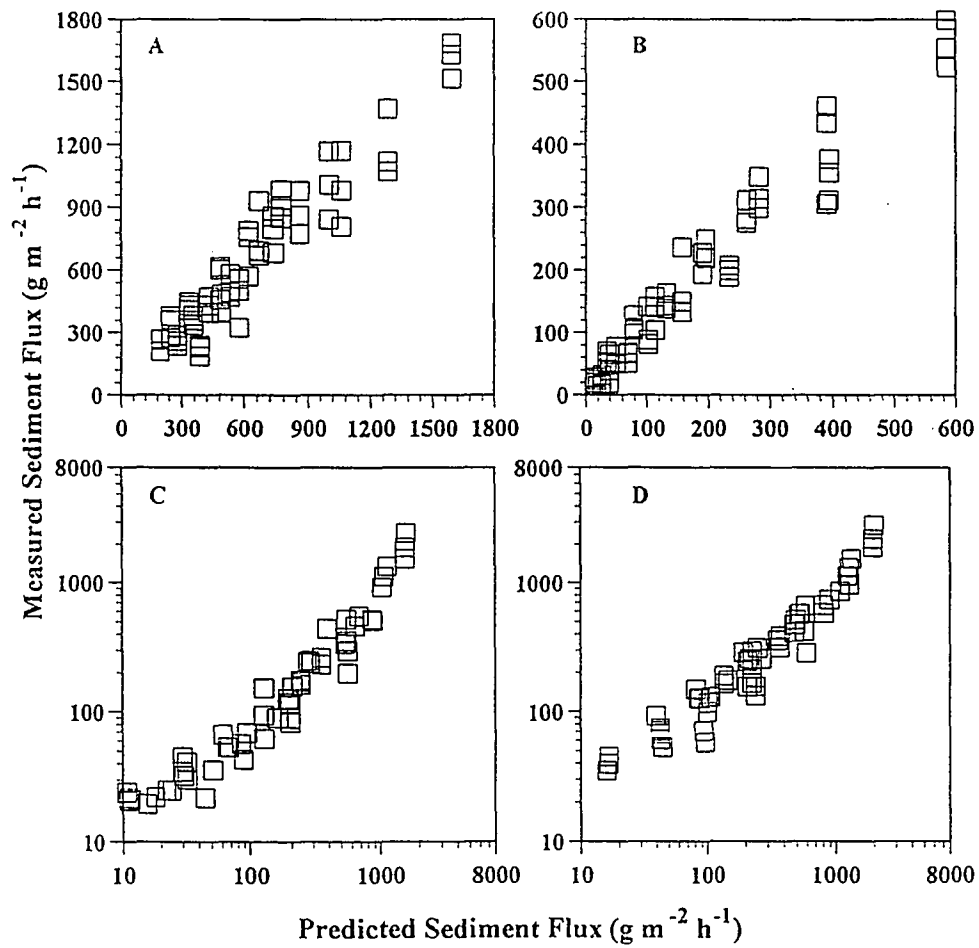


Figure 3.3. Measured sediment flux and predicted flux using Eq. [3.14] for total splash (A), Eq. [3.15] for downslope splash (B), Eq. [3.16] for wash (C), and Eq. [3.17] for interrill sediment delivery (D).

that from K_w increased with increasing Q . When Q was held constant, the contribution of K_w increased with decreasing S and that from K_s increased with increasing S . This analysis agrees with the experimental observations about the relative contribution of wash and splash to sediment delivery. Figure 3.2. indicated that splash dominated sediment transport under high slope and low flow flux conditions (45 and 65 mm h⁻¹ runs) and wash dominated sediment transport under high flow flux (95 and 135 mm h⁻¹ runs at all slopes) and low slope conditions (65 mm h⁻¹ runs at 4 and 9% slopes). Therefore, interrill erodibility can be either dominated by splashability or washability, depending on slopes and runoff conditions. This may partially explain the significant differences in the WEPP interrill erodibility values measured with "flat" plots and "ridged" plots (Kinnell, 1993a). Although partitioning of sediment transport by splash and wash was not attempted during the WEPP interrill erodibility measurements, it can reasonably be assumed that wash dominated sediment transport at low slopes (4-6%) with "flat" plots, and splash would play a more important role in sediment transport at high slopes (>30%) with "ridged" plots. The lumped nature of interrill erodibility may also be partially responsible for the difficulties encountered in relating measured soil properties with interrill erodibility. While the present study does not allow for comparisons of splashability and washability between soils, information available in the literature does suggest that a soil with high splashability may not necessarily have high washability (Bollinne, 1978; De Ploey and Mucher, 1981; Parsons et al., 1994). Further experimental study is required to confirm this point.

3.4 Conclusions

With the interrill splash and wash partitioning system, it was found that the power function model, $E = aI^b$, well quantified the rainfall intensity effects on sediment fluxes from all splash and wash components studied. Values of b in this equation increased with increasing slope for all the splash and wash components due to the interaction between rainfall intensity and slope. However, b -values for splash were close to 1 and for wash were well above 2, indicating the different dynamics for the two processes. Therefore, it should be realized that I (rainfall intensity), in splash equations, is a surrogate for rainfall kinetic energy, and in wash equations, is endowed with the physical meaning of the interaction between raindrop kinetic energy and interrill flow flux. To be more process-based, Kinnell (1993b) suggested using IQ , and Sharma et al. (1995) proposed $I(E-E_0)$, where E and E_0 (dimensions of $J\ m^{-2}\ mm^{-1}$) are rainfall kinetic energy and the threshold kinetic energy for raindrop detachment, to replace the erosivity term I^2 in the WEPP model. Apparently, a more fundamental erosivity term would be to combine kinetic energy and flow flux. This is particularly true when data obtained from simulated rainfall are extrapolated to natural rainfall conditions or when data with different raindrop sizes and soil characteristics are compared.

This study also indicated that slope controls on interrill splash and wash dynamics were well described by either a linear function or a power function, both showing a monotonic increase with increasing slope except for the upslope splash component. The data set obtained in this study does not fit the slope function factor presently used in the WEPP model. This is partially due to the well-aggregated nature of the soil studied.

Since interrill sediment delivery was partitioned into downslope splash and wash components, the additive or lumped effects of the two components were investigated. By differentiating the erosivity factors between splash and wash, it was found that interrill erodibility was essentially a dynamic combination of splashability and washability. Thus, the measured interrill erodibility depends, in part, on the processes, i.e., splash or wash, controlling sediment delivery under specific environmental conditions. The splashability can be comparable to any other erodibility indexes obtained solely from raindrop impact such as rainfall detachability in the model of Rose (1985; 1993). The washability can be transferable to runoff related erodibility parameters such as the K-factor in the USLE model or the rill erodibility factor in the WEPP Model which was studied Chapter 4.

CHAPTER 4
INFLUENCE OF PLASTIC MULCH AND FLOW HYDRAULIC REGIMES ON
RUNOFF GENERATION AND RILL EROSION

Abstract

Field rainfall simulation and added inflow experiments were conducted on a well-aggregated Oxisol commonly used in Hawaii for pineapple production. Four treatments were no cover (hereafter called bare), plastic mulch as the sole cover (plastic), pineapple crowns as the sole cover (crown), and both plastic and crowns as covers (plastic-crown). The average slope of these plots was 4.2% and all were shaped into ridge-and-furrow configurations. For each of the treatments, three successive storms were imposed: a "dry run" with an intensity of 35 mm h⁻¹ on the initially dry soil, a "wet run" with the same intensity on the following day; this was followed immediately by a "very wet run" with an intensity of 62 mm h⁻¹. Runoff was measured and sampled every 5 to 10 minutes until a steady state was reached and then flow velocity and width were measured. A series of inflows was introduced into the rill (furrow) from the top of the plots after rainfall simulation and similar out-flow measurements were made.

Compared to bare conditions, plastic mulch substantially accelerated runoff generation and soil erosion due to its impervious nature. The simultaneous presence of plastic mulch and pineapple crowns, however, tended to retard runoff generation and decrease soil erosion. For all the storms, runoff and erosion rates in the plastic-crown plot were smaller than those of the bare plot and the crown plot. Visual observations during the simulated storms indicated that rainfall intercepted over the plastic mulch was funneled into the ground through holes in the mulch where the crowns were planted. Plots without plastic

mulch displayed soil surface sealing which impeded infiltration. The data combining simulated rainfall and added inflow showed that a critical Reynolds number (Re) of 1000 distinguished laminar or quasi-laminar regimes from turbulent regimes. The rill erodibility and critical shear stress obtained for $Re > 1000$ were significantly larger than those for $Re < 1000$ due to more vigorous flow detachment under turbulent regimes.

4.1 Introduction

On a hillslope, rill erosion may occur either in randomly distributed rills produced by overland flow concentration and channelization, or in artificially defined rills which are formed by agricultural operations such as tillage. The furrow of the ridge-and-furrow system, commonly practiced for cultivation of row crops, is a typical example of artificially defined rills. In such an agriculturally managed system, runoff in the ridge (interrill) area is delivered laterally into the furrow (rill), producing concentrated flow (rill flow). This concentrated flow possesses higher erosive power than unconcentrated flow under the same slope and rainfall conditions, and serves as the primary vector for sediment transport. For a given ridge-and-furrow system, rill erosion is largely determined by flow rate, which, in turn, depends on rainfall intensity, antecedent soil moisture content, and the plantation practices applied in the system. In Hawaii, the ridge-and-furrow system is typically used for pineapple culture, and plastic mulching over the ridge area has been a common practice for several reasons, including nematode control. However, the effect of plastic mulch on the dynamics of runoff generation and soil erosion are poorly understood and not covered in available literature. Hypotheses for the mulch effect range from acting as a protective barrier on one extreme to acting as a "water shedding", runoff-inducing impervious surface

on the other. It is clear that a quantitative understanding of the role of plastic mulch requires empirical experimentation. Therefore, the first objective of this study was to assess the effect of plastic mulch on runoff generation and soil loss under varying antecedent soil moisture contents and rainfall intensities.

At the process level, rill erosion is conceptualized as the detachment and transport of sediment solely by concentrated overland flow. The driving force of this process is commonly recognized to be the mutual shear stress developed at the interface between rill flow and the soil surface, which is given as:

$$\tau = \rho g S R \quad [4.1]$$

where τ = average flow shear stress acting on soil surface (Pa), ρ = density of water (kg m⁻³), g = acceleration of gravity (m s⁻²), S = slope (m m⁻¹), and R = hydraulic radius of the flow (m), which is defined as:

$$R = A/P \quad [4.2]$$

where A = cross-sectional flow area (m²), and P = wetted perimeter (m). For a rectangular flow with width W (m) and depth D (m), then:

$$R = DW/(W+2D) \quad [4.3]$$

The WEPP model relates rill flow detachment linearly to the excess flow shear stress:

$$D_c = K_r(\tau - \tau_c) \quad [4.4]$$

where D_c = rill flow detachment capacity ($\text{kg s}^{-1} \text{m}^{-2}$), K_r = soil rill erodibility (s m^{-1}), τ = defined as above, and τ_c = critical shear stress for soil detachment to be overcome by flow (Pa). The two soil parameters: K_r and τ_c in Eq. [4.4] have been experimentally determined by a procedure developed by Laflen et al. (1987). The method employed initial rainfall simulation followed by adding clear water inflow at varying discharge rates to the upper end of a preformed rill, which was similar to a ridge-and-furrow system, and making flow measurements within the rill to calculate the shear stress exerted at each flow rate. One assumption implicitly underlying Eq. [4.4] and the rill erodibility measurement method is that K_r and τ_c are constant (purely intrinsic soil parameters) for a given soil and are independent of flow discharge rate and thus flow hydraulic regimes. During a measurement of K_r and τ_c in the field, the hydraulic regimes involved may cover both laminar and turbulent flows. The effects of flow hydraulic regimes on flow detachment are not well documented in the literature, and examination of their dynamics and effects was the second objective of this study.

4.2 Flow Hydraulic Regimes and Resistance

Flow hydraulic regimes i.e., laminar or turbulent, are defined by a dimensionless parameter, Reynolds number (Re), which is given as:

$$Re = VR/\nu \quad [4.5]$$

where V = mean flow velocity (m s^{-1}), ν = water kinematic viscosity at a given temperature ($\text{m}^2 \text{s}^{-1}$), and R = defined as above. For overland flow, the critical Re value to differentiate laminar and turbulent flows is not well defined. A range from 1000 to 2440 has been proposed in the literature (Savat, 1978; 1980). One approach to determine flow regimes is to relate Re with the resistance of the solid surface to overland flow. One of the most widely used flow resistance equations is the Darcy-Weisbach equation (Savat, 1980; Gilley and Kottwitz, 1993; Abrahams et al., 1994), which is defined as:

$$f = 8gSR/V^2 \quad [4.6]$$

where f = Darcy-Weisbach roughness coefficient, which is a dimensionless parameter, and g , S , R , V = defined as above. According to the f - Re relationship developed for pipe flow (the Moody diagram) and for overland flow (Savat, 1980; Abrahams et al., 1994), three f - Re relationships are identified: (i) f decreases in an inversely proportional manner to Re under laminar flow regimes according to:

$$f = K/Re \quad [4.7]$$

where K = constant; (ii) f decreases slightly with increasing Re under smooth turbulent flow regimes where a laminar sublayer covers the solid surface roughness and this can be described as (Savat, 1980):

$$f = k/Re^{0.25} \quad [4.8]$$

where k = constant for a given solid surface; and (iii) f is independent of Re under rough turbulent regimes since the surface roughness protrudes through the laminar sublayer into the turbulent region and causes additional flow mixing. Most turbulent flows in open channel are presumed to be in rough turbulent regimes.

4.3 Materials and Methods

Field rainfall simulation experiments were conducted on the Wahiawa silty clay soil (a Rhodic Eutrostoxx) at the Poamoho Experimental Station on the island of Oahu, Hawaii (Selected soil properties are shown in Table 2.1). Prior to rainfall simulation, the field site was disked and smoothed with a rototiller to simulate conventional seed-bed conditions and to minimize soil spatial variability. The plots prepared for rainfall simulation consisted of two 8.5 m long and 0.6 m wide ridges with a 0.6 m wide and 0.15 m deep triangular furrow in between. A plastic border was inserted in the center of each ridge, leaving about 0.03 m above the soil surface as the drainage divide. The average furrow slope was 4.2 %. The ridge sideslope was not uniform with the top half fairly level and bottom steep, resulting in an average of about 30%. This plot setup was prepared to mimic the ridge-and-furrow system used for pineapple culture in Hawaii. Since the ridge-and-furrow configuration is uniform in the field, the plot set-up described above is representative of a hydrological unit in the field. A total of four plots were prepared, representing four different treatments: a control plot with the bare soil (hereafter called bare), a plot with plastic mulch as the sole cover (plastic), a plot with the pineapple crowns as the sole cover (crown), and a plot with plastic mulch and crowns as the cover (plastic-crown). For plots with plastic mulch, a standard plastic sheet (60 cm wide), which is commercially available for pineapple culture,

was laid over the bed and the edges were covered with soil, providing about 45% coverage for the ridge area. The crowns were planted by insertion through the plastic according to the marks in the sheet. The areal coverage of the pineapple crowns in the plot was about 20%. The plot set-up for the plastic-crown treatment, as an example, is shown in Figure 4.1.

A programmable rainfall simulator based on the design of Foster et al. (1982) was used (Figure 4.1). Raindrops were emitted through six oscillating V-jet spray nozzles from low line pressure (6.9×10^4 Pa). The median drop diameter of simulated rainfall was 2.2 mm. Rain fell from a height of 3 m above the soil surface resulting in a kinetic energy flux of $20 \text{ J m}^{-2} \text{ mm}^{-1}$ of rainfall. Domestic water supply with an average temperature of $25 \text{ }^\circ\text{C}$ was used. Wind effects were minimized by use of a wind shield around the rainfall simulator. For each of the plots, three rainfall events were simulated. The first storm (dry run) was applied at the soil moisture condition prevailing at the time (about 20% for top soil) with a rainfall intensity of 35 mm h^{-1} . The second storm (wet run) with the same rainfall intensity was imposed on the following day to simulate wet antecedent soil water conditions and to determine the influence of surface sealing or compaction on runoff generation. The third storm (very wet run) was applied following the wet run and had a rainfall intensity of about 62 mm h^{-1} . For each of the runs, time to runoff initiation was recorded. Runoff rate was volumetrically measured and sampled every 5 to 10 min for sediment concentration determination until a steady state was reached. This steady state was deemed present when runoff discharge rate did not change with time. This took 3-5 h for the dry runs. For the wet and very wet runs, the steady state was reached within 30 min, but the rainfall was extended for about 1 h. Three measurements of rill flow width and velocity were made within the furrow at 1, 2, and 3 m upslope from the sampling outlet. A fluorescent dye was



Figure 4.1 Plot setup for the plastic-crown treatment (a) and the rainfall simulator (b).

used for flow velocity measurement (Abrahams et al., 1986; Gilley et al., 1990) and a mm-scale ruler was used to determine flow width.

After the very wet run was completed, inflow was added at the top of each plot. A total of 10 inflow rates ranging from 10 to 100 L min⁻¹ were used, with each plot receiving only two or three different rates. Such a limited number of inflow rates was applied for each plot to avoid possible exposure of the non-erodible sublayer. For each inflow rate, three measurements of flow rate, flow width, and flow velocity were conducted as were done for the rainfall simulation, and three runoff samples were taken for determination of sediment concentration.

4.4 Results and Discussion

4.4.1 Runoff generation and runoff rate

The plastic mulch and antecedent soil moisture conditions significantly influenced runoff generation (Table 4.1). For the dry run, runoff was initiated about 75 min after rainfall started on the bare control plot. Visual observations indicated that the ridge area generated a thin layer of overland flow which laterally drained into the furrow, and contributed to rill flow. This thin sheet flow was an essential component of runoff generated in the plot. For the plastic mulch plot, runoff was generated about 50 min after rainfall started due to the impermeable nature of the plastic mulch. Intercepted rain formed ponds on the plastic mulch. However, under continuous raindrop impact, the ponds broke and water flowed into the furrow. Unlike the continuous sheet overland flow on the bare plot, runoff from the interrill area was channelled into the furrow through a system of small rills. For the crown plot, runoff was not generated until 120 min after rainfall started. Reasons for this delayed

runoff initiation include rainfall interception by crowns which also efficiently slowed down sheet flow into the furrow and prevented soil surface from sealing. For the plastic-crown plot, no runoff was generated until 210 min after rainfall started. Visual observations indicated that each crown formed a tiny basin and ponded water in the plastic sheet was funnelled into the hole where the crowns were planted. For the wet run and very wet run, however time to runoff generation was similar and short for all the treatments (1-5 min), and thus the difference between treatments was limited.

Table 4.1 Time to runoff initiation in simulated storms

Treatment	Dry Run	Wet Run	Very Wet Run
	<----- min ----->		
Bare	75	3.0	2.5
Plastic	57	5.1	0.8
Crown	120	4.2	0.7
Plastic-crown	210	3.9	1.5

The effect of plastic mulch on runoff generation under dry conditions has significant implications from a management perspective since low intensity events occur more frequently than high intensity events. Rainfall infiltrates through the plastic-crown interfaces is stored in the soil profile and is thus available for post-rain plant growth. The time required to reach steady state after runoff initiation for the plastic-crown plot was about 40 min while that for the other treatments ranged from 1 to 2 h (Figure 4.2). This suggested that before runoff initiation a more uniform soil moisture distribution existed in the soil with the plastic-crown treatment than with other treatments.

The presence of plastic mulch also influenced runoff rate. Table 4.2 shows the steady state runoff rates and runoff coefficients (ROC). The runoff coefficient is defined as

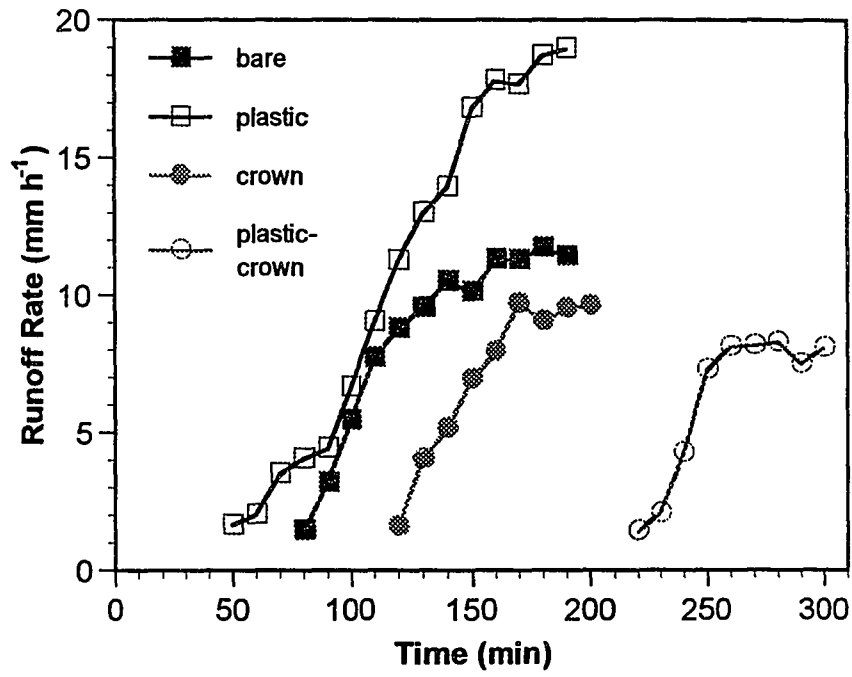


Figure 4.2 Change of runoff rate with time during the dry run (rainfall intensity = 35 mm h⁻¹)

the percentage of rainfall converted into overland flow during an event. As expected, the plastic mulch plot had the highest ROC value, with mean steady runoff rates ranging from about 19 mm h⁻¹ for the dry run to 47 mm h⁻¹ for the very wet run. The bare plot and the crown plot had similar runoff rates and ROC values, indicating that the limited crown cover was not effective in preventing surface sealing. The plastic-crown plot had consistently lower runoff rates and ROC values when compared to other treatments for all the runs. This was mostly because surface soil covered by plastic mulch

Table 4.2 Treatment effects on steady state runoff rates and runoff coefficients.

Treatment	Dry Run	Wet Run	Very Wet Run
	<-----Steady Runoff Rate (mm h ⁻¹)†----->		
Bare	11.45(0.19)	13.56(0.40)	37.24(0.45)
Plastic	18.43(0.56)	19.89(0.21)	47.12(0.15)
Crown	9.382(0.25)	13.99(0.34)	37.37(0.26)
Plastic-crown	8.271(0.34)	11.65(0.23)	31.67(0.43)
	<-----Runoff Coefficient (%)‡----->		
Bare	15.40	38.26	57.32
Plastic	23.95	48.83	74.10
Crown	9.534	39.11	57.50
Plastic-crown	5.432	26.96	48.35

† Mean of the final three measurements with standard deviation (SD) in parentheses.

‡ Rainfall duration was 300 min for the plastic-crown plot and 190 min for other plots during the dry run, and 60 min for all the plots during the wet and very wet runs.

was protected from raindrop impact, and thus maintained a higher infiltration capacity than the bare or crown plots. Bulk density measurements in five locations within the plot after rainfall simulation indicated that the mean bulk density of surface soil covered by plastic mulch (1.01 kg m⁻³) was significantly smaller ($P < 0.01$ with a t test) than that of surface soil without this cover (1.17 kg m⁻³). This suggested that surface compaction and sealing

was induced by rainfall impact as were found by Sutherland et al. (1996) in a laboratory study. This compaction and sealing effect may also be partially responsible for the slightly higher runoff rates for the wet run in comparison with that of the dry run as indicated in Table 4.2.

4.4.2 Soil loss and sediment concentration

Table 4.3 shows steady state sediment concentrations and soil loss rates. The plastic mulch plot always produced the highest sediment concentrations and soil loss rates due to its high runoff rates and thus larger erosive power. For the other three treatments, differences in sediment concentration for the same storm sequence were relatively small in comparison with those between runs. Soil loss rates were therefore mainly controlled by runoff rates: i.e., the plastic-crown plot always displayed smaller soil loss rates than the bare or the crown plots.

Table 4.3 Treatment effects on steady state sediment concentrations and soil loss rates[†]

Treatment	Dry Run	Wet Run	Very Wet Run
	<-----Sediment concentration (g L ⁻¹) ----->		
Bare	1.69(0.02)	2.65(0.38)	12.46(0.85)
Plastic	2.44(0.11)	5.07(0.46)	13.87(0.66)
Crown	1.80(0.19)	2.69(0.12)	10.22(0.19)
Plastic-crown	1.45(0.10)	1.66(0.07)	9.25(0.78)
	<-----Soil loss rate (g m ⁻² h ⁻¹) ----->		
Bare	19.41(0.08)	36.13(4.85)	462.1(27.7)
Plastic	44.99(3.37)	95.68(7.44)	653.2(25.4)
Crown	16.97(2.14)	37.34(1.26)	389.2(13.7)
Plastic-crown	12.08(1.66)	17.20(1.76)	292.8(23.7)

[†] Mean of the final three measurements with SD in parentheses.

It is well known that detached sediment is entrained more easily by flow than undetached soil due to greater cohesion between the undetached soil particles (Rose, 1993). Under the experimental conditions, interrill erosion in the ridge area delivered sediment into the furrow bottom for further detachment and transport by rill flow. Thus the plastic mulch acted as a non-erodible soil cover in terms of interrill erosion. The amount of sediment delivered into the furrow for plots with plastic mulch should be correspondingly less than the plots without plastic mulch given similar flow discharge conditions. The estimated sediment delivery rates for the bare plot using the interrill erosion model obtained in Chapter 3 (Eq. [3.17]) were 63, 74, and 361 g m⁻² h⁻¹, respectively for the dry, wet, and very wet runs. According to the coverage provided by plastic mulch and crowns, the interrill sediment delivery rates were at most 50% of the above estimates for the plastic-crown plot and 80% for the crown plot. Comparing these estimated interrill sediment delivery rates with soil loss rates in Table 4.3, it can be well assumed that the amount of sediment delivered by interrill erosion exceeded rill flow detachment capacity during the dry run and wet run but was below flow detachment capacity during the very wet run. This assumption can be further confirmed by the data in Figure 4.3 in which sediment concentration is plotted against time for the crown and plastic-crown plots. It shows that sediment concentration during the dry and wet runs was low, ranging between 1.5-3.0 g L⁻¹ and the temporal variation during a run was limited. However, for the very wet runs sediment concentration declined with time initially, and reached a constant value of about 10 g L⁻¹. This temporal variation during the very wet runs probably resulted from an initial entrainment and transport of deposited sediment from previous runs and a following detachment of in-situ soil after the deposited sediment was depleted. The relationship between flow hydraulic shear and flow detachment will be further examined in the next section.

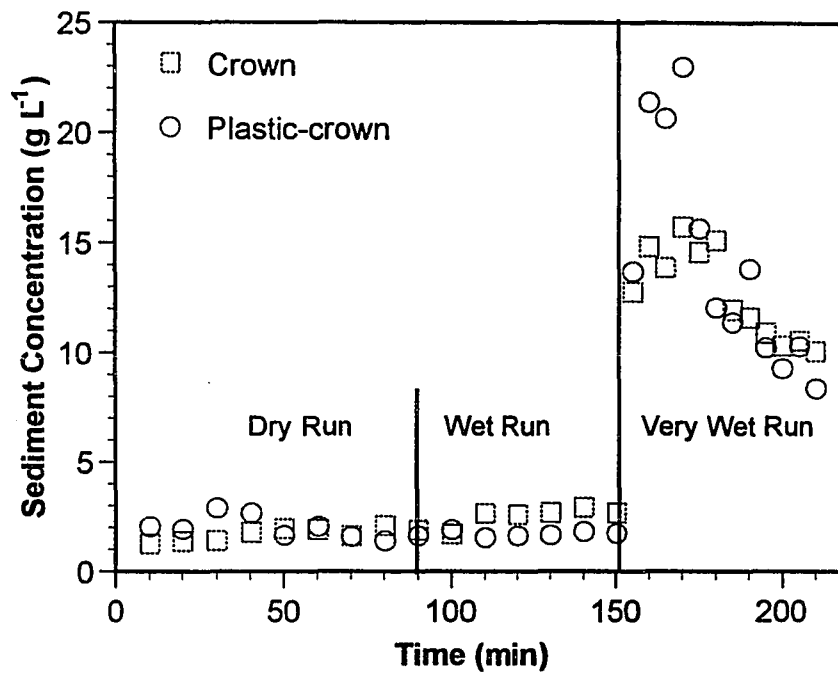


Figure 4.3 Change in sediment concentration with time during rainfall simulation

4.4.3 Flow hydraulic regimes and rill detachment

The steady state flows from rainfall simulation and from added inflows for all plots were combined in this analysis. This provided Re values ranging from 200 to 6000, and ensured that both laminar and turbulent regimes were covered. To determine the critical Re value, f was plotted against Re as shown in Figure 4.4. It was noted that f initially decreased with increasing Re. As Re exceeded 1000, the change in f with increasing Re was not significant. Thus the f -Re relationship can be described with the following equations:

$$f = 415.8/Re \quad r^2 = 0.61, n = 39, P < 0.001, Re < 1000 \quad [4.9]$$

$$f = 0.28 \pm 0.09 \text{ (mean } \pm \text{ SD)}, n = 27, Re > 1000 \quad [4.10]$$

These f -Re relationships indicate that 1000 was the critical Re value differentiating laminar or quasi-laminar flow (including transitional regimes from fully laminar to turbulent) from turbulent flows under the conditions of these experiments.

Figure 4.5 shows the increase of flow detachment capacity, expressed as soil loss per unit rill flow area per unit time ($\text{g m}^{-2} \text{ s}^{-1}$), with the increase in Re. This increase was best described by a power function (exponent = 2.18), showing that more vigorous flow detachment occurred in the turbulent flow regimes than in the laminar flow regimes. Similar observations have also been made by Nearing and Parker (1994) in a controlled flume study. The change of flow detachment with flow hydraulic regimes was mostly associated with the different shearing actions under laminar and turbulent conditions. Laminar flows are characterized by fluid particles moving along distinct and smooth layers with no flow mixing. Thus shearing in laminar flows can be visualized as a purely frictional action between adjacent fluid layers. Turbulent flows, in contrast, incorporate mixing actions, and

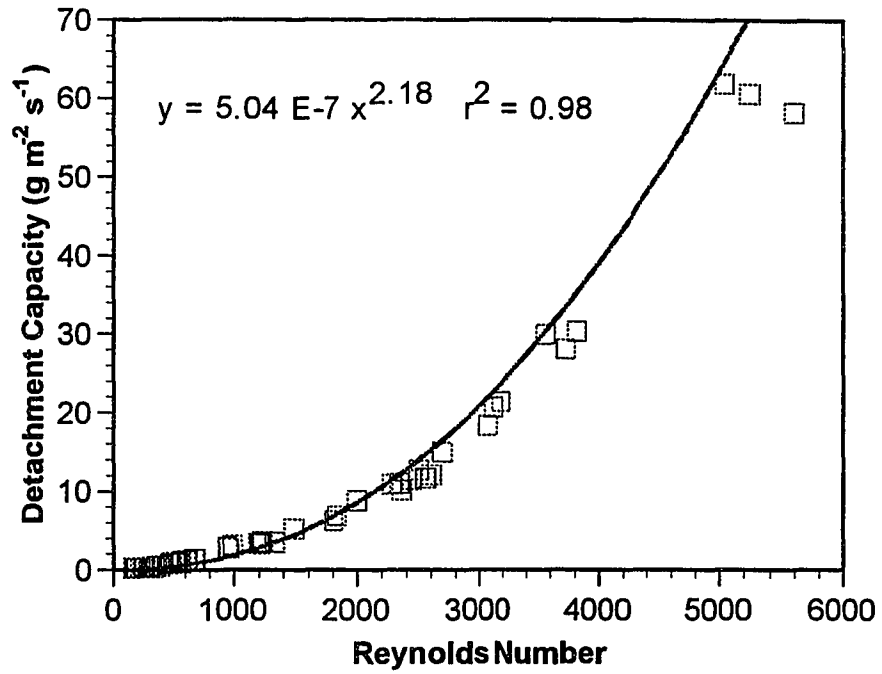


Figure 4.5 Flow detachment capacity versus flow Reynolds number. Data from simulated rainfall and inflows were combined (n = 66).

fluid motions are irregular and involved with fluctuations in velocity and direction. Thus shearing in turbulent flows is associated with mixing actions (called turbulent bursts) and is highly localized. The localized shear stress associated with burst events was estimated to be approximately 150 times greater than the average shear stress of flow (Nearing, 1991).

To determine the relationship between flow detachment and mean flow shear stress under different flow regimes, the data were divided into two groups: $Re < 1000$ and $Re > 1000$. Figure 4.6 shows flow detachment capacity plotted against flow shear stress. Linear regression analyses were conducted separately for these two groups of data to fit Eq. [4.4]. The following relationships were obtained:

$$D_c = 1.12 (\tau - 1.18) \quad r^2 = 0.90, n = 39, P < 0.001, Re < 1000 \quad [4.11]$$

$$D_c = 17.8 (\tau - 2.31) \quad r^2 = 0.84, n = 27, P < 0.001, Re > 1000 \quad [4.12]$$

It was indicated that the rill erodibility K_r and the critical shear stress τ_c for $Re < 1000$ were both smaller than these for $Re > 1000$. This difference was again mostly because the shear stress calculated with Eq. [4.1] was the mean flow shear stress which tended to underestimate the actual shear stress of turbulent flow. If, however, this mean shear stress is to be used in rill erosion modeling, it seems reasonable to determine the rill erodibility K_r and the critical shear stress τ_c separately for laminar and turbulent flows, and this is currently not addressed in the WEPP model. The WEPP model has the capacity to predict overland flow hydraulics (Lane and Nearing, 1989). However, it is not linked with the erosion component in terms of flow detachment modeling. Other alternatives to account for the increased flow detachment under turbulent regimes are to use a power function

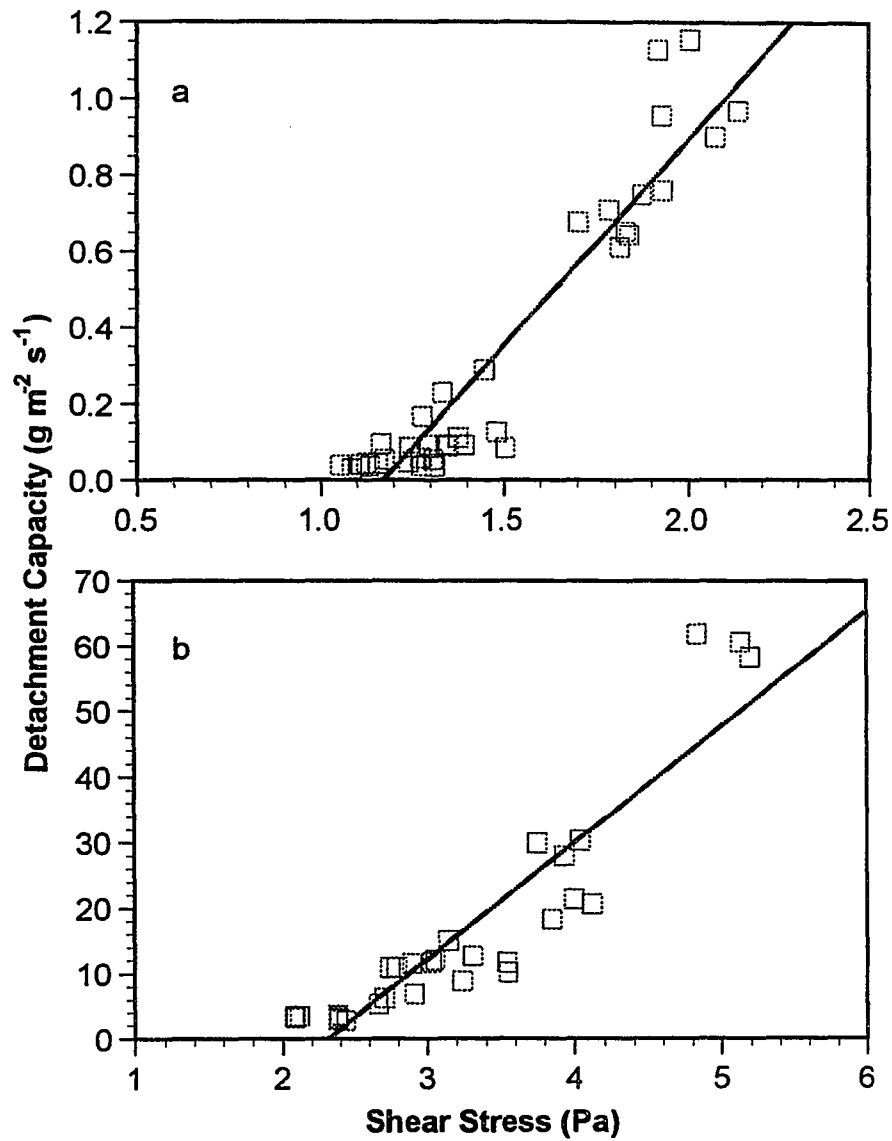


Figure 4.6 Flow detachment capacity versus shear stress for $Re < 1000$ (a) and $Re > 1000$ (b). Note scale difference.

model of Eq. [4.4] as suggested by Meyer (1964) or to apply a probabilistic model proposed by Nearing (1991).

Noting the pronounced flow detachment under turbulent flow regimes also has important implications in erosion control. It is apparent that when only a limited amount of residue mulch is to be applied, the most effective approach is to apply it in areas where flows are more likely to be turbulent. The downslope area of long and steep slopes is typically suited for the development of turbulent flows.

4.5 Conclusions

Plastic mulch substantially accelerates runoff generation and soil erosion due to its impervious nature. The simultaneous presence of plastic mulch and pineapple crowns, however, tended to retard runoff generation and decrease soil erosion. For all the storms, runoff and erosion rates for the plastic-crown treatment were smaller than those from the bare or the crown treatments. Plots without plastic mulch displayed soil surface sealing which impeded infiltration. The practical implication of this finding is that the plastic mulch used in Hawaiian pineapple plantations may not necessarily increase runoff and soil erosion as was commonly believed. However, this study was conducted on a relative mild slope and results can not be easily extrapolated to steeper slopes.

The data combining simulated rainfall and added inflow showed that a critical Reynolds number of 1000 distinguished laminar or quasi-laminar flows from turbulent flows. The rill erodibility and critical shear stress obtained for turbulent regimes were both larger than for laminar regimes due to more vigorous flow detachment caused by flow mixing under turbulent regimes. The implication of this finding was that alternative approaches for

rill erosion modeling are required to successfully account for flow detachment under both laminar and turbulent flow regimes, especially on well-aggregated soils.

CHAPTER 5
SIZE CHARACTERISTICS OF INTERRILL SPLASH AND WASH SEDIMENTS
OVER A RANGE OF RAINFALL INTENSITIES AND SLOPE ANGLES

Abstract

Simultaneous measurements were made of the sediment aggregate size distribution of interrill directional splash and wash from an Oxisol at 4, 9, 18, 27, and 36% slopes under simulated rainfall with 45, 65, 90, and 135 mm h⁻¹ intensities. Results indicated that sediment geometric mean diameter (GMD) varied significantly with wash and directional splash components following the sequence of downslope splash > lateral splash > upslope splash > wash. Both splash and wash preferentially transported the aggregate size fraction <0.063 mm. However, mean enrichment ratios (ER) for this fraction were < 2 for splash and about 12 for wash, reflecting the dynamic differences between the two processes. All sand-sized fractions were depleted in wash sediment but some were enriched in splash sediment, depending on directional components. Rainfall intensity and slope gradient had significant influences on both directional splash GMD (at $\alpha = 0.05$) and wash GMD (at $\alpha = 0.001$). However, the interaction between rainfall intensity and slope angle was significant only for wash GMD. Splash GMD was weakly correlated with the corresponding sediment flux, suggesting that the noted sediment size sorting was in a matrix-limited regime. In contrast, wash sediment GMD strongly correlated with the corresponding sediment flux and the sediment size sorting was force-limited. The study also indicated the splash-dominated regime generated sediment which had similar size characteristics to the in-situ soils while the wash-dominated regime produced sediment which was much finer than the in-situ soil.

5.1 Introduction

Research on the size characteristics of erosional sediment has received increasing attention due to its relevance in the understanding of the erosion processes involved and in quantifying nonpoint source pollution, including transport of sediment-sorbed chemicals. Available literature has generally shown that interrill erosion results in selective removal of silt and clay sized particles while rill erosion is less selective or non-selective after a specific critical flow shear stress is exceeded (e.g. Swanson et al. 1965; Govers, 1985; Hamlett et al. 1987; Miller and Baharuddin, 1987; Parsons et al. 1991). The selective transport of fine sediment produced by interrill erosion has been attributed to either the insufficient ability of interrill overland flow to transport large detached particles (Parsons et al. 1991) or the selective deposition of coarse detached sediment (Proffitt and Rose, 1991b). Yet, even for this general observation, conflicting reports exist in the literature. For example, Young and Onstad (1978), in a laboratory study with three soil types, found that sediment from interrill areas was coarser than the in-situ soils and the rill sediment. Young (1980) further pointed out that on poorly aggregated soils eroded sediment tends to have the same size distribution as the matrix soil. It is apparent that sediment size characteristics vary with soil erosion processes and soil aggregation characteristics, and that the relationship between interrill erosion and sediment size characteristics is not yet fully understood.

As illustrated in Chapters 2 and 3, interrill erosion is a dynamic combination of detachment and transport by impact of rainfall (splash) and transport by thin and unconcentrated overland flow (wash). Most information about sediment size characteristics and selective transport of interrill erosion is obtained from research which only considered

the wash process (e.g., Alberts et al., 1983; Ghadiri and Rose, 1991b) or failed to partition splash and wash processes (e.g., Miller and Baharuddin, 1987). Limited information on simultaneous measurements of splash and wash sediment size distribution indicated that wash sediment was finer than splash sediment (Gabriels and Moldenhauer, 1978; Sutherland et al., 1996). Thus, sediment produced by interrill erosion is sorted differently by splash or wash, and its ultimate size distribution partly depends on which process is dominant in sediment transport. In addition, splash sediments in the literature were not directionally partitioned and were mostly tested under a single rainfall intensity and slope gradient (hereafter shorted as "slope"). The influence of rainfall intensity and slope on sediment size characteristics of directional splash and wash as separate components is not yet well understood. The objectives of this study were (i) to determine the size characteristics of directionally partitioned splash sediment and wash sediment from a well aggregated Oxisol; (ii) to determine the effect of rainfall intensity and slope on splash and wash sediment size characteristics; and (iii) to assess the relative importance of splash and wash on interrill sediment size characteristics.

5.2 Materials and Methods

The soil, interrill splash and wash partitioning system, and experimental procedures were as described in Chapter 2. Briefly, soil samples (Wahiawa silty clay) were collected from the upper 0.1 m at the Poamoho Experimental Station on the island of Oahu, Hawaii, and were air-dried and sieved through a sieve with 6-mm openings. The interrill splash and wash partitioning system consisted of a drip-type rainfall simulator, a soil tray, a runoff collector, and four splash collectors. A glass bead layer of about 20 mm was evenly placed

at the bottom of the soil tray to provide free drainage. A metal screen separated the glass beads and a 20-mm pre-wet soil layer (soil moisture \approx 35% mass). This "horizon" was compacted to a bulk density of approximately 1.3 Mg m^{-3} to simulate a subsoil layer found in the field (Table 2.1). Air-dried soil was packed uniformly in the soil tray to produce a soil bed of 60 mm in depth with a level surface. The soil bed was wetted to near saturation through input water from the bottom percolation outlet prior to slope adjustment. Slopes studied were 4, 9, 18, 27, and 36 %. The rainfall intensities studied were 45 ± 2.1 , 65 ± 1.1 , 90 ± 4.2 , and $135 \pm 3.0 \text{ mm h}^{-1}$ (± 1 standard deviation). For each slope and rainfall intensity combination, runoff and percolate were measured every 5 min once rainfall was started. After achieving a steady state (about 20-30 min), the splash collectors were attached for 20-min. Wash and splash sediment was separately collected with sediment from the two lateral collectors combined. Each combination of slope and rainfall intensity was replicated three times and a new soil sample was used for each replicate.

The collected wash and splash sediment was wet sieved through a nest of sieves with openings of 2, 1, 0.5, 0.25, 0.125, and 0.063 mm. The wet-sieving procedure was similar to that discussed by Gabriels and Molderhauer (1978). Aggregate size distribution of the in-situ soil was obtained as follows. Five 50-g air-dried soil samples were wetted slowly by adding water from a wash bottle and received 20 min of rainfall at an intensity of 65 mm h^{-1} under the laboratory rainfall simulator. The samples together with the collected splash sediment and percolation water were wet sieved as was done for sediment. Wet-sieved aggregates were oven dried for 16 h at $105 \text{ }^\circ\text{C}$ and mass determinations were made. Aggregate geometric mean diameters were determined using the equation of Mazurak(1950) and Gardner (1956):

$$GMD = \exp\left(\frac{\sum_{i=1}^n w_i \log x_i}{\sum_{i=1}^n w_i}\right) \quad [5.1]$$

where GMD is the geometric mean diameter (mm), w_i is the mass (g) of an individual size fraction, x_i is the mean sieve size (mm). Aggregate size distribution and GMD for the in-situ wet-sieved soil are shown in Table 5.1. These data were used for determination of aggregate size enrichment ratio (ER), which was defined as:

$$ER = \frac{\text{Wet-sieved aggregate fraction (\% in sediment)}}{\text{Wet-sieved aggregate fraction (\% in in-situ soil)}} \quad [5.2]$$

Statistical analyses used in this study were mainly the analysis of variance (ANOVA) and Fisher's Protected Least Significant Different Test (LSD).

Table 5.1 Wet-sieved aggregate size fraction (%) and GMD (mm) for the in-situ soil

Aggregate size fractions (mm)	Description	Mean (n = 5)	Standard deviation
2-6	Gravel	6.43	0.42
1-2	Very coarse sand	15.07	1.34
0.5-1	Coarse sand	24.11	2.21
0.25-0.5	Medium sand	20.73	2.29
0.125-0.25	Fine sand	18.95	1.41
0.063-0.125	Very fine sand	10.05	1.23
<0.063	Silt and clay	4.66	1.81
GMD		0.728	0.027

5.3 Results and Discussion

5.3.1 Overall splash and wash GMD and ER

Table 5.2 shows sediment GMD for lateral splash, downslope splash, upslope splash, total splash (combination of all the three directional components), and wash. One-way ANOVA followed by the LSD test indicated that the mean GMD values for the directional splash components differed significantly from one another ($P < 0.001$) following the order: downslope > lateral > upslope. This variation was mostly associated with the directional forces exerted by rain drops on an inclined surface (Chapter 2), i.e., a larger sediment GMD indicates a larger force exerted and vice versa. The mean GMD of splash components, ranging from 0.59 mm for upslope splash to 0.74 mm for downslope splash, was significantly larger than that of wash (0.40 mm). This distinction indicated the dynamic difference between the ability of splash and wash to induce particle size sorting i.e., splash was driven by rainfall energy and so was less selective than wash which was

Table 5.2 Splash and wash sediment GMD: n = 60.

Statistic	Total splash	Lateral splash	Downslope splash	Upslope splash	Wash
	----- mm ----->				
Low 95% confidence interval	0.67	0.66	0.72	0.57	0.36
Mean	0.68	0.67	0.74	0.59	0.40
High 95% confidence interval	0.69	0.68	0.75	0.61	0.44
Median	0.68	0.66	0.75	0.59	0.38
Range	0.63-0.82	0.61-0.79	0.67-0.85	0.48-0.79	0.23-0.69
Coefficient of variation (%)	4.87	5.06	7.97	10.58	37.70

under the action of thin and unconcentrated overland flow. This finding supports the results of Gabriels and Moldenhauer (1978) and Sutherland et al. (1996).

The average GMD for total splash and wash sediments (Table 5.2) was significantly smaller (at $\alpha = 0.05$ with a t test) than the wet sieved in-situ soil (Table 5.1), suggesting that both splash and wash were selective. The average ER values of all aggregate size fractions for splash and wash components are shown in Table 5.3. An ER value larger than 1 indicates enrichment of the fraction in sediment and that less than 1 indicates that the fraction was depleted. The results showed that the silt and clay fraction (<0.063 mm) was significantly enriched in all splash and wash sediments. However, the mean ER values were < 2 for splash and about 12 for wash, indicating that the overland flow was considerably less powerful and, thus, more selective for fine sediment than were raindrops. The enrichment of fine aggregates in splash sediment was mostly due to continuous aggregate breakdown by rainfall impact, a process which was further studied in Chapter 7. The enrichment of the fine fraction in splash sediment can be compared to studies by Poesen and Savat (1980) and Parsons et al. (1990) who found that the silt plus clay fractions in splash sediment were under represented. This contradiction was mostly associated with the different soils used. In the above studies sandy and poorly-aggregated soils were used and thus production of the fine fraction by rainfall impact was not possible. Instead, Poesen and Savat (1980) suggested that finer fractions were carried downwards into the parent material by percolating water, a migration mechanism they called "filtration pavement". Clearly, the relative enrichment or depletion of the fine fraction in splash sediment is highly soil-dependent.

Table 5.3 Mean ER for splash and wash sediment (means of 60 measurements with 95% confidence intervals in parentheses).

Fraction (mm)	Total splash	Downslope splash	Lateral splash	Upslope splash	Wash
2-6	0.00(0.00)	0.00(0.00)	0.00(0.00)	0.00(0.00)	0.12(0.05)
1-2	0.54(0.04)	0.87(0.09)	0.46(0.04)	0.23(0.06)	0.38(0.09)
0.5-1	1.29(0.04)	1.47(0.05)	1.27(0.05)	0.94(0.09)	0.47(0.09)
0.25-0.5	1.35(0.04)	1.23(0.05)	1.36(0.04)	1.45(0.04)	0.57(0.11)
0.125-0.25	1.01(0.04)	0.76(0.04)	1.05(0.05)	1.39(0.08)	0.47(0.08)
0.063-0.125	0.67(0.04)	0.51(0.08)	0.69(0.04)	0.94(0.07)	0.41(0.07)
<0.063	1.48(0.12)	1.42(0.19)	1.56(0.14)	1.70(0.15)	12.33(1.69)

For sand size fractions (0.063-2 mm), ER values for wash were significantly < 1, indicating that interrill overland flow had limited power for transporting large aggregates. In splash, however, there were some sand-sized fractions which were selectively transported. For total splash, the enriched sand-sized fractions were 1-0.25 mm, i.e., coarse sand to medium sand fractions. Similar observations were also made by Poesen and Savat (1980), Proffitt et al. (1993), and Sutherland et al. (1996). The other fractions (1-2 mm and 0.063-0.125 mm) were depleted in splash sediment. Depletion of these fractions in splash sediment was linked to the larger physical mass of coarser fractions and the stronger cohesion between particles in the finer fractions (Farmer, 1973; Mazurak and Mosher, 1968). For gravel size fraction (2-6 mm), ER values for splash were all close to 0, indicating that splash was unable to transport aggregates of this fraction under the experimental condition. The ER value for wash was 0.12 and transport of this fraction was associated with events of high intensity (90 and 130 mm h⁻¹) with steep slope angles (>18%).

While previous research studied only total splash sediment size characteristics, the directionally partitioned splash ER data in Table 5.3 revealed several interesting patterns. Note that the enriched fractions and the ER values varied with directional components. For very coarse sand and coarse sand fractions (1-2 mm and 0.5-1 mm), ER values decreased following the sequence of downslope > lateral > upslope while for smaller sand size fractions ER values increased in this sequence. This variation was again associated with the directional force available for splash transport, i.e., the downslope force was larger than the upslope force due to the inclined slopes studied, and thus favored transport of large aggregates. An important implication of this difference was that, with time, sediment in the downslope area tended to become coarser by splash erosion. This may also provide an explanation for the field observations reported by Poesen and Savat (1980).

5.3.2 Effect of rainfall intensity and slope gradient

Table 5.4 shows the results of ANOVA of rainfall intensity and slope effects on splash and wash sediment GMD. Rainfall intensity and slope significantly influenced the GMD of splash components ($P < 0.05$) except for the slope effect on total splash. These

Table 5.4 P values of the F test in ANOVA for the rainfall intensity and slope effects on GMDs of splash and wash sediments.

Source of variance	df	Total Splash	Upslope Splash	Lateral Splash	Downslope Splash	Wash
Rain intensity (I)	3	0.006	0.001	0.018	0.003	<0.001
Slope (S)	4	0.394	<0.001	0.026	0.003	<0.001
I x S	12	0.957	0.296	0.968	0.525	<0.001
Error	40					

main effects on wash sediment GMD were highly significant ($P < 0.001$). It was interesting to note that the interaction between rainfall intensity and slope gradient did not have a significant ($P > 0.2$) influence on sediment GMD for any of the splash components. This interaction effect was, however, highly significant ($P < 0.001$) for wash, indicating that the response of splash and wash to rainfall intensity and slope angle, in terms of sediment size sorting, was different.

Since the interaction effect between slope and rainfall on splash GMD was not significant, it was desirable to compare splash GMD means between slope with the average of all rainfall intensities and between rainfall intensity with the average of all slopes to obtain a greater number of degrees of freedom (Table 5.5). For mean comparisons by slope, GMD means for total splash were generally not significantly different from each other. However, average GMD values for directionally partitioned splash sediments varied significantly with slope angles. For example, downslope splash displayed smaller GMD at 4% slope than at the other slopes. This was mostly associated with the cushioning effect of ponded water in the downslope area (discussed earlier in Chapters 2 and 3), which retarded large aggregates from being detached and transported. As slope gradient increased, this cushioning effect became less significant, resulting in similar sediment GMDs. This also indicated that particle size sorting by downslope splash was not limited by rainfall impact forces, which increased with increasing slope. For upslope splash, however, sediment GMD decreased significantly with increasing slope angle (Table 5.5). This decrease in GMD suggested a progressively smaller force available for upslope transport with increasing slope angle.

Table 5.5 Comparison of GMD means by slope and rainfall intensity for splash[†].

By slope (%)	Total	Lateral	Downslope	Upslope
	←----- mm ----->			
4	0.689a	0.691a	0.688b	0.671a
9	0.682a	0.679ab	0.759a	0.613b
18	0.677a	0.655b	0.741a	0.586c
27	0.683a	0.660b	0.764a	0.559d
36	0.679a	0.657b	0.735a	0.518e
LSD(0.05)	0.023	0.023	0.038	0.023
By rainfall intensity (mm h ⁻¹)				
45	0.660b	0.651b	0.695b	0.576b
65	0.700a	0.683a	0.764a	0.570b
90	0.691a	0.681a	0.742a	0.605a
135	0.684a	0.667ab	0.749a	0.609a
LSD(0.05)	0.023	0.023	0.034	0.023

[†] Means in a column for a category followed by the same letter are not significantly different at $\alpha = 0.05$ according to the LSD test. Each GMD mean in the table is an average of 12 observations for comparison by slope and of 15 observations for comparison by rainfall intensity.

For comparisons by rainfall intensity, the average GMD values for 45 mm h⁻¹ were significantly smaller than those for other intensities. Similar observations were also made by Farmer (1973) who found that splash sediment detached by high-intensity rainfall contained coarser-grained sediment than that by low-intensity rainfall. The smaller GMD for 45 mm h⁻¹ was possibly due to the limited rainfall kinetic energy flux under this rainfall intensity. This suggested that a critical rainfall kinetic energy was required to change splash sediment GMD or to transport larger particles.

The effect of slope gradient and rainfall intensity on size characteristics of splash sediment can also be seen from Figure 5.1, which shows changes in ER values for the <0.063 mm and 1-2 mm fractions, with slopes and rainfall intensities, for downslope and upslope splash components. These two fractions were selected since the finest fraction was generally enriched and is of environmental significance (Chapters 6 and 7), and the coarser fraction was depleted and the depletion varied with directional splash components. For downslope splash, ER values for the <0.063 mm fraction at 4% slope was significantly higher than that for the other slopes (Figure 5.1a). This was again due to the cushioning effect of ponded water in the downslope area. ER values for the 1-2 mm fraction did not significantly increase with increasing slope angle (Figure 5.1b). It was, however, interesting to note that ER values for both fractions increased with increasing rainfall intensity. For the finest fraction this was possibly due to the increased aggregate breakdown under high rainfall intensity while for the coarser fraction this may indicate efficient sediment transport associated with high rainfall kinetic energy flux. For upslope splash, ER values increased with increasing slope for the <0.063 mm fraction and decreased with increasing slope for the 1-2 mm fraction (Figure 5.1c&d). Variations of ER values with rainfall intensity were, however, not significant.

Changes in wash GMD and ER values for the <0.063 mm fraction with rainfall intensity and slope are shown in Table 5.6 and Figure 5.2, respectively. Overall, sediment GMD increased and ER values for the <0.063 mm fraction decreased with increasing slope and rainfall intensity. This reflected the effect of increased flow shear force or stream power with increasing slope and runoff flux on transport of large aggregates. It is, however, necessary to note several exceptions to this general pattern. Wash sediment GMD did not significantly change with slope at a rainfall intensity of 45 mm h⁻¹. Figure 5.2 also indicated

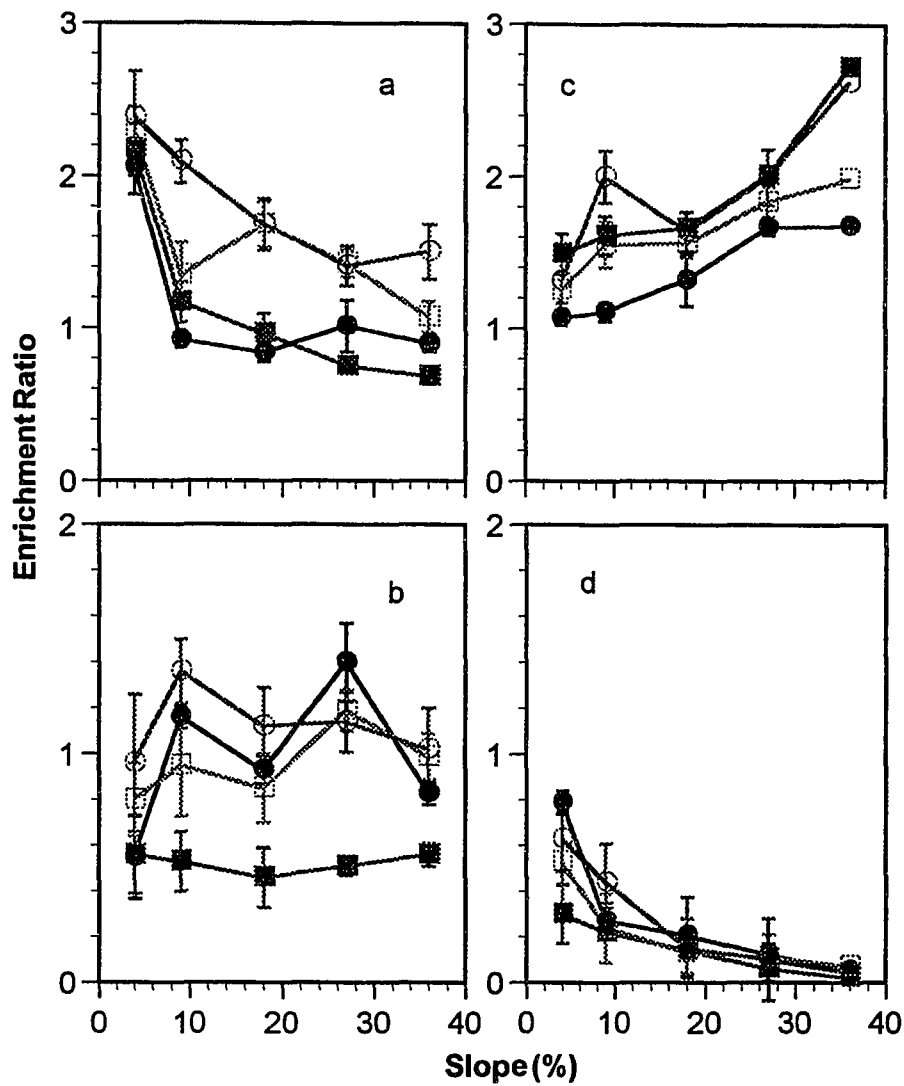


Figure 5.1 Change in ER values with slope and rainfall intensity (■: 45 mm h⁻¹, ●: 65 mm h⁻¹, □: 90 mm h⁻¹, and ○: 130 mm h⁻¹) for a: <math><0.063\text{ mm}</math> fraction of downslope splash; b: <math><2-1\text{ mm}</math> fraction of downslope splash; c: <math><0.063\text{ mm}</math> fraction of upslope splash; and d: $2-1\text{ mm}$ fraction of upslope splash. Error bars are standard errors for the mean of three replicates.

that ER values <0.063 mm fraction at 45 mm h⁻¹ did not change significantly with slope. This confirms the observation made in Chapter 3, that flow flux under this condition was small and the resulting flow shear stress was lower than the critical level required for transporting large aggregates. Wash sediment GMD also did not significantly change with rainfall intensity at 45, 65, and 90 mm h⁻¹ for the 4% slope. Further increase in rainfall intensity significantly increased wash sediment GMD. This trend again suggested that a critical shear stress or stream power was required for transporting large aggregates. It was also interesting to note that the increase of sediment GMD with slope generally diminished as the slope angle exceeded 18%. This critical change was also apparent from Figure 5.3. It shows the ER decrease with increasing slope and supports the observation made earlier (in Chapter 3) that a rapid increase occurred in wash transport as slope angle increased from 9% to 18%.

Table 5.6 Comparison of GMD means by slope and rainfall intensity for wash[†]

Slope (%)	rainfall intensity (mm h ⁻¹)				LSD(0.05)
	45	65	90	135	
	<----- mm ----->				
4	0.248g	0.267g	0.257g	0.375f	0.050
9	0.232g	0.323f	0.379f	0.452e	0.055
18	0.239g	0.402e	0.493c	0.609b	0.067
27	0.232g	0.460d	0.521c	0.643b	0.035
36	0.246g	0.487d	0.542c	0.679a	0.033
LSD(0.05)	0.029	0.050	0.054	0.069	

[†] Means in a row or a column followed by the same letter are not significantly different at $\alpha = 0.05$ according to the LSD test. Each GMD mean in the table is an average of 3 observations.

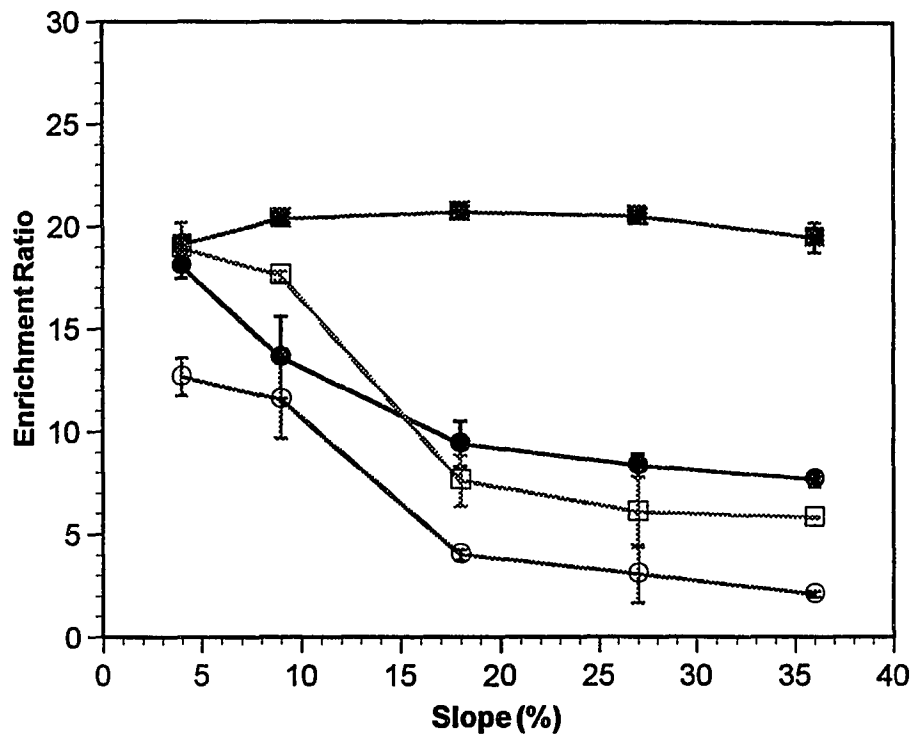


Figure 5.2 Change in ER values of wash <0.063 mm fraction with slope and rainfall intensity (■: 45 mm h⁻¹, ●: 65 mm h⁻¹, □: 90 mm h⁻¹, and ○: 130 mm h⁻¹). Error bars are standard errors for the mean of three replicates.

Data in Chapter 3 indicated that sediment flux can be modeled with rainfall intensity and slope for splash and with rainfall intensity, runoff flux, and slope for wash. The different relationships between splash and wash sediment size characteristics and rainfall intensity and slope suggest that splash and wash sediment sizes respond differently to sediment flux. Regression analyses of sediment GMD with the corresponding sediment flux indicated that splash sediment GMD, in general, had weak correlation with sediment flux (correlation coefficient $r = -0.17, 0.22, -0.25, \text{ and } 0.40$, respectively for total splash, downslope splash, lateral splash, and upslope splash; only that for upslope splash was significant at $\alpha = 0.05$) while wash GMD strongly correlated with sediment flux ($r = 0.62$ for linear correlation and 0.92 if sediment flux was \log_{10} transformed, both highly significant at $\alpha = 0.001$). The implication of this difference is that particle size sorting of splash and wash are related with different regimes. Selective transport can be limited by the magnitude of the erosive force involved in the specific erosion process and the size characteristics of the soil matrix. In a force-limited regime, an erosion process (such as the wash discussed previously) will produce coarser sediment as the force becomes larger. In a matrix-limited regime, sediment size will not increase significantly with increasing the force involved (such as splash) until a critical level associated with the transport of large fractions is exceeded. For a soil consisting of a wide spectrum of size fractions such as the Oxisol in this study (Table 5.1), erosional consequences may be limited alternatively by the matrix or force in response to the increase of erosive force. Aselective erosion occurs only when neither the force nor the matrix are limiting factors. Mass movement and rill detachment are examples of aselective erosion.

5.3.3 Interrill sediment delivery

Data in Chapters 2 and 3 indicated that interrill sediment delivery can be dominated by either splash or wash, depending on slope and runoff conditions. Figure 5.3 shows the aggregate size distribution of wash, downslope splash, and total interrill sediment (combining wash and downslope splash) for the rainfall events of 45 mm h⁻¹ at 36% slope and 135 mm h⁻¹ at 4% slope. These two events were selected to represent contrasting conditions: the first one represents splash-dominated regime (splash flux: wash flux = 8.16 : 1) and the second wash-dominated regime (splash flux: wash flux = 1 : 7.48). The aggregate size distribution of total interrill sediment was essentially the cumulative result of the contributions of wash sediment and downslope splash sediment to overall interrill sediment delivery. It was clear that interrill sediment size characteristics depend highly on the predominant process responsible for sediment transport. It is, thus, not surprising that vastly different reports about interrill sediment size characteristics exist in the literature (e.g., Young and Onstad, 1978; Parsons et al., 1991; Ghadiri and Rose, 1991b). It is very likely that in the study of Young and Onstad (1978), interrill sediment delivery was dominated by splash, resulting in sediment size characteristics which were similar or even coarser than for the in-situ soil. However, in the studies of Parsons et al. (1991) and Ghadiri and Rose (1991b) the sediment was primarily transported by overland flow, which generated much finer sediment than splash, due to the limited flow shear stress.

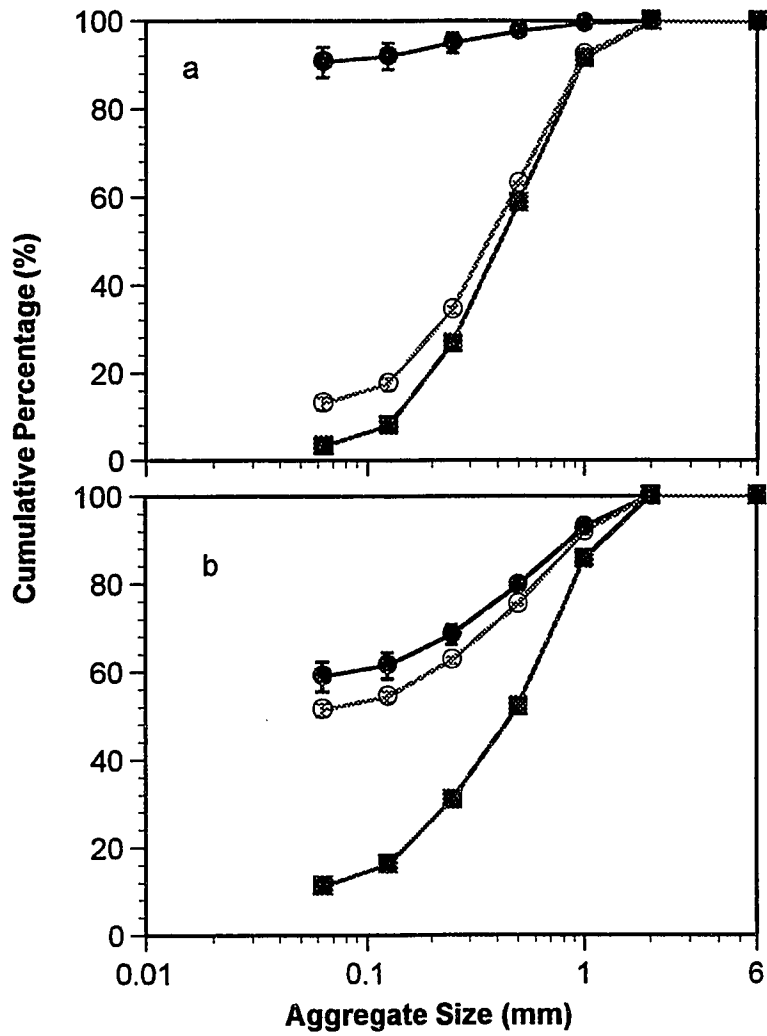


Figure 5.3 Aggregate size distribution of splash (■), wash (●), and total interrill sediment (○) for the events of (a) 45 mm h⁻¹ at 36% slope and (b) 135 mm h⁻¹ at 4% slope. Error bars are standard errors for the mean of three replicates.

5.4 Conclusions

In this study, sediment geometric mean diameter varied significantly with wash and directional splash components following the sequence of downslope splash > lateral splash > upslope splash > wash. Both splash and wash preferentially transported the aggregate size fraction <0.063 mm. However, mean enrichment ratios for this fraction were < 2 for splash and about 12 for wash, showing that wash was more selective in terms of fine particles. All sand-sized fractions were depleted in wash sediment but certain fractions were enriched in splash sediment, depending on directional components. Rainfall intensity and slope had significant influences on both directional splash GMD (at $\alpha = 0.05$) and on wash GMD (at $\alpha = 0.001$). However, the interaction effect was significant only for wash GMD. Splash GMD had a poor correlation with the corresponding sediment flux, suggesting that sediment size sorting was controlled by the soil matrix. In contrast, wash sediment GMD strongly correlated with the corresponding sediment flux and the sediment size sorting was force-limited. The study also indicated that interrill sediment size characteristics depended highly on sediment transport regimes, i.e., a splash-dominated regime generated coarse sediment whereas wash-dominated regime produced fine sediment. The implication of the study was that, with time, interrill splash and wash processes tended to produce a coarser and nutrient-depleted surface soil matrix and finer and chemically-enriched sediment. This is verified by research presented in Chapters 6 and 7.

CHAPTER 6
SEDIMENT ENRICHMENT DURING FLOW TRANSPORT
FROM A WELL-AGGREGATED AND UNIFORMLY-TEXTURED OXISOL

Abstract

Sediment enrichment and transport from a well-aggregated and uniformly-textured Oxisol were determined using field rainfall simulation on an agriculturally-managed ridge-and-furrow system. Overland flow was generated by applying four successive rainfall events: a dry run on bare soil with a rainfall intensity of 35 mm h⁻¹, a wet run on bare soil with the same rainfall intensity on the second day, followed by a very wet run on bare soil with a rainfall intensity of 62 mm h⁻¹ and a final run on partially plastic-mulched soil (to simulate pineapple culture) with a rainfall intensity of 50 mm h⁻¹. Results indicated that the stream power and shear stress of overland flow during the dry and wet runs did not exceed the critical level for rill flow detachment, and resulted in runoff sediment concentrations between 1.7-3.5 g L⁻¹, with 70-90% of sediment consisting of fine aggregates (<0.063 mm). As flow rate and thus flow stream power and shear stress increased, sediment concentration increased to over 12 g L⁻¹ for the subsequent two runs. Elevated sediment concentrations were associated with the increased transport of sand-sized aggregates. Elimination of interrill erosion due to the presence of plastic mulch reduced transport of fine aggregates in comparison with the very wet run on the bare soil. Due to the high clay content and uniform texture of the Oxisol, sediment from the four events displayed similar primary particle size distribution, with the enrichment ratio (ER) of clay particles not significantly different from 1.0. However, organic carbon (OC) and extractable phosphorus (Ext-P) were enriched in sediment. The ER magnitudes followed the order: dry run (1.2 for

OC and 1.4 for Ext-P) > wet run (1.1 for OC and 1.2 for Ext-P) > very wet run (1.03 for OC and 1.1 for Ext-P) > plastic mulch run (close to 1 for both OC and Ext-P). This enrichment was associated with selective transport of fine aggregates which were chemically richer than the coarser fractions.

6.1 Introduction

Sediment transported by overland flow has long been recognized to be enriched with fine soil particles (e.g., silt and clay), organic matter, nutrients and other associated chemicals when compared with the in-situ soil (Massey and Jackson, 1952; Stoltenberg and White, 1953; Bhatt, 1976; Alberts and Moldenhauer, 1981; Alberts et al., 1983; Sharpley, 1985; McIsaac et al. 1991). This sediment enrichment phenomenon is commonly described by an empirically derived enrichment ratio (Menzel, 1980; Lane and Nearing, 1989). The enrichment ratio (ER) is defined as the ratio of a specific constituent (e.g., organic matter or a particular nutrient) concentration in sediment to that of the same constituent in the in-situ soil. Thus, in the case of nutrients:

$$ER = \frac{\text{Nutrient concentration in sediment}}{\text{Nutrient concentration in bulk soil}} \quad [6.1]$$

Such ER computations have been integrated into several water quality and soil erosion models such as CREAMS (Menzel, 1980), GLEAMS (Leonard et al., 1987), and WEPP (Lane and Nearing, 1989) for predicting potential on-site and off-site impacts of soil erosion.

Sediment enrichment can occur in two ways, namely physical enrichment of fine particles which arises from selective size sorting of detached sediment and chemical enrichment of organic matter, nutrients, pesticides and other chemicals (Young et al., 1985). The selectivity of soil erosion processes is responsible for physical enrichment. Most controlled studies dealing with selectivity of erosional processes have focused on interrill erosion (e.g. Swanson et al., 1965; Hamlett et al., 1987; Miller and Baharuddin, 1987; Parsons et al. 1991), and these studies generally showed that interrill erosion resulted in selective removal of silt and clay sized particles. Limited information about rill erosion indicated that concentrated flow is less selective or non-selective after a critical shear stress is exceeded (Govers, 1985; Proffitt and Rose, 1991b). In an agriculturally managed system, sediment transport is often accomplished by concentrated overland flow while interrill erosion contributes sediment to channels carrying the concentrated flow (Chapter 4). Little information is available about sediment size characteristics from such a dynamic interrill-rill erosion system.

The chemical enrichment of organic matter, nutrients or pesticides in sediment is commonly considered a consequence of physical enrichment. The rationale for this is that fine particles have a larger specific surface area than coarse ones, and thus have a larger capacity for retaining chemicals via sorption and ionic exchange (Foster et al., 1985; Sharpley, 1985; Flanagan and Foster, 1989). However, this explanation is valid only for non-uniformly textured soils, and only if fine particles are rich in the specific chemical of concern. Characteristics and mechanisms of chemical enrichment for well-aggregated and uniformly-textured soils are yet not well understood.

This chapter reports on measured sediment loss and enrichment characteristics for a well-aggregated and uniformly-textured Oxisol under controlled rainfall and overland flow

conditions in the field. The objectives were: (i) to delineate temporal variations of sediment transport and physical and chemical enrichment under different flow conditions; (ii) to determine the effect of interrill sediment delivery on sediment size characteristics and thus sediment enrichment of concentrated rill flow; and (iii) to further elucidate the relationship between physical enrichment and chemical enrichment of sediment from this Oxisol.

6.2 Materials and Methods

The Wahiawa silty clay soil (a Rhodic Eustrtox) at the Poamoho Experimental Station on the island of Oahu, Hawaii was again selected for this study. Field rainfall simulation was conducted in the same site as for that in Chapter 4. The field had been cultivated for the past ten years and is heavily fertilized with inorganic fertilizers. The plot prepared for rainfall simulation consisted of two 8.5 m long and 0.6 m wide ridges and a 0.5 m wide and 0.15 m deep triangular furrow in between, similar to that in Chapter 4. A plastic border was inserted in the center of each ridge as the drainage divide, resulting in a plot width of 1.2 m. The average slope for the furrow was 4.2 % and that for the row side was about 30%. This plot setup was prepared to mimic the agricultural ridge-and-furrow system, which is typical of pineapple culture in Hawaii.

A programmable rainfall simulator based on the design of Foster et al. (1982) was used. Raindrops were emitted through six oscillating V-jet spray nozzles from low line pressure (6.4×10^4 Pa). The median drop diameter of simulated rain was 2.2 mm. Rain fell from a height of 3 m above the soil surface resulting in a kinetic energy flux of $20 \text{ J m}^{-2} \text{ mm}^{-1}$ of rainfall. Domestic water supply with an average water temperature of 25 °C was used. Wind effects were minimized by use of a wind shield around the rainfall simulator.

Four storms with predetermined rainfall intensities were applied. Rainfall duration was 3.2 h for the first event and about 1 h for each of the remaining three events. The first storm (dry run) applied at the soil moisture condition prevailing at the time (about 20%) had a rainfall intensity of 35 mm h⁻¹. This rainfall intensity was selected so that the stream power or shear stress of the generated overland flow did not exceed the critical value required for flow detachment of this soil (Chapter 4). During the dry run, runoff was generated about 1.2 h after rainfall and the storm was extended for another 2 h until runoff rate was unchanged with time (steady state). The second storm (wet run) with the same rainfall intensity was imposed on the following day to simulate high antecedent soil water conditions (about 40 %) and determine the influence of surface sealing or compaction on runoff flux and thus sediment enrichment.

The third storm (very wet run) was applied immediately following the wet run and had a rainfall intensity of about 62 mm h⁻¹. This rainfall intensity was selected so that the overland flow generated was planned to be powerful enough to perform sediment detachment (Chapter 4). After the third storm was finished, two strips of plastic mulch (0.6 m wide and 9 m long) were laid over the two ridges, leaving a 0.4 m bare soil strip in the center of the furrow. The plastic sheets were carefully anchored to the soil surface to allow for direct delivery of rain water into the furrow. Due to the impervious nature of the plastic sheet, a rainfall intensity of about 50 mm h⁻¹ was employed for the last storm (plastic mulch run) with the intention of providing comparable flow to that in the very wet run. The time interval separating storms 2-3 and 3-4 was about 30 min.

For each of the runs, time for runoff generation was recorded. Runoff was volumetrically measured and sampled every 5 to 10-min. After steady state was reached, rill flow width and velocity at 1, 2, and 3 m upslope from the sampling outlet were

measured. A fluorescent dye was used for flow velocity measurement (Abrahams et al., 1986; Gilley et al., 1990) and a mm-scale ruler was used to determine flow width. Visual observations of sediment transport and soil surface conditions were made both during and after simulated storms. The above experiments were replicated two times.

Runoff samples were processed in the laboratory by passing them through a nest of sieves of 4, 2, 1, 0.5, 0.25, 0.125, 0.063 mm openings without dispersion. The fractions of smaller aggregates (< 0.063 mm) were further determined by a plummet balance method (El-Swaify, 1980). After this determination, sediment in the mixture was allowed to settle and water was decanted. Aggregates in each size fraction were oven dried at 35–40 °C for about 48 h and mass determinations were made. This low drying temperature was used to avoid possible alteration of nutrient extractability. However, this mass was further corrected based on a subsample oven dried at 105 °C. These laboratory measurements were conducted within 5 days after sampling. It is realized that disintegration of aggregates by raindrop impact occurs during rainfall simulation, particularly at the beginning of the first storm. A "reference" aggregate size distribution was obtained for the in-situ soil using the method of Proffitt et al. (1991). About 100 g of field-dry soil sample, evenly placed in a 0.1 m diameter container, was exposed to 62 mm h⁻¹ rainfall for 1 h. The container bottom was pervious so that ponding did not occur. This container was placed in another larger container to collect all sediment lost in percolate and as splash. Aggregate size distribution was determined on five replicates as done for the runoff samples. Preliminary trials indicated that aggregate size distribution obtained as such did not differ significantly (at $\alpha = 0.05$ with a t test) from that obtained with rainfall extended for 2 h. So this reference aggregate size distribution was considered appropriate for representing "in-situ" soil for all storms in this study.

Dispersed particle size distribution, organic carbon (OC), and extractable phosphorus (Ext-P) were determined for selected samples of the whole soil, sediment, and aggregate size fractions of the reference samples. Dispersion for particle size distribution analysis was enhanced by applying ultrasonic energy (350 W h^{-1}) for 20 min over the soil and 5% calgon solution mixture (soil solution ratio = 1:5). The quantity of particles $< 0.002 \text{ mm}$ was determined by the pipette method (Day, 1965). Organic C was determined with a LECO Carbon Analyzer. Phosphorus was extracted with Mehlich 3 solution (Mehlich, 1985), and determined following the procedure of Murphy and Riley (1962). Analysis results for the in-situ soil are shown in Table 6.1, and these data were used as the basis for ER determinations with Eq. [6.1].

Table 6.1 Selected soil properties of the in-situ Wahiawa Oxisol

Soil Property	Replicates	Mean	Standard deviation
pH (soil : water = 1:1)	3	5.80	0.04
Organic C (%)	5	1.52	0.03
Extractable P (mg kg^{-1})	5	96.51	3.57
Dispersed particle size distribution (%)			
Sand ($>53 \mu\text{m}$)	3	1.33	0.12
Silt ($2-53 \mu\text{m}$)	3	9.59	0.50
Clay ($<2 \mu\text{m}$)	3	89.08	0.47

6.3 Results and Discussion

6.3.1 Flow hydraulics and sediment concentration

The properties of overland flow at steady state in the downstream area where measurements were made, are given in Table 6.2 for the four rainfall events. Flow for all

events was laminar (Reynolds Number: $Re < 1000$), though the Re values for the later two storms were 2-3 times larger than that of the first two (Table 6.2). Data in Chapter 4 indicated that critical shear stress for sediment detachment of the soil was about 1.1 Pa, which corresponded to a stream power of 0.12 W m^{-2} . So the flow shear stress and stream power for the very wet run and the plastic mulch run substantially exceeded these values while those for the dry and wet runs were close to the critical values (not significantly different).

Table 6.2 Flow properties at steady state for the four rainfall events

Event	Dry run	Wet run	Very wet run	Plastic mulch run
Flow rate ($\times 10^{-5} \text{ m}^3 \text{ s}^{-1}$)	3.24	3.92	9.90	11.16
Flow width (m)	0.12	0.13	0.16	0.17
Flow Depth ($\times 10^{-3} \text{ m}$)	4.5	5.0	7.0	8.0
Flow velocity (m s^{-1})	0.11	0.13	0.16	0.18
Hydraulic radius [†] ($\times 10^{-3} \text{ m}$)	2.3	2.5	3.5	4.0
Reynolds number [‡]	283	351	613	795
Stream power [§] (W m^{-2})	0.11	0.12	0.25	0.27
Shear stress [¶] (Pa)	0.93	1.03	1.44	1.65

[†] $R = WD/(D+ 2W)$ rectangular rill where R = hydraulic radius (m), W = flow width (m) and D = flow depth (m).

[‡] $Re = VR/v$ where Re = Reynolds number (dimensionless), V = flow velocity (m s^{-1}), R = as defined above, and v = water kinematic viscosity at a given temperature ($\text{m}^2 \text{ s}^{-1}$).

[§] $\omega = \rho g S Q / W$ where ω = stream power (W m^{-2}), ρ = water density at a given temperature (kg m^{-3}), g = acceleration of gravity (9.81 m s^{-2}), S = slope (m m^{-1}), Q = flow rate ($\text{m}^3 \text{ s}^{-1}$), and W = as defined above.

[¶] $\tau = \rho g S R$ where τ = shear stress (Pa) and ρ , g , R , S = as defined above.

Figure 6.1 shows variations in runoff rate and sediment concentration with time for the four storms. Runoff rate for the dry run increased with time, approaching steady state in about 90 min after runoff initiation. Sediment concentration was high for the first 10 min due to the initial flush of loose sediment, and then approached a constant of about 1.7 g L^{-1} . The increase in runoff rate and thus flow shear stress or stream power in the dry run did not increase sediment concentration, suggesting that the critical value for flow detachment was not yet exceeded under this flow condition. The mechanism responsible for sediment transport was mainly the rainfall impacted flow called "rain flow transport" by Moss (1988) or rainfall detachment and redetachment as defined by Rose (1993). Steady state runoff rate for the wet run (same rainfall intensity as dry run) was slightly higher than that of the dry run, indicating the influence of reduced soil water saturation deficit, surface sealing and compaction on infiltration rate. It should be noted that a slight increase in runoff rate and thus flow shear stress and stream power for the wet run (Table 6.2) increased sediment concentration up to about 3.5 g L^{-1} when compared with the dry run. This increase in sediment concentration was possibly associated with the initiation of runoff entrainment or re-entrainment as defined by Hairsine and Rose (1992). A further increase in runoff rate during the last two runs (Figure 6.1 c&d) and thus flow shear stress and stream power resulted in a steady state sediment concentration over 12 g L^{-1} . This significant increase in sediment concentration with increased runoff rate suggested that flow shear stress and stream power had significantly exceeded the critical value required for rill erosion.

It was originally intended to obtain the same flow rate for the very wet run and the plastic mulch run, but there were experimental difficulties which prevented this. These data showed that the runoff rate for the plastic mulch run was higher than that of the very wet run (Figure 6.1 c&d). However, sediment concentration for the plastic mulch run was slightly

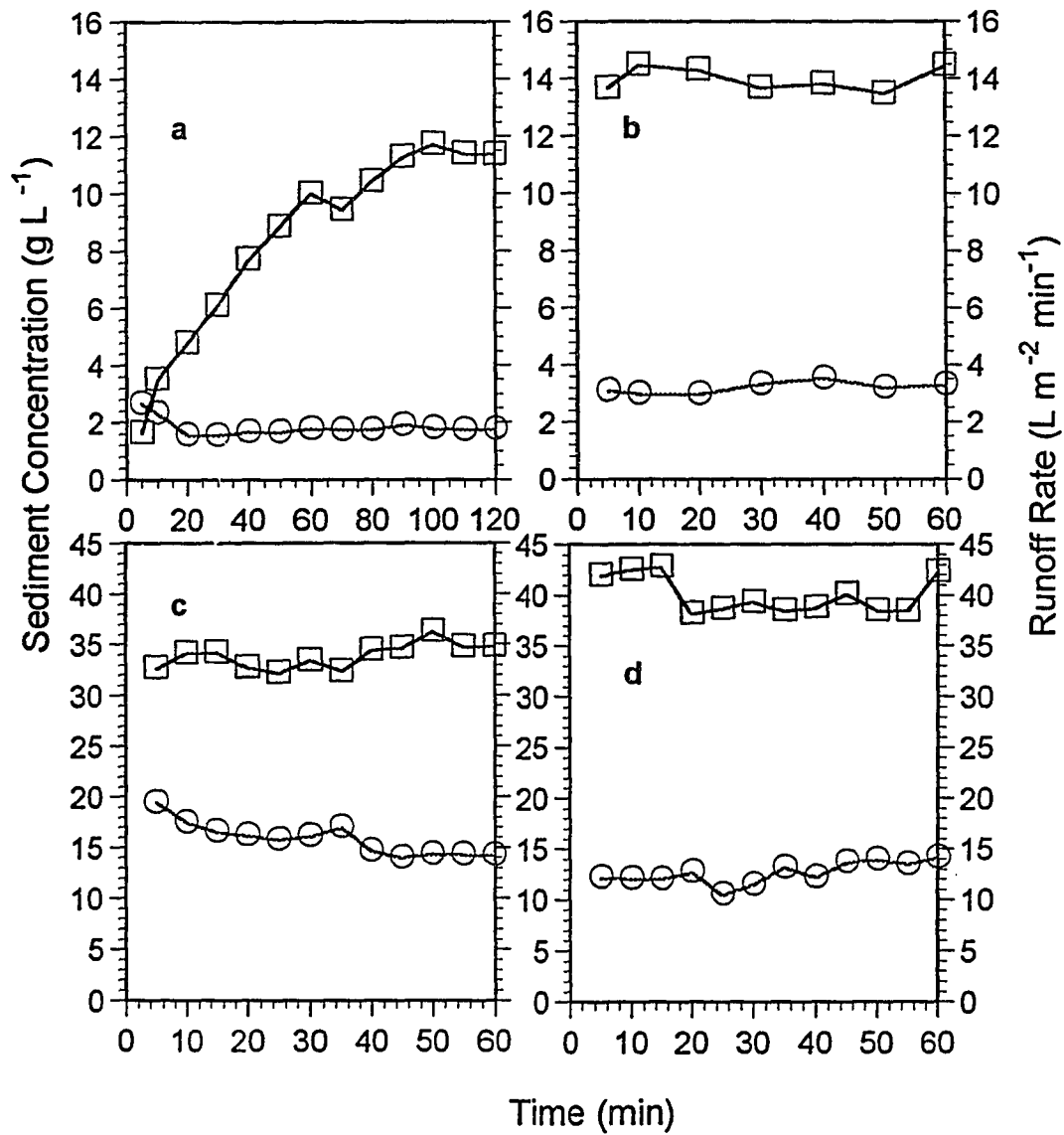


Figure 6.1 Temporal variation in sediment concentration (O) and runoff rate (□) during a. dry run, b. wet run, c. very wet run, and d. plastic mulch run.

lower than that for the very wet run. This is likely because the plastic mulch protected the ridge area from interrill erosion, and sediment delivery into the rill flow was less than in the very wet run. As a result, sediment available for flow transport or re-entrainment with the plastic mulch was less than without it, so that more flow energy had to be dissipated to overcome inter-aggregate cohesion of the undetached soil. These data support the concept of runoff entrainment and re-entrainment proposed by Hairsine and Rose (1992).

6.3.2 Aggregate size distribution

Figure 6.2 shows the temporal variations in aggregate size composition of sediment from the four events. For the dry run (Figure 6.2a), sediment was principally composed of fine aggregates (0.005-0.063 mm and < 0.005 mm) which accounted for about 90% of the whole sediment. These fine aggregates were largely transported in suspended form. The initial high content of coarse aggregates were associated with the initial flush of loose sediment during the first 10 min. After that time, the concentrations of different size fractions varied little throughout the duration of the run. Under low flow energy conditions, Proffitt et al. (1991) noted a gradual increase in coarseness of transported sediment with time due to development of a coarser deposited layer. This was not observed in this study, possibly due to the ridge-and-furrow plot configuration used. Under this condition, interrill erosion in the ridge area provided a continuous source of sediment for transport by flow in the furrow. The interrill sediment, though transported largely by splash, was enriched with aggregates < 0.063 mm (Chapter 5). However, visual observations after the dry run did indicate the existence of a coarser deposition layer in the downslope area of the furrow, due to the limited power of the flow to transport coarse aggregates.

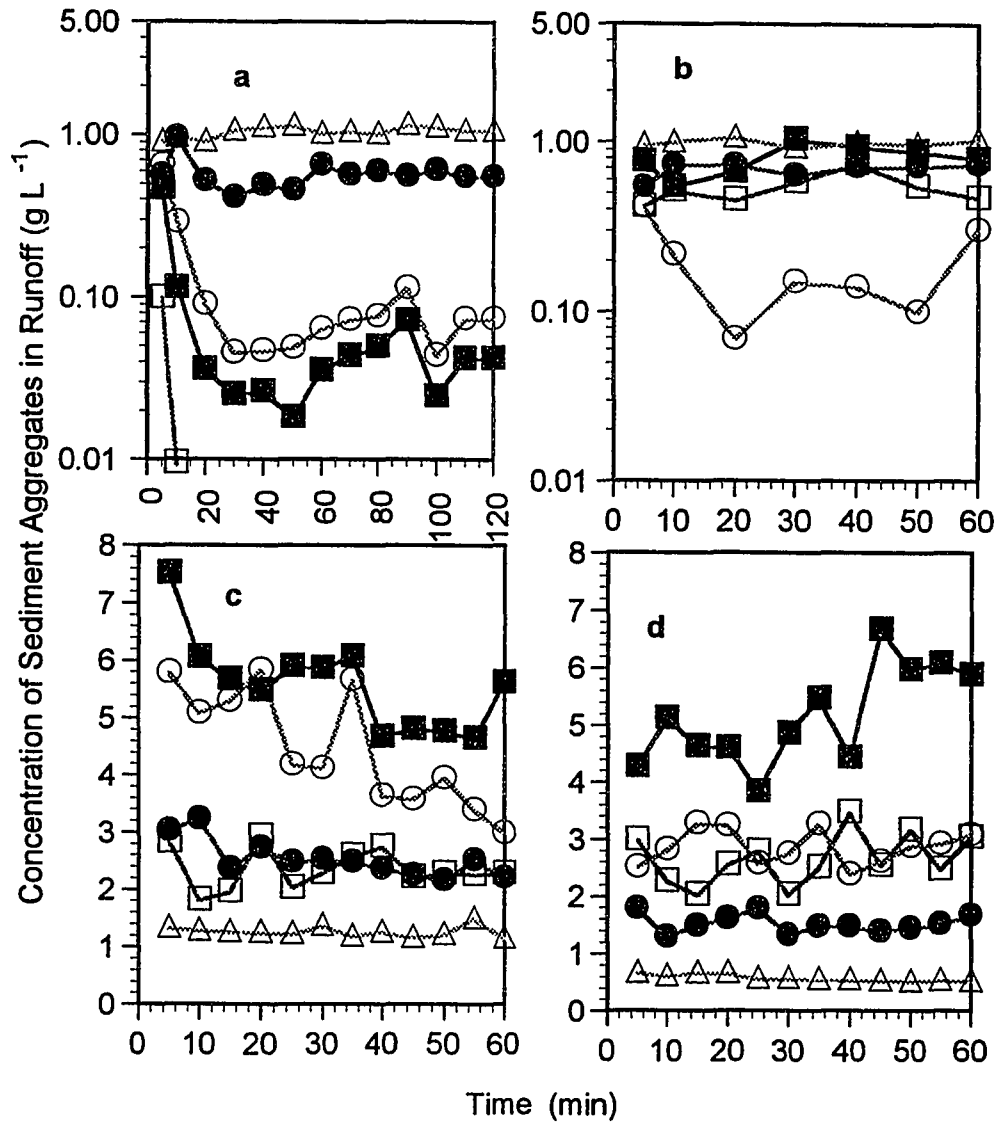


Figure 6.2 Temporal variation in concentrations of aggregate size fractions: (\square) >2 mm, (\blacksquare) 2-0.5 mm, (\circ) 0.5-0.063 mm, (\bullet) 0.063-0.005 mm, and (\triangle) <0.005 mm) in runoff during a. dry run, b. wet run, c. very wet run, and d. plastic mulch run .

A slight increase of flow energy (about 10% increase in stream power) in the wet run resulted in elevated concentrations of sand-sized aggregates (Figure 6.2b). The concentration of fine aggregates <0.063 mm remained almost the same as that for the dry run. The concentrations of various sediment size fractions in runoff varied over a narrow range during the run. The increased coarseness of sediment with increased flow energy was more pronounced in the very wet and the plastic mulch runs (Figure 6.2 c&d). Under these conditions flow detachment prevailed and thus coarse aggregates (>2 mm, 0.5-2 mm, and 0.063-0.5 mm), somewhat representative of the soil matrix, dominated sediment output.

During the very wet run (Figure 6.2c), sand-sized aggregates (0.5-2 mm and 0.063-0.5 mm) constituted over 60% of the sediment load. The concentration of these aggregates declined slightly with time, probably due to the initial transport of the coarse deposited layer formed during the previous runs. Concentrations of the other fractions stayed almost unchanged during the entire run. It is interesting to note that the concentration of fine aggregates (<0.063 mm) was even higher than that of the dry run. This elevated concentration was associated with increased interrill sediment delivery rate under high rainfall intensity. This suggested that the loss of these fine aggregates per unit volume of runoff should be correspondingly higher in the very wet run than in the dry run.

During the plastic mulch run (Figure 6.2d), sand-sized aggregates were still dominant. However, the concentrations of the finer fractions: 0.063-0.5 mm, 0.005-0.063 mm, and <0.005 mm were less than those for the very wet run. This decline in transport of finer aggregates was again mostly associated with the virtual absence of interrill erosion which restricted the sediment availability for rill flow transport. Since the plastic mulch eliminated the interrill sediment delivery into the rill flow, there was less fine sediment

available for transport than for the unmulched soil. Instead, the transported sediment was mostly derived directly from the in-situ soil in the furrow bed as it was entrained by rill flow. This process is commonly considered to be aselective (Rose, 1993). The increased concentration of the 0.5-2 mm fraction with time suggested that sediment detachment by runoff was active in the plastic mulch run.

The change of sediment aggregate size fractions relative to the "reference" aggregate size distribution of the in-situ soil can be seen from Figure 6.3. The median aggregate size (D_{50}) was 0.01 mm for the dry run, 0.05 mm for the wet run, 0.47 mm for the very wet run, and 0.85 mm for the plastic mulch run, which was similar to that of the in-situ soil. Sediments from the dry and wet runs showed significant enrichment of fine aggregates (<0.063 mm). Aggregate size distributions for sediment from the very wet and plastic mulch runs approached that of the in-situ soil though fine aggregates were still somewhat enriched. These differences again reflected the influence of flow hydraulics, the interrill-rill erosion dynamics, and sediment availability on sediment size composition discussed earlier.

6.3.3 Primary particle size distribution

Particle size distribution was determined on three composite sediment samples from each storm since the amount of sediment available was limited for this analysis (Table 6.3). These composite samples for each event were prepared by combining three to four sediment samples taken in a temporal sequence during the storm so the difference of particle size distribution between samples in a specific event also reflected the temporal variation. The results indicated that only minor variations existed for sand and silt fractions between the dry run and other storms. The sediment from the dry run consisted primarily

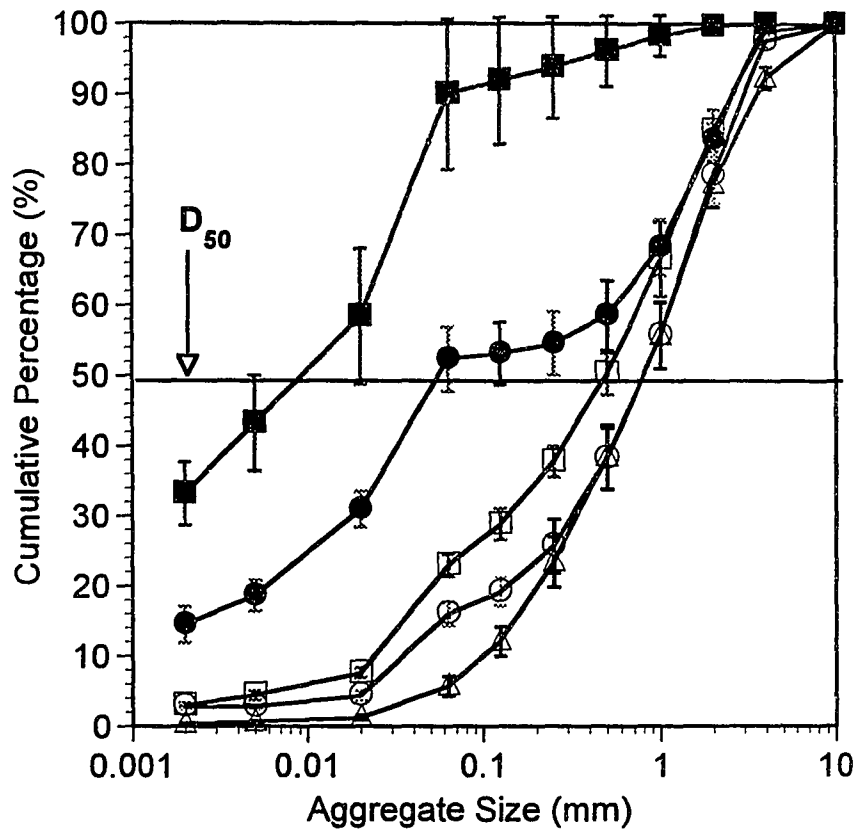


Figure 6.3 Aggregate size distributions of sediment from the four events: (■) dry run, (●) wet run, (□) very wet run, (○) plastic mulch run and of (Δ) in-situ soil. Error bars are 95% confidence intervals.

Table 6.3 Primary particle size distributions and clay enrichment ratios of sediment from the four rainfall events †

Event	Sample	Sand ($>53 \mu\text{m}$)	Silt ($53\text{-}2\mu\text{m}$)	Clay ($<2 \mu\text{m}$)	ER of clay
		<----- % ----->			
Dry run	1	0.24	10.61	89.15	1.00
	2	0.19	10.74	89.07	1.00
	3	0.20	10.47	89.33	1.00
	Mean	0.21b	10.61a	89.18a	1.00a
Wet run	1	1.49	9.55	88.96	1.00
	2	1.67	10.04	88.29	0.99
	3	1.52	9.71	88.77	1.00
	Mean	1.56a	9.76ab	88.68a	1.00a
Very wet run	1	1.44	10.44	88.12	0.99
	2	1.47	9.64	88.89	1.00
	3	1.03	10.43	88.54	0.99
	Mean	1.32a	10.16ab	88.52a	1.00a
Plastic mulch run	1	1.37	9.19	89.44	1.00
	2	1.32	8.84	89.84	1.01
	3	1.54	10.28	88.18	0.99
	Mean	1.41a	9.43b	89.16a	1.00a

† Means in a column followed by the same letter are not significantly different at $\alpha = 0.05$ with the Fisher's Protected Least Significant Difference (LSD) test.

of aggregates $< 0.063 \text{ mm}$, and thus had less sand. Other than that sediment from these four storms, though characterized with distinct aggregate size distributions, did not show a significant difference in dispersed particle size distributions either between events or between samples within an event. This was particularly true for the clay fraction which had ER values not significantly different from 1.0. This finding is contrary to many studies on temperate soils which indicated that overland flow, particularly in interrill area, selectively transports clay particles (e.g., Sharpley, 1985; Parsons et al., 1991). However, this finding

is not surprising in view of the very high content of clay-sized primary particles and strong intra-aggregate bonds in this Oxisol (El-Swaify, 1980). Table 6.4 shows particle size distributions of various aggregate size fractions of the in-situ soil (obtained from the reference aggregate size distribution analysis). The average clay content in all aggregate size fractions (88-89%) was similar to that of the whole soil and collected sediment shown in Tables 6.1 and 6.3. The aggregate enrichment ratio (AER), which is defined as the clay content or nutrient concentration in a specific aggregate size fraction divided by that of the whole soil (ER is reserved for use with the whole sediment), is used here to compare clay distribution within aggregate size fractions. The calculated clay AER values were all close to 1, indicating that clay is uniformly distributed in all aggregate size fractions. With less uniformly textured temperate soils, Meyer et al. (1992) found that larger aggregates contained more sand and clay than smaller aggregates.

Table 6.4 Primary particle size distributions and clay aggregate enrichment ratios for aggregates of varying size fractions[†]

Size (mm)	Sand ($>53 \mu\text{m}$)	Silt ($53\text{-}2\mu\text{m}$)	Clay ($<2 \mu\text{m}$)	AER of clay
	←----- % ----->			
>4	1.17ab	9.94a	88.89a	1.00a
2-4	1.35a	10.62a	88.03a	0.99a
1-2	1.27a	9.95a	88.78a	1.00a
0.5-1	1.26a	9.96a	88.79a	1.00a
0.25-0.5	1.10ab	9.11a	89.78a	1.01a
0.125-0.25	1.00ab	9.10a	89.90a	1.01a
0.063-0.125	0.80b	9.53a	89.67a	1.01a
<0.063	0.09c	10.82a	89.09a	1.00a
LSD (0.05)	0.39	2.95	2.72	0.00

[†] Means in a column followed by the same letter are not significantly different at $\alpha = 0.05$ with the LSD test.

6.3.4 Organic carbon and extractable phosphorus

Table 6.5 and Figure 6.4 shows the time-averaged OC enrichment ratio (ER_{oc}) and its change with with time for the four storms, respectively. Temporal variations in ER_{oc} were apparent for the dry run. The ER_{oc} was low initially for the first 5 min, peaked at 20-30 min, and then declined to an equilibrium value of about 1.2. This temporal variation was partially associated with the transport of the fine and easily removable organic residues. The existence of fine organic constituents in runoff was visually observed during wet sieving analyses and the amount decreased with time. This temporal variation was also observed by Palis et al. (1990 a&b) with a less well-aggregated soil. The ER_{oc} values for other events were lower than that of the dry run, decreasing in the sequence of wet run (about 1.1) > very wet run (about 1.03) ≈ plastic mulch run (about 1), a trend which is similar to that of median aggregate size diameter. The ER_{oc} values for these latter storms stayed nearly unchanged during the entire duration of specific rainfall events.

Table 6.5 Comparison of time-averaged ER values for OC and Ext-P †

Event	Mean	Standard deviation	Mean	Standard deviation
	<----- ER_{oc} ----->		<----- ER_p ----->	
Dry run	1.216a	0.059	1.394a	0.071
Wet run	1.098b	0.022	1.237b	0.053
Very wet run	1.030c	0.027	1.102c	0.030
Plastic mulch run	1.000c	0.016	1.029d	0.045
LSD(0.05)	0.040		0.068	

† Means in a column followed by the same letter are not significantly different at $\alpha = 0.05$ with the LSD test

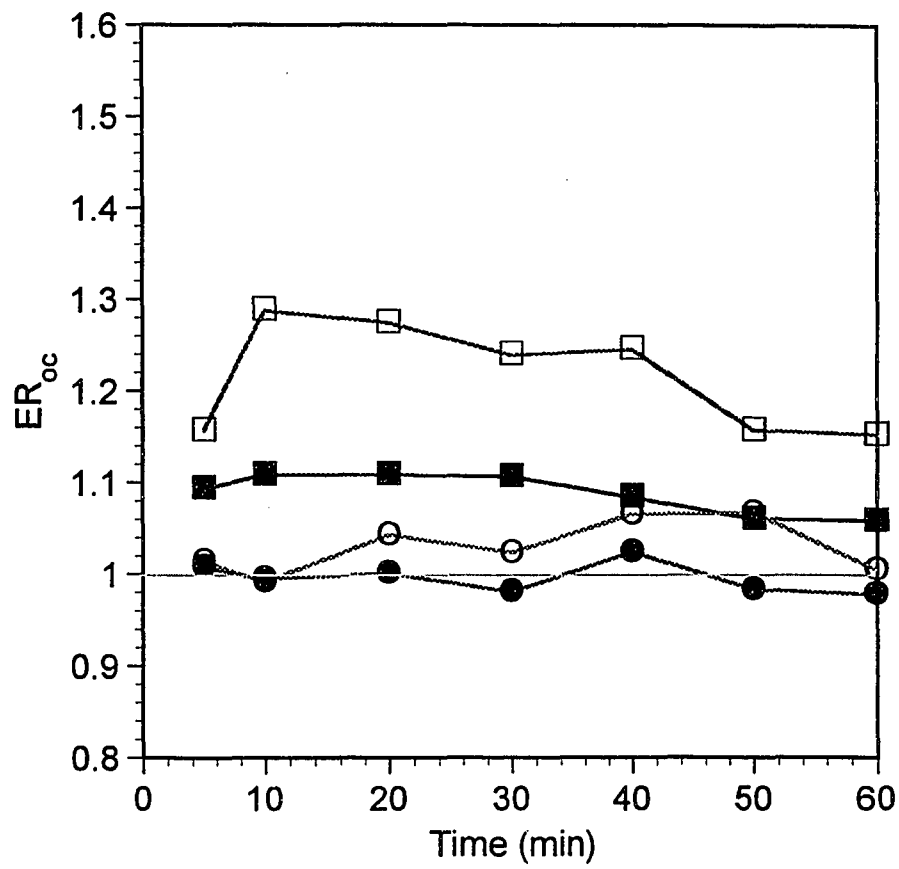


Figure 6.4 Temporal variation in enrichment ratio of organic carbon (ER_{oc}) during (\square) dry run, (\blacksquare) wet run, (\circ) very wet run, and (\bullet) plastic mulch run.

In nonpoint source pollution by nutrients, transport of P has been commonly considered to be in a sorbed form by fine soil mineral particles (Sharpley, 1980 & 1985; Avnimelech and McHenry, 1984). The similarity between clay content in sediments and the in-situ soil is expected to produce no P enrichment in sediments. Contrary to this assumption, Figure 6.5 and Table 6.5 indicated that values of ER for sorbed P extracted by Mehlich 3 solution (ER_p) were mostly above 1. Values of ER_p were about 1.4 for the dry run and 1.2 for the wet run, which were larger than those of ER_{oc} . For the very wet and the plastic mulch runs, ER_p values were about 1.1 and 1.03, again smaller than those of the dry and wet runs. The ER_p for the dry run was lower than 1.3 initially, increased to nearly 1.5 and then leveled off after 30 min. Variations of ER_p with time for other storms were relatively small.

The similarity between trends in ER_{oc} , ER_p , and sediment aggregate size composition (Figures 6.2 and 6.3) suggested that the enrichment of OC and Ext-P were closely associated with sediment aggregate size distributions. Table 6.6 shows the concentration of OC and Ext-P in various aggregate size fractions obtained from the reference soil aggregate size analysis. The AER was again used to quantify the enrichment of OC and Ext-P in specific aggregate size fractions relative to the whole soil. The results showed that OC and Ext-P concentrations generally increased with decreasing aggregate size. When compared with the whole soil, micro-aggregates (<0.25 mm) were enriched with OC and Ext-P. This is particularly true for aggregates < 0.063 mm. Therefore, selective erosion of these chemically enriched fractions was responsible for the high ER_{oc} and ER_p values measured for the dry and wet runs (Figures 6.4 and 6.5), though transport of discrete fine organic residue particles may also have contributed to high ER_{oc} values. The low E_{oc} and ER_p values for the very wet run, the plastic mulch run, and the first 10 min of

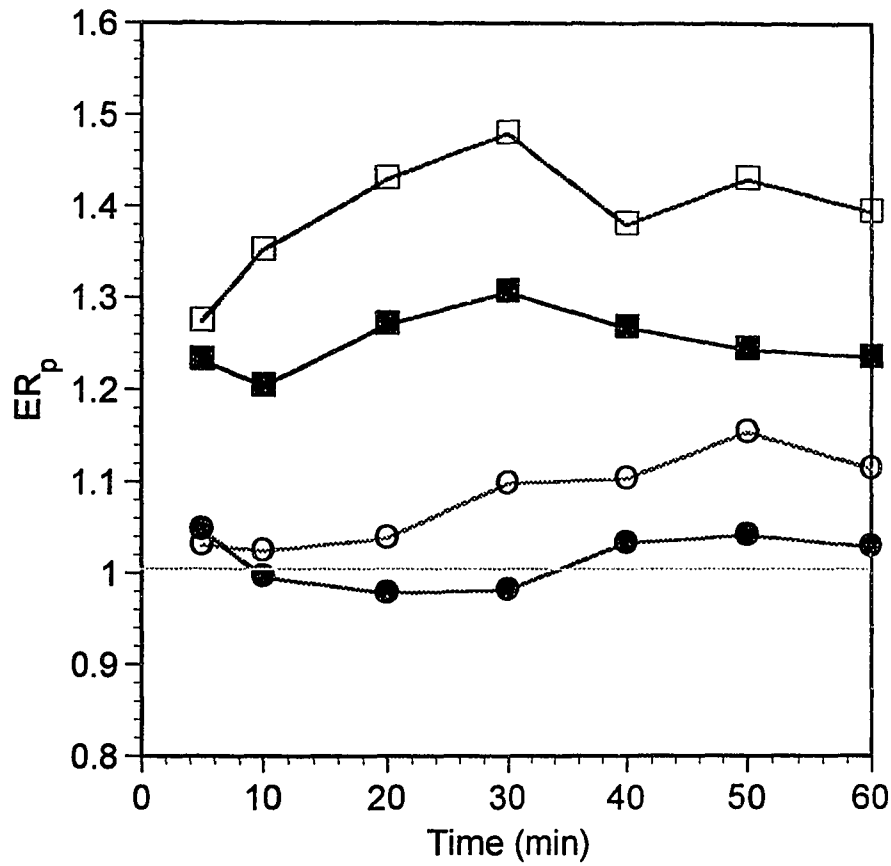


Figure 6.5 Temporal variation in enrichment ratio of extractable phosphorus (ER_p) during (□) dry run, (■) wet run, (○) very wet run, and (●) plastic mulch run.

the dry run can also be attributed to significant transport of large aggregates. The higher dependence of Ext-P on aggregate size was responsible for the larger values of ER_p than ER_{oc} . Since soil OC and P can both be sorbed onto certain soil minerals and inorganic Fe and Al compounds in highly weathered soils, it is unlikely that there was a cause-and-effect relationship between the high concentration of Ext-P in micro-aggregates and their high OC content. Two possible mechanisms may be responsible for the unexpected OC and P enrichment in fine aggregates. First, the fabric of soil aggregates might have blocked or retarded sorption inside large aggregates and resulted in preferential accumulation of P and OC in fine (highly exposed surface) aggregates. Second, accumulation of OC and P was uniform among various aggregate fractions but rainfall impact may produce fine aggregates which are richer in OC and chemical than larger aggregates (Ghadiri and Rose, 1991a&b). These potential mechanisms were further studied in Chapter 7.

Table 6.6 Organic C and Ext-P concentrations and aggregate enrichment ratio (AER) for aggregates of varying size fractions[†]

Size (mm)	OC (%)	AER _{oc}	Ext-P (mg kg ⁻¹)	AER _p
>4	1.49cd	0.98	72.01e	0.75
2-4	1.48cd	0.96	85.73d	0.89
1-2	1.40d	0.93	89.13d	0.92
0.5-1	1.48cd	0.98	92.41d	0.96
0.25-0.5	1.51bc	1.00	102.2c	1.06
0.125-0.25	1.54bc	1.02	117.4b	1.22
0.063-0.125	1.60b	1.05	122.7ab	1.27
<0.063	1.89a	1.41	130.6a	1.35
LSD (0.05)	0.10		8.90	

[†] Means followed by the same letter in a column are not significantly different at $\alpha = 0.05$ with the LSD test.

6.4 Conclusions

The concentration and aggregate size distribution of sediment transported by overland flow in a ridge-and-furrow system was influenced by flow hydraulics, interrill-rill erosion dynamics, and sediment availability for transport. The shear stress or stream power of the flow in the dry and wet runs (rainfall intensity of 35 mm h^{-1}) did not significantly exceed the threshold value required for flow detachment, resulting in a low sediment concentration (about $1.7\text{-}3.5 \text{ g L}^{-1}$) and preferential transport of fine aggregates $<0.063 \text{ mm}$. In addition to the initial flush of loose sediment, sediment concentration and aggregate size distribution stayed nearly unchanged with time and flow rate. Increase in flow rate and thus flow stream power and shear stress elevated sediment concentration to 12 g L^{-1} for the very wet and the plastic mulch runs. The increase in sediment concentration was mainly associated with transport of sand-sized aggregates. Elimination of interrill erosion with plastic mulch decreased sediment concentration and the content of fine aggregates in comparison with the bare soil condition in the very wet run. Sediment from the four events did not display physical enrichment of dispersed clay particles due to the strong aggregation, high clay content, and the uniformly-textured nature of the soil. However, OC and Ext-P were both enriched in sediment with ER magnitudes in the following order: dry run > wet run > very wet run > plastic mulch run. The enrichment of OC and Ext-P was associated with selective transport of fine aggregates which were chemically richer than the coarser ones. Since primary particle size distribution does not vary with aggregate size, the mechanism responsible for the enrichment of OC and P in fine aggregates requires further study.

CHAPTER 7

SEDIMENT ENRICHMENT BY ORGANIC CARBON AND PHOSPHORUS: IMPLICATIONS OF FERTILIZATION, AGGREGATE BREAKDOWN BY RAINFALL, AND SELECTIVE TRANSPORT OF FINE AGGREGATES

Abstract

Three interrelated experiments were carried out to study the effects of fertilization and aggregate breakdown by rainfall on organic carbon (OC) and extractable phosphorus (Ext-P) concentrations in aggregate size fractions of a well-aggregated and uniformly-textured Oxisol. Soil samples presented four field treatments: no fertilization (NF), long-term P fertilization (LTP), short-term P fertilization (STP), and organic waste fertilization (OW). Organic C content in dry-sieved aggregates increased for all treatments with decreasing aggregate size, suggesting that OC in small aggregates is more persistent and protected from microbial attack. Ext-P concentration in aggregates from the NF treatment did not vary with aggregate size. Upon addition of P in STP and OW treatments, Ext-P concentration increased significantly with decreasing aggregate size. This was attributed to the blockage of interior P sorption sites within aggregates. Selected large aggregate fractions (4-10 mm and 2-4 mm) from STP and OW treatments were exposed to 20 and 60 min of simulated rainfall. These fractions were broken down into a wide spectrum of finer and more stable aggregates within 20 min of rainfall, suggesting that the rapid breakdown of large aggregates or "crumbs" upon wetting and rainfall impact (slaking) occurred. The resulting fine aggregates (mainly <0.063 mm) were richer in OC and Ext-P than the larger ones. Extended rainfall impact (60 min) only slightly increased the content of small aggregates (<0.25 mm), indicating that further breakdown of fine water stable aggregates (peeling or

stripping) was more difficult and slow. An interrill erosion experiment with a liquid-P treated and incubated soil sample further verified the aggregation blockage mechanisms for P sorption. Selective transport of OC and Ext-P rich fine aggregates (<0.25mm) was responsible for sediment enrichment. Continuous aggregate breakdown by rainfall produced aggregates containing less OC and Ext-P than those in the original soil and was partially responsible for the decline in enrichment ratio with time. For the LTP treatment, however, differences between Ext-P concentrations in various aggregate size fractions were not significant, suggesting that P sorption and desorption, P diffusion into inner regions of aggregates, and P mixing by aggregate breakdown and reaggregation had effectively brought about a uniform Ext-P distribution. Thus selective transport of fine aggregates may not necessarily result in Ext-P enrichment when soils are allowed sufficient time to equilibrate with the applied fertilizer.

7.1 Introduction

The loss of soil organic carbon (OC) and phosphorus (P) in runoff is of increasing concern due to the resulting impact on soil and water quality. This concern is especially acute considering that OC and P are often enriched in sediment in comparison with the in-situ soil (Massey and Jackson, 1952; Stoltenberg and White, 1953; Bhatt, 1976; Alberts and Moldenhaur, 1981; Alberts et al., 1983; Sharpley, 1985; McIsaac et al. 1991). Since both OC and P are strongly sorbed, or in close association with soil clay particles, selective or preferential erosion of fine primary particles has been proposed to be the mechanism responsible for this enrichment (Foster et al. 1985; Sharpley 1985; Flanagan and Foster 1989). This mechanism explains sediment enrichment of OC and P for poorly aggregated

and non-uniformly textured soils, where clearly preferential transport of primary fine particles is the consequence of selective soil erosion processes (Sharpley, 1985).

Mechanisms other than enrichment of clay may play a major role when sediment is mostly transported as aggregates. Results reported in Chapter 6 indicated that sediment enrichment of OC and Extractable P (Ext-P) for a well-aggregated and uniformly-textured Oxisol (containing about 90% clay) was not due to selective erosion of clay particles since sediment exhibited a similar particle size distribution in comparison with the in-situ soil. Instead, the potential mechanism was associated with selective erosion of fine aggregates which were richer in Ext-P and OC than the coarser ones. The question left unanswered is whether these chemically enriched fine aggregates are intrinsic in the soil or are produced during the soil erosion process. For a well aggregated soil containing 55% clay, Ghadiri and Rose (1991a&b) found that differences between concentrations of OC and sorbed chemicals in various aggregate size fractions were not significant. However, OC and sorbed chemicals mainly coated on the outside layer of an individual soil aggregate. They therefore hypothesized that raindrops initially performed an overall washing to remove the thin chemically enriched layer of fine aggregates from the surface of larger aggregates and preferential transport of these stripped fine aggregates were responsible for sediment enrichment. It is, however, not clear whether this stripping mechanism is also responsible for sediment enrichment for the stable and well-aggregated Oxisol used in this study. In addition, immediate breakdown of unstable aggregates may coexist with the gradual stripping process. Investigation of aggregate breakdown by raindrop impact and its contribution to sediment enrichment was one of the objectives of this study.

The distribution of OC and P in aggregate size fractions is also influenced by soil fertilization practices. Bhatnagar et al. (1985), using a loam soil, observed that sediment

from manure treated plots was less enriched with Ext-P than that from inorganic P fertilizer treated plots. They suggested that this was because large aggregates (> 2 mm) adsorbed more P and OC than smaller ones upon the addition of manure (Bhatnagar et al., 1985; Bhatnagar and Miller, 1985). Mbagwu (1990), on the other hand, reported that upon applying organic waste, preferential accumulation of OC and P occurred with smaller aggregate size fractions due to their larger clay content. In Hawaii, large amounts of inorganic P fertilizers are required for agriculture on highly weathered soils. Organic wastes are also used, or proposed, as a substitute for chemical fertilizers to correct P deficiency (Hue, 1990). Investigation of the influence of these fertilization practices on OC and P accumulation in aggregate size fractions and thus on sediment enrichment was another objective of this study.

7.2 Materials and Methods

The following experiments were conducted with the Wahiawa silty clay (Rhodic Eutrodox). All soil samples (0-10 cm) were taken from the Poamoho Experiment Station, Oahu, Hawaii. Organic C was analyzed with a LECO Carbon analyzer. Discrete and visible plant residues not associated with aggregates were carefully removed during sample preparation. Ext-P was extracted with the Mehlich 3 solution (Mehlich, 1985) and was determined following the procedure of Murphy and Riley (1962).

7.2.1 Dry-sieving experiment

This experiment was designed to examine the influence of soil fertilization practices on OC and Ext-P distributions in different dry-sieved aggregate size fractions. Dry-sieving

was used since it provided the least breakdown of aggregates or "crumbs". Four sampling plots were chosen to represent different soil fertilization treatments: no fertilization (NF), short-term P application (STP), long-term P application (LTP), and organic waste application (OW). The NF plot was a control plot with no fertilization or cultivation in the past 30 years. The STP plot was used for the soil erosion study in Chapters 4 and 6, and had received inorganic P fertilizer over the last 10 years. The average application rate in the most recent five years was about $150 \text{ kg P ha}^{-1} \text{ y}^{-1}$. The LTP plot was used for a long-term soil fertility study by Fox and Yost (personal communication). Initial P fertilization (inorganic) was applied at the rate of $700 \text{ kg P ha}^{-1} \text{ y}^{-1}$ to provide a soil solution P of 0.4 mg L^{-1} in 1970. Additional fertilizer at the rate of $40\text{-}490 \text{ kg P ha}^{-1} \text{ y}^{-1}$ had been applied to "maintain" this P level in solution until 1992. Since then the plot has been left fallow in an uncultivated condition. The OW plot was used for long-term organic waste studies by Hue (1990). In 1983 sewage sludge was initially applied at the rate of 180 Mg ha^{-1} , and in 1994 a commercial compost was applied at the rate of 30 Mg ha^{-1} (the soil sample was taken 12 months later). The organic wastes applied contained about 1.2% P, serving as the major P source for plant growth. During this period, only limited inorganic P fertilizer (120 kg P ha^{-1}) was applied in 1987. Selected soil physical and chemical properties of the soil subjected to these treatments are given in Table 7.1.

Three replicated soil samples were taken from each of the plots. The samples were air-dried and passed through a nest of sieves with 10, 4, 2, 1, 0.5, 0.25, 0.125, and 0.063 mm openings. Remaining crumbs $> 10 \text{ mm}$ were carefully broken by hand to pass through the 10 mm sieve. The OC and Ext-P concentrations in these "aggregate" fractions were determined.

Table 7.1 Selected soil properties of the Wahiwa soil receiving different fertilization treatments

Properties	NF	STP	OW	LTP
pH	5.31	5.91	4.90	5.90
Exchangeable Cations (+cmol/kg)				
Ca	2.06	3.25	3.09	2.96
Mg	0.36	0.40	0.38	0.48
K	2.48	2.02	2.83	2.88
Na	0.60	0.65	0.63	0.77
Particle size distribution (%)				
Sand (>53 μm)	2.563	1.329	2.264	2.103
Silt (53-2 μm)	9.277	9.601	9.216	8.167
Clay (<2 μm)	88.16	89.08	88.54	89.73
Dry-sieved aggregate size distribution (%)				
4-10 mm	19.23	25.18	28.69	22.22
2-4 mm	13.39	16.57	14.34	18.77
1-2 mm	16.47	16.10	17.14	17.40
0.5-1 mm	17.48	15.35	16.84	15.95
0.25-0.5 mm	16.59	13.44	14.16	13.57
0.125-0.25 mm	9.994	8.125	5.502	7.154
0.063-0.125 mm	4.964	4.094	2.513	3.583
<0.063 mm	1.882	1.161	0.824	1.373

7.2.2 Aggregate breakdown experiment

The breakdown of aggregates by rainfall impact and its contribution to sediment enrichment were studied in this experiment. Only the 4-10 mm and 2-4 mm fractions of dry-sieved aggregates with STP and OW treatments were used. These two fractions were selected since they accounted for about 40% of the whole soil, and they are more likely to be disrupted by rainfall impact than the smaller ones. A 50-g sample of dry-sieved

aggregates was evenly placed on the bottom of a 10 cm diameter sieve with 0.063 mm openings. A 30 cm PVC pipe with the same diameter was connected to the sieve to act as a splash guard so that only aggregates < 0.063 mm may leave the sieve with drainage water. The whole setup was placed in a bucket to allow the capture of breakdown products. The drip-type laboratory rainfall simulator described in detail in Chapter 2 was used. The bucket containing the aggregate sample was placed under the rainfall simulator and received rainfall with a constant intensity of 65 mm h⁻¹ for 20 and 60 min. During rainfall simulation ponding did not occur, due to percolation through the sieve, and this allowed the aggregates to directly receive raindrop impact. This simulated the effect of splash in interrill erosion (Chapters 2&3) or the effect of rainfall detachment and redetachment as defined by Proffitt et al. (1991).

Immediately after the simulated rainfall, the sample in the system was passed through a nest of sieves with 4, 2, 1, 0.5, 0.25, 0.125, and 0.063 mm openings, and aggregate size distributions were determined. Concentrations of OC and Ext-P in these aggregates size fractions were determined only for samples receiving 20 min rainfall. This experiment was replicated three times.

7.2.3 Interrill erosion experiment

This experiment was designed to further elucidate how the P fertilizer was associated with various aggregates and its relationship to sediment enrichment. Only the NF soil sample was used. About 13 kg of air-dried soil was uniformly mixed with a liquid P fertilizer containing Ca(H₂PO₄)₂ at a rate equivalent to surface application of 500 kg P ha⁻¹, which is typical for this soil during initial P fertilization. The fertilized soil had a soil moisture content of about 33%, close to well-drained field soil moisture conditions 2-3 days after

rainfall. This mixture was left for 24 h to allow for partial equilibrium between P and the soil and thus only "fast reactions" occurred. The fertilized soil was then uniformly packed in a 60 (length) by 30 (width) cm soil tray, resulting in a soil bulk density of about 1 Mg m^{-3} . The soil tray was placed under the drip-type rainfall simulator with a 9% slope. A 2-h storm with a constant rainfall intensity of 130 mm h^{-1} was applied. Runoff was collected and measured every 10 min after rainfall started. Immediately after the simulated rainfall, collected runoff samples were passed through a nest of sieves with 4, 2, 1, 0.5, 0.25, 0.125, and 0.063 mm openings, and aggregate size distributions were determined. Concentrations of OC and Ext-P in these aggregate size fractions were determined. Aggregate size distribution of the eroded surface samples taken after rainfall was also determined. This experiment was not replicated.

7.3 Results and Discussion

7.3.1 Dry sieving experiment

Tables 7.2 shows OC contents in various dry-sieved aggregate size fractions of the soil receiving different soil fertilization treatments. The one-way analysis of variance performed with these data indicated significant differences of OC content between aggregate size fractions within a treatment and between treatments within a specific aggregate size fraction ($P < 0.001$). Overall OC content increased with decreased aggregate size. For the NF treatment, OC in macro-aggregate fractions ($> 0.25 \text{ mm}$) was around 1.5%, and increased significantly with decreased size for micro-aggregate fractions ($< 0.25 \text{ mm}$). For STP and LTP treatments, OC content in most aggregate size fractions was lower than for the NF treatment, probably due to the accelerated decomposition of OC under cultivated

conditions. The variation of OC content with aggregate size was similar to that for the NF treatment, with the LTP treatment showing more depletion within large aggregates. The OW treatment resulted in elevated OC content in all aggregate size fractions. The increase of OC content with decreasing aggregate size was particularly evident, with OC ranging from 1.5% in the 4-10 mm fraction to 3.5% in the <0.063 mm fraction.

Table 7.2 Contents of OC in dry-sieved aggregates of varying size for the Oxisol receiving different fertilization treatments[†]

Size fraction (mm)	NF	STP	OW	LTP
	<----- % ----->			
Bulk soil	1.620	1.512	2.209	1.298
4-10	1.500e	1.490c	1.550g	1.082g
2-4	1.535de	1.482c	1.625g	1.110fg
1-2	1.570de	1.510bc	1.877f	1.126f
0.5-1	1.592d	1.491c	2.058e	1.318e
0.25-0.5	1.604d	1.500c	2.351d	1.369d
0.125-0.25	1.750c	1.550cb	2.735c	1.531c
0.063-0.125	1.981b	1.622b	3.307b	1.838b
<0.063	2.169a	2.013a	3.540a	1.839a
LSD(0.05)	0.092	0.113	0.128	0.039

[†] Means in a column followed by the same letter are not significantly different at $\alpha = 0.05$ with the Fisher's Protected Least Significant Difference (LSD) test.

The Ext-P distribution among aggregates of various sizes responded differently with soil fertilization treatments. Table 7.3 indicated that Ext-P concentration with the NF treatment was low and uniform among aggregate size fractions (about 10 mg kg⁻¹). Upon addition of P fertilizers, either in inorganic form (STP) or in organic form (OW), there existed a preferential accumulation of P in small aggregates. As shown in Table 7.3, the

concentration of P increased from 93.2 mg kg⁻¹ in the 4-10 mm fraction to 161.1 mg kg⁻¹ in the <0.063 mm fraction for the STP treatment. This increase was even more pronounced for the OW treatment (from 81.8 mg kg⁻¹ in the 4-10 mm fraction to 205.2 mg kg⁻¹ in the <0.063 mm fraction). However, such preferential accumulation of P in small aggregates vanished in the LTP treatment as evidenced by a rather uniform P concentration around 185 mg kg⁻¹ for all aggregate sizes.

Table 7.3 Concentrations of Ext-P in dry-sieved aggregates of varying size for the Oxisol receiving different fertilization treatments[†]

Size fraction (mm)	NF	STP	OW	LTP
	<----- mg kg ⁻¹ ----->			
Bulk soil	11.25	108.1	151.3	187.6
4-10	10.74a	93.16f	81.81f	188.9a
2-4	10.00a	103.4e	87.08f	184.3a
1-2	10.75a	111.0ce	121.9e	184.2a
0.5-1	11.26a	109.4ce	128.1e	180.6a
0.25-0.5	10.57a	116.4cd	151.0d	185.4a
0.125-0.25	11.60a	123.4c	167.2c	184.2a
0.063-0.125	11.77a	141.5b	182.6b	184.7a
<0.063	12.28a	161.2a	205.2a	180.6a
LSD(0.05)	2.73	9.16	6.45	8.44

[†] Means in a column followed by the same letter are not significantly different at $\alpha = 0.05$ with the LSD test.

It has been well documented that OC and P concentrations in aggregates are closely related to their clay contents (Christensen, 1986; Mbagwu, 1990). For this uniformly-textured soil (Table 7.1), there are, however, other mechanisms responsible for the preferential accumulation of OC and P in small aggregates. The most plausible

explanation for OC is that soil organic matter associated with micro-aggregates is more persistent or is more protected from microbial attack and decomposition while that associated with macro-aggregates is more labile or more decomposable (Elliot, 1986). This may be partially responsible for the reduced OC content in macro-aggregates of STP and LTP treatments. Decreased P concentration with increasing aggregate size in the OW and STP treatments is most likely due to the reduced accessibility of intra-aggregate surfaces to P in soil solution (Horn et al., 1994). This aggregation "blockage" mechanism may also be applicable for sorption of newly added organic substances as evidenced by OC accumulation in aggregates under the OW treatment. The aggregation blockage mechanism will be further clarified later within the context of the interrill erosion experiment.

Unlike OC, soil solution P entrapped in intra-aggregate pores as an "immobile" phase may undergo further diffusion into the inside of aggregates. Kinetics of this diffusion process, however, are likely very slow (Vaidyanathan and Talibudeen, 1968), and depend primarily on time. The relative uniformity of P in aggregates size fractions for the OW, STP, and LTP treatments may shed some light on the effect of fertilization history on this diffusion process. Given a finite P source and time, uniform distribution within aggregate size fractions may be eventually reached as evidenced by the LTP treatment. The aggregate breakdown and reaggregation process through tillage, irrigation and rainfall impact can also contribute to a more uniform distribution of OC and P within aggregates. The rainfall impact on this process will be further discussed in the next section.

7.3.2 Aggregate breakdown experiment

To investigate the breakdown process of an individual aggregate fraction under rainfall impact and the contribution of this process to sediment enrichment, aggregate

fractions of 4-10 and 2-4 mm from STP and OW treatments were exposed to simulated rainfall under an intensity of 65 mm h⁻¹ for 20 and 60 min, consecutively. The obtained aggregate size distributions are shown in Figure 7.1. For the two largest fractions studied, a broad spectrum of aggregates with varying sizes were produced upon rainfall impact, indicating that these large "aggregates" are actually unstable crumbs formed by a collection of smaller but more stable aggregates. The distribution was skewed to >0.5 mm fractions which accounted for about 85% of the total mass of aggregates. This skewness was particularly apparent for the 2-4 mm fraction, indicating that the smaller dry aggregates are more stable. These results are supported by the "aggregate hierarchy concept" of Dexter (1988), who stated that larger aggregates will be weaker because they contain large pores which constitute planes of failure when an aggregate is stressed.

Tables 7.4 and 7.5 show OC and P concentrations in these aggregates as produced by a 20 min rainfall. For most cases, OC and Ext-P contents in aggregates >0.063 mm were similar and not significantly different from one another ($\alpha = 0.05$). The finest fractions (<0.063 mm), however, consistently contained significantly more OC and Ext-P than the rest. This suggested that aggregate breakdown by rainfall further produced fine aggregates which were richer in OC and P. Thus selective transport of these fine aggregates, as well as those originally in the in-situ soil matrix (as shown in the dry-sieving experiment) is responsible for sediment enrichment.

Figure 7.1 indicated that the 60 min rain produced more fine aggregates than the 20 min one with further breakdown of larger ones. However, this continued aggregate breakdown process was much slower than that during the initial 20 min in terms of production of fine aggregates due to the high aggregate stability of the soil studied (El-Swaify, 1980). It should be noted that this exercise was conducted with the least stable

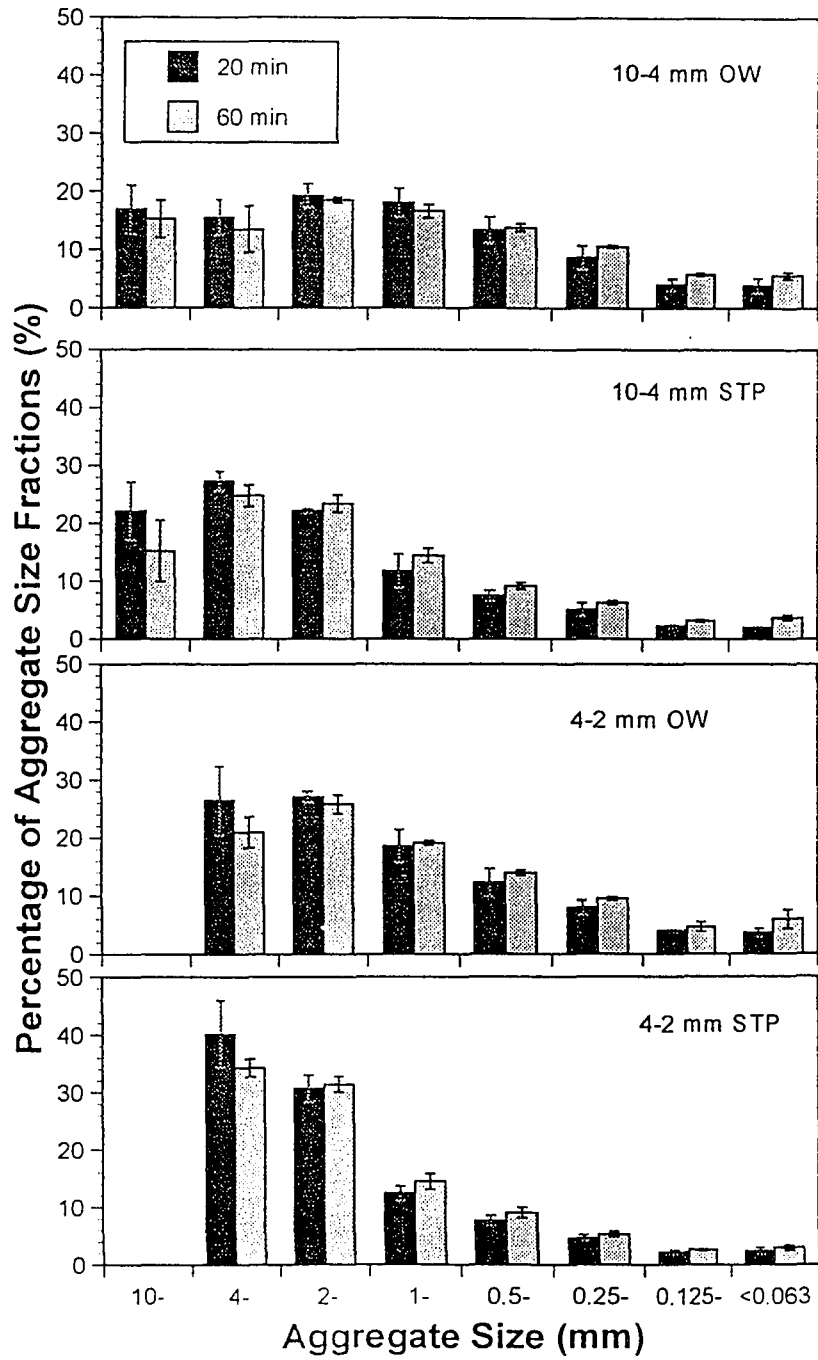


Figure 7.1 Water stable aggregate size distributions of selected dry-sieved fractions under rainfall impact. Error bars are 95% confidence intervals.

Table 7.4 Organic carbon contents in aggregates of varying size produced by a 20-min rainfall from dry-sieved aggregates†

Size fraction (mm)	10-4mm OW	4-2 mmOW	10-4mm STP	4-2 mm STP
	<----- % ----->			
4-10	1.529c		1.436c	
2-4	1.529c	1.481c	1.453bc	1.422bc
1-2	1.500c	1.480c	1.406cd	1.450bc
0.5-1	1.448d	1.518cb	1.362d	1.435bc
0.25-0.5	1.413d	1.485c	1.393cd	1.407c
0.125-0.25	1.429d	1.493c	1.414c	1.434bc
0.063-0.125	1.553b	1.568b	1.496b	1.477b
<0.063	1.805a	1.913a	1.692a	1.691a
LSD(0.05)	0.041	0.051	0.048	0.053

† Means in a column followed by the same letter are not significantly different at $\alpha = 0.05$ with the LSD test.

Table 7.5 Extractable P concentrations in aggregates of varying size produced by a 20-min rainfall from dry-sieved aggregates†

Size fraction (mm)	10-4mm OW	4-2mm OW	10-4mm STP	4-2mm STP
	<----- % ----->			
4-10	64.30c		85.72e	
2-4	73.48b	81.30c	85.55e	101.9bc
1-2	77.90b	83.68c	90.48de	101.7bc
0.5-1	78.24b	84.19c	88.29de	99.15bc
0.25-0.5	75.18b	81.65c	94.05cd	97.11c
0.125-0.25	73.65b	82.19c	98.81bc	101.0bc
0.063-0.125	78.92b	88.59b	100.6b	105.8bc
<0.063	87.59a	105.3a	107.5a	118.7a
LSD(0.05)	8.64	3.64	5.75	6.86

† Means in a column followed by the same letter are not significantly different at $\alpha = 0.05$ with the LSD test.

fractions. Thus for smaller and more stable aggregates, this continued breakdown process should be of even less significance in changing aggregate size distributions. Therefore, the overall aggregate disruption under rainfall impact can be conceptualized as a combination of two processes: rapid slaking and slow stripping. Rapid slaking occurred in the early stages of rainfall, involving aggregate failure along weak planes upon wetting and raindrop impact. This can result in rapid changes in the aggregate size distribution and a significant increase in fine aggregate fractions. The newly produced fine aggregates are likely to be enriched in chemicals since these intra-aggregate pores which act as failure planes are often the most available paths to sorption sites for chemicals. Slow stripping is a "peeling" phenomenon associated with the breakdown of water stable aggregates, described in detail by Ghadiri and Rose (1991a&b). The rate of producing fine aggregates is much less than that of the fast slaking process. The data in Tables 7.1, 7.2, 7.3 and 7.4 indicate that aggregates produced by rainfall contained less OC and Ext-P than those of the same size in the dry-sieving experiments. This may imply that sediment will be less enriched with time as the richer fine aggregates are depleted during an event. A temporal variation of P and OC concentrations in aggregates under rainfall impact will be further discussed in the next section.

7.3.3 Interrill erosion experiment

This experiment was designed specifically to allow newly added P to react with aggregates within a limited time frame (fast reactions) under a soil moisture condition close to field capacity before interrill erosion was imposed. The simulated interrill erosion provided a setting for aggregate breakdown by rainfall and transport by interrill splash and wash. Figure 7.2 shows the changes of runoff rate and sediment concentration with time. During

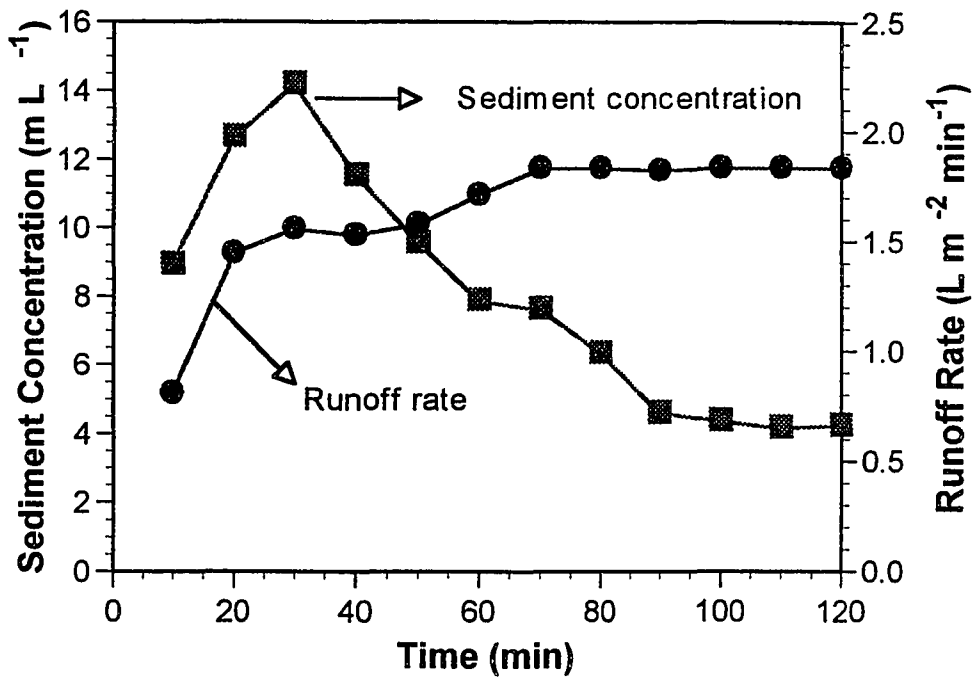


Figure 7.2 Changes of sediment concentration and runoff rate with time during the interrill erosion experiment (rainfall intensity = 130 mm h^{-1}).

the first 10 min sediment concentration and runoff rate were both low. Afterwards, sediment concentration peaked at about 30 min and then declined with time while runoff rate increased with time and reached a steady state after 60 min. This temporal variation has been attributed to either the build-up of a seal (Bradford et al., 1987) or the formation of a selectively deposited layer of coarse particles (Proffitt et al., 1991).

Figure 7.3 shows wet-sieved sediment aggregate size composition and enrichment relative to the in-situ soil. It is noted that the concentration of the <0.063 mm fraction stayed higher than for other fractions and this fraction was highly enriched during the 2-h rainfall. This supports earlier studies on the selectivity of interrill erosion (e.g. Ghadiri and Rose, 1991b). The other fractions enriched included 0.125-0.25 mm and 0.063-0.125 mm. The rest were either depleted or close to unity. Figure 7.3a also shows that the concentration of most fractions in runoff was initially high and then decreased with time. This is particularly so for the <0.063 mm fraction, implying that fine aggregates were produced by the fast slaking process at the beginning of rainfall and were more available for transport. As time went on, a deposit of large and water stable aggregates existed on the soil surface as shown in Figure 7.4. So the initially produced fine aggregates or those originally existing in the soil may be shielded by the deposited layer. These coarse aggregates may further undergo breakdown by the slow stripping process. However, this process was not as efficient in producing fine aggregates for transport as was the fast slaking process. The fine aggregates transported in the later stage of rainfall was only partially derived from stripping since vigorous splash by rainfall can detach sediment from soil in the unshielded areas, and may effectively bring fine aggregates into runoff.

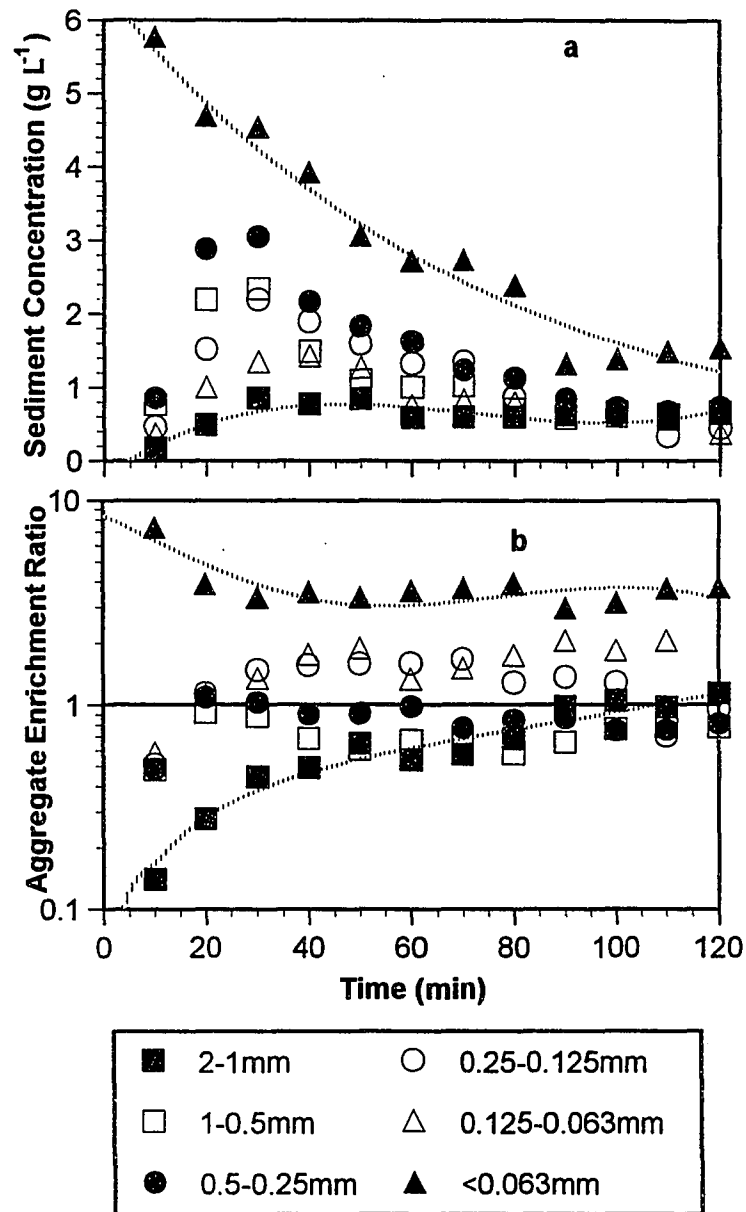


Figure 7.3 Changes of sediment aggregate size composition (a) and enrichment ratios (b) with time during the interrill erosion experiment (rainfall intensity = 130 mm h⁻¹). Dotted lines are fitted to 1-2 mm and <0.063 mm fractions.

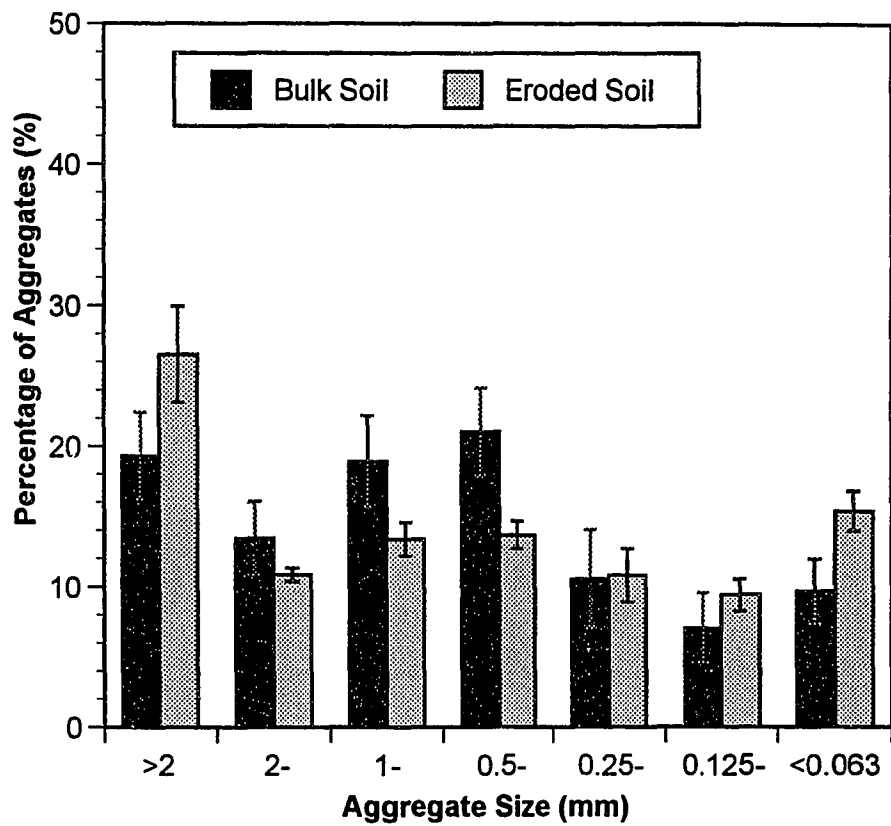


Figure 7.4 Comparison of aggregate size distribution of eroded soil with the in-situ soil. Error bars are 95% confidence intervals.

Figure 7.5a shows P concentration in aggregates and its changes with time. It is clear that P concentration increased as aggregate size became smaller. This confirmed the observations made in the previous section. The only exception was that P concentration in the smallest fraction (<0.063 mm) was only slightly higher than in the 0.063-0.125 mm fraction. This was likely because the finest fraction was left in runoff water longer than the other fractions during wet sieving analysis and some of the sorbed P may have been desorbed. When P is firmly sorbed after a few drying and wetting cycles in the field, desorption may not be as active as for this newly fertilized condition. Figure 7.5a also shows that P concentration for most fractions decreased slightly with time. As mentioned earlier, sediment deposition was active and thus sediment collected in a temporal manner reflected the time of sediment experiencing rainfall impact. The decrease in P concentration with time can, therefore, be attributed to the continuous stripping of the outer P-enriched layer of aggregates as suggested by Ghadiri and Rose (1991a&b). Due to the P concentration gradient within an aggregate, the stripping process produces aggregates with lower P concentration than those of the same size originally existing in the soil or produced by the initial fast slaking process. Gradual P desorption might have occurred during rainfall for this newly fertilized soil and contributed to the decline in P concentration with time.

The OC content in aggregates and its change with time (Figure 7.5b) displayed a different pattern from these of P due to its more uniform distribution within aggregates. An apparent decrease in OC content with time was observed only in the fractions of 0.125-0.25 mm and 0.063-0.125 mm and only in the first 40 min. These initially high OC values were mostly associated with selective transport of OC-rich micro-aggregates which have a low density. The low density of these micro-aggregates, which are likely to be in the early stage of the organic-inorganic complex process, were visually observed during wet-sieving. These

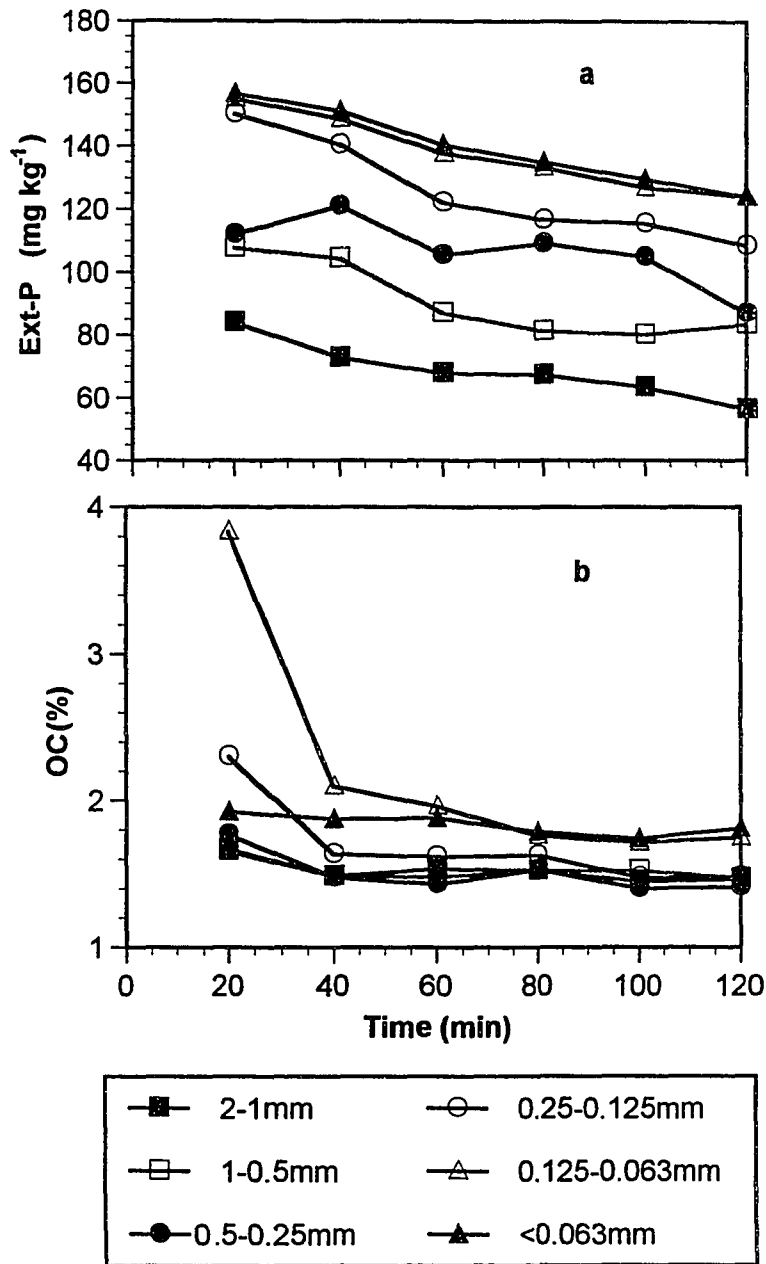


Figure 7.5 Changes of Ext-P concentration (a) and OC content (b) in sediment aggregate fractions with time during the interrill erosion experiment (rainfall intensity = 130 mm h⁻¹).

aggregates were either released during the fast slaking process or existed originally in the soil but interrill flow brought them together in runoff. After this initial transport of OC-rich micro-aggregates, the remaining micro-aggregates as well as those produced by the slow stripping process were transported and exhibited a nearly constant OC content.

Figure 7.6 shows the sediment enrichment by Ext-P and OC relative to the in-situ fertilized soil. The changes in enrichment ratio values with time of OC and Ext-P can thus be understood in a context of selective transport of Ext-P and OC rich fine aggregates (Figure 7.3) and the temporal variations of Ext-P and OC concentration in individual aggregate size fractions (Figure 7.5). Both processes were influenced by aggregate breakdown by the slaking and stripping mechanisms.

7.4 Conclusions

Sediment enrichment by OC and Ext-P and its variation with time can now be understood by combining the results of the dry-sieving, aggregate breakdown, and interrill erosion experiments. For the studied Oxisol, fine aggregates generally displayed higher OC content than large ones irrespective of fertilization treatments. Application of P fertilizer, either in inorganic form or organic form, resulted in preferential accumulation of P in fine aggregates since P sorption sites inside large aggregates were not fully accessed. Aggregate breakdown upon rainfall impact, mainly through the initial fast slaking process, produced additional fine aggregates which were richer in OC and Ext-P than larger ones. Selective transport of these chemically rich aggregates was responsible for sediment enrichment of OC and Ext-P as shown in the interrill erosion experiment. Deposition of large

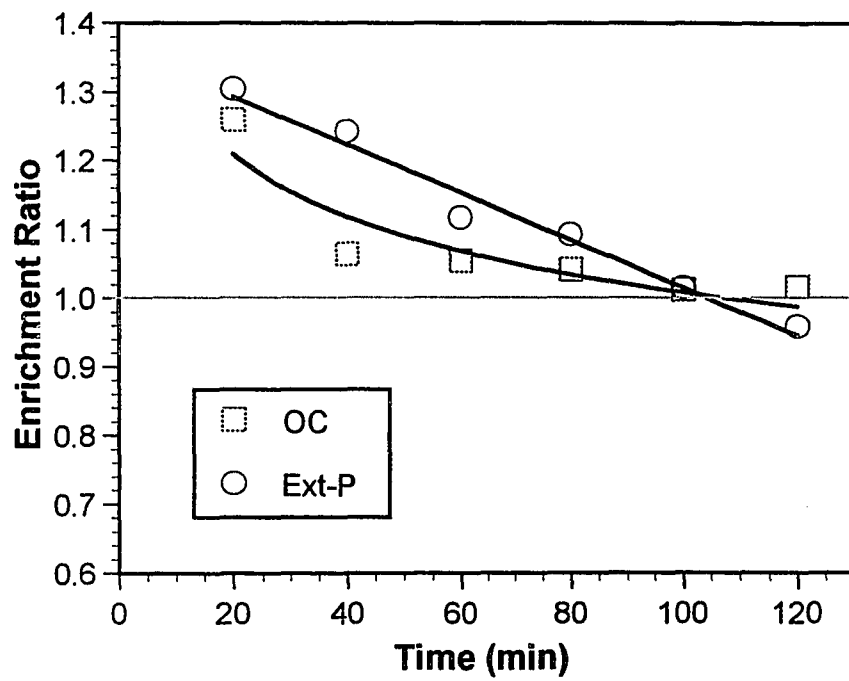


Figure 7.6 Changes of sediment enrichment ratio of Ext-P and OC with time during the interrill erosion experiment (rainfall intensity = 130 mm h⁻¹).

water stable aggregates on the soil surface may shield the underlying soil from further detachment. The slow stripping process working on these large water stable aggregates was not effective in producing fine aggregates, thereby resulting in a decline in sediment transport. The stripped aggregates were less rich in OC and Ext-P compared with those of the same size in the original soil or those produced by fast slaking. This is at least partially responsible for the decline in sediment enrichment with time during rainfall.

The above conclusions likely represent a transient situation in the chemical enrichment process. Phosphorus diffusion into soil aggregates is a time dependent process, and uniform distribution of P within aggregates of varying size may be eventually reached as evidenced by the LTP treatment. Thus, selective transport of fine aggregates from soil following long equilibration with applied fertilizers may not necessarily result in sediment enrichment by Ext-P. Further research is necessary to study the kinetics of P sorption processes for soils with different aggregation characteristics.

CHAPTER 8

OVERALL SUMMARY AND CONCLUSIONS

A detailed and comprehensive study on sediment detachment and transport, selectivity, and sediment enrichment of interrill erosion and rill erosion in a well-aggregated and uniformly-textured Oxisol was hereafter completed. The overall objective addressed was to advance the present state of our knowledge about the processes and mechanisms responsible for soil erosion and sediment enrichment. This objective was fulfilled with the following conclusions obtained from this study.

It has been recognized for some time, but hitherto unsuccessfully partitioned, that interrill erosion consists of sediment detachment and transport by raindrop impact (splash) and sediment transport by interrill overland flow(wash). In this study, an innovative experimental set-up was developed to allow for the partitioning of total splash into directional components and interrill sediment transport into downslope splash and wash components. With this approach, the common notation about "wash as the major sediment transport process for interrill erosion" was examined under a range of slope gradients and rainfall intensities. It was concluded that either splash or wash can dominate sediment transport in interrill area, depending mainly on runoff and slope conditions. The studied Oxisol tends to favor splash erosion due to its highly-aggregated and well-drained nature. This finding implied that the traditional methodology using open-troughs for interrill sediment measurements may generally underestimate total soil loss and interrill sediment delivery into rills.

With this approach, the rainfall intensity and slope steepness effects were quantitatively determined for splash and wash, respectively. Results showed that the

commonly used power law function, $E = aI^b$ (where E = erosion rate, I = rainfall intensity, and a and b are fitted constants), though, may well model the rainfall intensity effects on splash and wash sediment fluxes, the b values for splash were close to 1 and those for wash were well above 2. This may explain why a wide range of b values are reported in the literature when splash and wash are lumped together. In addition, the rainfall intensity term in the equation has distinct physical meaning for splash and wash, i.e., " I " represents rainfall kinetic energy (E) for splash and the excess rainfall impacted flow flux ($Q - Q_{cr}$) for wash (Q_{cr} is the critical flow flux for significant variation in sediment transport with changing slope angle). The result justified the use of $E(Q - Q_{cr})$, instead of I^2 , as the erosivity term for modeling interrill erosion. It was also found that rainfall intensity effects were highly dependent on the slope steepness effect which was described by either a linear function or a power function. This slope effect showed a monotonic increase of erosion with increasing slope angle and can not be simply explained by the interrill erosion slope function in the WEPP model. This difference was mostly due to the empirical origination of the WEPP slope function and the transport-limited regime prevailed at high slope angles studied with the well-aggregated Oxisol.

Erodibility factors were analyzed for both interrill erosion and rill erosion. It was indicated that the commonly measured interrill erodibility is a dynamic combination of splashability and washability, the erodibility factor defined for splash and wash respectively. For rill erosion, results showed that the rill erodibility and the critical shear stress changed with flow hydraulic regimes, i.e., these two factors were larger under turbulent flow regimes than under laminar flow regimes. A critical Reynolds number of 1000 distinguished laminar or quasi-laminar flow from turbulent flow under the studied experimental condition. It was

implied that the current WEPP rill erosion model may need modifications, especially with regards to the linkage with flow hydraulics.

Sediment aggregate size characteristics and the selectivity of erosion processes were studied separately for interrill erosion and rill erosion. For interrill erosion, sediment geometric mean diameter (GMD) varied significantly with wash and directional splash components following the sequence of downslope splash > lateral splash > upslope splash > wash. Both splash and wash preferentially transported the aggregates in the size fraction <0.063 mm. However, mean enrichment ratios (ER) for this fraction were < 2 for splash and were about 12 for wash. Sand-sized fractions were depleted in wash sediment but certain fractions (generally coarse to medium sand size fractions) were enriched in splash sediment, and ER values of these fractions varied with directional components. Rainfall intensity and slope had a significant influence on both directional splash GMD (at $\alpha = 0.05$) and on wash GMD (at $\alpha = 0.001$). However, the interaction effect was significant only for wash GMD. Interrill sediment size characteristics partially depended on the sediment transport regimes, i.e., splash-dominated regimes produced sediment with size characteristics similar to that of in-situ soil while wash-dominated regimes produced sediment which was much finer than in-situ soil. For rill erosion, sediment size distribution was mainly influenced by flow hydraulics. When the erosive force available for sediment transport is unchanged, interrill sediment delivery and sediment availability for transport tend to play major role in the size characteristics of sediment transported by rill flow.

Although sediments from this Oxisol had distinct aggregate size distributions, their dispersed particle size distributions were similar, with the ER of dispersed clay particles not significantly different from 1.0. This implied that organic carbon (OC) and extractable phosphorus (Ext-P) concentrations in sediment should correspondingly be the same as for

the in-situ soil. However, it was found that sediment contained significantly higher OC and Ext-P than the in-situ soil, and the magnitudes of ER varied with sediment aggregate size distributions. This sediment enrichment can not be simply explained by the traditional mechanism suggested in the literature, i.e., selective transport of clay particles which have high specific surface areas to sorb chemicals. The alternative mechanism is associated with selective transport of fine aggregates which were chemically richer than the coarser ones.

The reasons responsible for preferential accumulations of Ext-P in fine aggregates were different as for OC. For Ext-P, it was mostly associated with the reduced accessibility for sorption inside large aggregates as evidenced by significantly higher Ext-P concentrations in fine aggregates than in coarser ones upon P application. However, the diffusion process eventually brought a uniform distribution of P among aggregates of varying size when the soil had been fertilized for a long time. For OC, however, the preferential accumulation in fine aggregates was possibly because organic matter in small aggregates was more persistent and protected from microbial attack through preferential sorption of organic matter by fine aggregates occurred when organic wastes were applied. A uniform distribution of OC among aggregates of varying size was not found in this study.

Breakdown of aggregates by rainfall impact further provided fine aggregates which were chemically richer than coarser ones. A two-step conceptual model was proposed for aggregate breakdown under rainfall impact: fast slaking of unstable aggregates occurring in the early stage of rainfall followed by slow stripping of water stable aggregates. The enriched fine aggregates were mainly produced by the fast slaking process, involving aggregate failures of weak planes. The slow stripping process was less effective in producing fine aggregates, and the produced fine aggregates were less rich in OC and Ext-P than those of the same size in the original soil or produced by fast slaking. This

concentration difference may be partially responsible for the decline in sediment enrichment with time during an erosion event.

Finally, the effect of plastic mulch, a common practice in Hawaiian pineapple plantation, on runoff generation and soil loss was studied. Results indicated that the presence of plastic mulch alone significantly accelerated runoff generation and soil erosion. However, the simultaneous presence of plastic mulch and pineapple crowns tended to retard runoff generation and decrease soil erosion, implying that the plastic mulch practice may not necessarily increase runoff and soil loss as was commonly believed.

REFERENCES

- Abrahams, A.D., A.J. Parsons, and S.H. Luk. 1986. Field measurements of the velocity of overland flow using dye tracing. *Earth Surface Processes and Landforms* 11: 653-657.
- Abrahams, A.D., A.J. Parsons, and J. Wainwright. 1994. Resistance to overland flow on semiarid grassland and shrubland hillslopes, Walnut Gulch, southern Arizona. *J. Hydrology* 156: 431-446.
- Alberts, E.E., and W.C. Moldenhauer. 1981. Nitrogen and phosphorus transported by eroded soil aggregates. *Soil Sci. Soc. Am. J.* 45: 391-396
- Alberts, E.E., R.C. Wendt, and R.F. Piest. 1983. Physical and chemical properties of eroded soil aggregates. *Trans. ASAE* 26: 465-471.
- Al-Durrah, M. and J.M Bradford. 1981. New methods of studying soil detachment due to waterdrop impact. *Soil Sci. Soc. Am. J.* 45: 449-953.
- Al-Durrah, M. and J.M. Bradford. 1982. Parameters for describing soil detachment due to single waterdrop impact. *Soil Sci. Soc. Am. J.*, 46: 836-840.
- Avnimelech, Y, and J.R. McHenry. 1984. Enrichment of transported sediments with organic carbon, nutrients, and clay. *Soil Sci. Soc. Am. J.* 48: 259-266.
- Bhatnagar, V.K. and M.H. Miller. 1985. Sorption of carbon and phosphorus from liquid manure by soil aggregates of differing size. *Can. J. Soil Sci.* 65: 467-473.
- Bhatnagar, V.K., M.H. Miller, and J.W. Ketcheson. 1985. Reaction of fertilizer and liquid manure phosphorus with soil aggregates and sediment phosphorus enrichment. *J. Environ. Qual.* 14: 246-251.
- Bhatt, P.N. 1977. Losses of plant nutrients through erosional process--a review. *Soil Conservation Digest* 5: 37-46.
- Bollinne, A. 1978. Study of the importance of splash and wash on cultivated loamy soils of Hesbaye (Belgium). *Earth Surface Processes* 3: 71-84.
- Bradford, J.M. and C. Huang. 1993. Comparison of interrill soil loss for laboratory and field procedures. *Soil Technology*: 6: 145-156.
- Bradford, J.M., J.E. Ferris, and A.P. Remley. 1987. Interrill soil erosion processes: I. Effect of surface sealing on infiltration, runoff, and soil splash detachment. *Soil Sci. Soc. Am. J.* 51: 1566-1571.
- Bryan, R.B. 1979. The influence of slope angle on soil entrainment by sheet wash and rainsplash. *Earth Surface Processes* 4: 43-58.

Chang, W.J. and D.J. Hills. 1993. Sprinkler drop effects on infiltration. I: Impact simulation. *J. Irrigation and Drainage Eng.* 119: 142-156.

Christensen, B.T. 1986. Straw incorporation and soil organic matter in macro-aggregates and particle size separation. *J. Soil Sci.* 41: 29-39.

Cooley, K.R. and J.R. Williams. 1985. Application of the universal soil loss equation (USLE) and modified USLE to Hawaii. In: S.A. El-Swaify, W.C. Moldenhauer, and A. Lo (eds.) *Soil Erosion and Conservation*. Soil Cons. Soc. Am., Ankeny, Iowa, pp. 509-523.

Day, P.R. 1965. Particle fractionation and particle size analysis. In: C.A. Black et al. (ed.), *Methods of Soil Analysis, Part I*. Am. Soc. Agr., Inc. Madison, Wisconsin. *Agronomy* 9: 545-624.

Dangler, E.W., S.A. El-Swaify, L.R. Ahuja, and A.P. Barnett. 1976. Erodibility of selected Hawaii soils by rainfall simulation. USDA-ARS, Western Region, CA.

De Ploey, J. and H.J. Mucher. 1981. A consistency index and rainwash mechanisms on Belgian loamy soils. *Earth Surface Processes and Landforms* 6: 319-330.

Dexter, A.R. 1988. Advances in characterization of soil structure. *Soil and Tillage Res.* 11: 199-238.

Ekern, P.C. 1954. Rainfall intensity as a measure of storm erosivity. *Soil Sci. Soc. Am. Proc.* 18: 212-216.

Elliot, W.J., Foster, G.R., and Elliot, A.V., 1991. Soil erosion: Processes, impacts and prediction. In: R. Lal and F.J. Pierce (eds.), *Soil Management for Sustainability*. Soil Cons. Soc. Am. Ankeny, Iowa, pp. 25-34.

El-Swaify, S.A. 1980. Physical and mechanical properties of Oxisols. In: B.K.G. Theng (ed.), *Soil with Variable Charge*. New Zealand Soc. Soil Sci., Wellington, pp. 303-324.

El-Swaify, S.A. 1992. Land degradation hazard and protection elements in small, tropical, volcanic island ecosystems. In: *Proceedings of 7th International Conference on Soil Erosion and Conservation*. Soil Con. Serv. of New South Wales, Sydney, Australia, pp: 281-287.

El-Swaify, S.A. 1993. Soil erosion and conservation in the tropics. In: D. Pimentel (ed.), *World Soil Erosion and Conservation*. Cambridge University Press, England, pp. 233-256.

El-Swaify, S.A. 1994. State of the art for assessing soil and water conservation needs and technologies: A global perspective. In: T.D. Napier, S.M. Camboni, and S.A. El-Swaify (eds.) *Adopting Conservation on Farm*. Soil and Water Cons. Soc. Ankeny, Iowa, pp. 13-27.

El-Swaify, S.A. and K.R. Cooley. 1980. Sediment loss from small agricultural watersheds in Hawaii (1972-1977). *USDA Agricultural Reviews and Manuals*, ARM-W-17.

El-Swaify, S.A. and J.H. Fownes. 1992. Erosion processes and models: Applications in the tropics. In: H. Hurni and K. Tato (eds.), *Erosion, Conservation, and Small-Scale Farming*, Geographica Bernesia, Missouri, pp. 135-149.

Evet, R.S. and G.R. Dutt. 1985. Effect of slope and rainfall intensity on erosion from sodium dispersed, compacted earth microcatchments. *Soil Sci. Soc. Am. J.* 49: 202-206.

Farmer, E.E. 1973. Relative detachability of soil particles by simulated rainfall. *Soil Sci. Soc. Am. Proc.* 37: 629-633.

Flanagan, D.C. and G.R. Foster. 1989. Storm pattern effect on nitrogen and phosphorus losses in surface runoff. *Trans. ASAE* 32: 535-544.

Foster, G.R. 1990. Process based modelling of soil erosion by water on agricultural land. In: J. Boardman, I.D.L. Foster, and J. A. Dearing (eds.), *Soil Erosion on Agricultural Land*. John Wiley, London, pp. 429-446.

Foster, G.R., L.D. Meyer, and C.A. Onstad. 1977. An erosion equation derived from basic erosion principles. *Trans. ASAE* 20: 678-682.

Foster, G.R., W.H. Neibling, and R.A. Nattermann. 1982. A programmable rainfall simulator. ASAE Paper No. 82-2570.

Foster, G.R., R.A. Young and W.H. Neibling. 1985. Sediment composition for nonpoint source pollution analysis. *Trans. ASAE* 28: 133-139&146.

Gabriels, D. and W.C. Moldenhauer. 1978. Size distribution of eroded material from simulated rainfall: Effect over a range of texture. *Soil Sci. Soc. Am. J.* 42: 954-958.

Gardner, W.R. 1956. Representation of soil aggregate size distribution by a logarithmic normal distribution. *Soil Sci. Soc. Am. Proc.* 20: 151-153.

Garnier, C.L. 1988. Residue effects on runoff and erosion under simulated rainfall from steeply sloping tropical soils. Ph.D. Thesis, University of Hawaii, Honolulu, HI.

Ghadiri, H. and D. Payne. 1981. Raindrop impact stress. *J. Soil Sci.* 32: 41-49.

Ghadiri, H. and D. Payne. 1988. The formation and characteristics of splash following raindrop impact on soil. *J. Soil Sci.* 39: 563-575.

Ghadiri, H. and C. W. Rose. 1991a. Sorbed chemical transport in overland flow: I. A nutrient and pesticide enrichment mechanism. *J. Environ. Qual.* 20: 628-633.

Ghadiri, H. and C. W. Rose. 1991b. Sorbed chemical transport in overland flow: II. Enrichment ratio variation with erosion processes. *J. Environ. Qual.* 20: 634-641.

- Gilley, J.E. and E.R. Kottwitz. 1994. Darcy-Weisbach roughness coefficients for selected crops. *Trans. ASAE* 37: 467-471.
- Gilley, J.E., E.R. Kottwitz, and J.R. Simanton. 1990. Hydraulic characteristics of rills. *Trans. ASAE*: 33: 1900-1906.
- Govers, G. 1985. Selectivity and transport capacity of thin flows in relation to rill erosion. *Catena* 12: 35-49.
- Hairsine, P.B. and C.W. Rose. 1992. Modelling water erosion due to overland flow using physical principles, I, Seet flow. *Water Resouces Res.* 28: 237-243.
- Hamlett, J. M., J. L. Baker, and H. P. Johnson, 1987. Size distribution of sediment transported within and from a small agricultural watershed. *Trans. ASAE* 30: 998-1004.
- Horn, R., H. Taubner, M. Wuttke, and T. Baumgartle. 1994. Soil physical properties related with soil structure. *Soil Tillage Res.* 30: 187-216.
- Huang, C. and J.M. Bradford. 1993. Analysis of slope and runoff factors based on the WEPP erosion model. *Soil Sci. Soc. Am. J.* 57: 1176-1183.
- Hue, N.V. 1990. Interaction of $C_a(H_2PO_4)_2$ applied to an Oxisol and previous sludge amendment: Soil and crop response. *Commun. in Soil Sci. Plant Anal.* 21: 61-73.
- Kinnell, P.I.A., 1990. The mechanics of raindrop induced flow transport. *Aust. J. Soil Res.* 28: 497-516.
- Kinnell, P.I.A. 1993a. Interrill erodibilities based on the rainfall intensity-flow discharge erosivity factor. *Aust. J. Soil Res.* 31: 319-332.
- Kinnell, P.I.A. 1993b. Runoff as a factor influencing experimentally determined interrill erodibilities. *Aust. J. Soil Res.* 31: 333-342.
- Lafren, J.M., A. Thomas and R. Welch. 1987. Crop land experiments for the WEPP project. ASAE Paper No. 87-2544. St. Joseph, MI.
- Lane, L. J. and M. A. Nearing (eds.). 1989. USDA- Water Erosion Prediction Project: Hillslope Profile Model Documentation. NSERL Report No. 2. USDA-ARS National Soil Erosion Research Laboratory, West Lafayette, Indiana.
- Leonard, R. A., W. G. Knisel, and D. A. Still. 1987. GLEAMS: Groundwater loading effects of agricultural management systems. *Trans. ASAE* 30: 1403-1418.
- Liebenow, A.M., W.J. Elliot, M.J. Lafren, and K.D Kohl. 1990. Interrill erodibility: Collection and analysis of data from cropland soils. *Trans. ASAE* 33: 1882-1888.

- Lindeburg, M.R. 1990. Engineer-In-Training Reference Manual. 7th edition, Professional Publication, Inc., CA.
- Lo, A., S.A. El-Swaify, and C.W. Rose. 1988. Analysis of erodibility of two tropical soils using a process model. *Soil Sci. Soc. Am. J.* 52: 781-784.
- Luk, S.H. 1979. Effect of soil properties on erosion by wash and splash. *Earth Surface Processes* 4: 241-225.
- Massey, H. F. and M. L. Jackson. 1952. Selective erosion of soil fertility constituents. *Soil Sci. Soc. Am. Proc.* 16: 353-356.
- Mazurak, A.P. 1950. Effect of gaseous phase on water-stable synthetic aggregates. *Soil Sci.* 69: 135-148.
- Mazurak, A.P. and P.N. Mosher. 1968. Detachment of soil particles in simulated rainfall. *Soil Sci. Soc. Am. Proc.* 32: 716-719.
- Mazurak, A.P. and P.N. Mosher. 1970. Detachment of soil aggregates by simulated rainfall. *Soil. Sci. Soc. Am. Proc.* 34: 798-800.
- Mbagwu, J.S.C. 1990. Carbon, nitrogen, and phosphorus concentrations in aggregates of organic waste-meneded soil. *Biological Wastes* 31: 97-111.
- Mclsaac, G.F., J.K. Mitchell, and M.C. Hirschi. 1987. Slope steepness effects on soil loss from disturbed lands. *Trans. ASAE* 30: 1387-1396.
- Mclsaac, F.G., M.C. Hirschi, and J.K. Mitchell. 1991. Nitrogen and phosphorus in eroded sediment from corn and soybean tillage system. *J. Environ. Qual.* 20: 663-670.
- Mehlich, A. 1985. Mehlich 3 soil test extractant: A modification of Mehlich 2 extractant. *Commun. in Soil Sci. Plant Anal.* 15: 1409-1416.
- Menzel, R.G. 1980. Enrichment ratios for water quality modelling. In W. G. Knisel (ed.), *CREAMS: A field scale model for chemical, runoff, erosion from agricultural management systems*. USDA Conservation Research Report No. 26, pp. 486-492.
- Meyer, L.D. 1964. Mechanics of soil erosion by rainfall and runoff as influenced by slope length, slope steepness, and particle size. Ph.D. thesis. Purdue Univ., West Lafayette, IN.
- Meyer, L.D. 1981. How rainfall intensity affects interrill erosion. *Trans. ASAE* 23:1472-1475.
- Meyer L.D. and W.C. Harmon. 1989. How row-sideslope length and steepness affect sideslope erosion. *Trans. ASAE* 32: 639-644.
- Meyer, L.P., D.E. Line, and W.C. Harmon. 1992. Size characteristics of sediment from agricultural soils. *J. Soil and Water Cons.* 47: 107-111.

- Miller W. P., and M. K. Baharuddin. 1987. Particle size of interrill-eroded sediment from highly weathered soils. *Soil Sci. Soc. Am. J.* 51: 1610-1615.
- Morgan, R.P.C. 1978. Field studies of rainsplash erosion. *Earth Surface Processes* 3: 295-299.
- Morgan, R.P.C., J.N. Quinton, and R.J. Rickson. 1992. EUROSEM, Documentation Manual, Version 1, Silsoe College, Bedford, U.K.
- Moss, A.J. 1988. Effects of flow velocity variation on rain-driven transportation and the role of rain impact in the movement of solids. *Aust. J. Soil Res.* 26: 443-450.
- Moss, A.J. and P.Green. 1983. Movement of solids in air and water by raindrop impact: Effect of drop-size and water depth variation. *Aust. J. Soil Res.* 21: 257-269.
- Munn, J.R.Jr. and G.L. Huntington. 1976. A portable rainfall simulator for erodibility and infiltration measurements on rugged terrain. *Soil Sci. Soc. Am. J.* 40: 622-624.
- Murphy, J, and J.P.Riley. 1962. a modified single solution method for the determination of phosphate in natural waters. *Anal. Chim. Acta.* 27: 31-36.
- Neal, J.H. 1938. Effect of degree of slope and rainfall characteristics on runoff and soil erosion. *Agr. Eng.* 19: 213-217.
- Nearing, M.A. 1991. A probabilistic model of soil detachment by shallow turbulent flow. *Trans. ASAE* 34: 81-85.
- Nearing, M.A. and S.C. Parker. 1994. Detachment of flow by flowing water under turbulent and laminar conditions. *Soil Sci. Soc. Am. J.* 58: 1612-1614.
- Nearing, M.A., L.J. Lane, E.E. Alberts, and J.M. Laflen. 1990. Prediction technology for soil erosion by water: Status and research needs. *Soil Sci. Soc. Am. J.* 54: 1072-1711.
- Palis, R.G., G. Okwach, C.W. Rose, and P.G. Saffigna. 1990a. Soil erosion processes and nutrient loss. I. The interpretation of enrichment ratio and nitrogen loss in runoff sediment. *Aust. J. Soil Res.* 28:623-639.
- Palis, R.G., G. Okwach, C.W. Rose, and P.G. Saffigna. 1990b. Soil erosion processes and nutrient loss. II. The effect of surface contact cover and erosion processes on enrichment ratio and nitrogen loss in eroded sediment. *Aust. J. Soil Res.* 28: 641-658.
- Parsons, A.J., A.D. Abrahams, and S.H. Luk, 1991. Size characteristics of sediment in interrill overland flow on a semiarid hillslope, southern Arizona. *Earth Surface Processes and Landforms* 16: 143-152.
- Parsons, A.J., A.D. Abrahams, and Wainwright, J., 1994. Rainsplash and erosion rates in an interrill area on semi-arid grassland, Southern Arizona. *Catena* 22: 215-226.

- Poesen, J. and J. Savat. 1980. Particle size separation during erosion by splash and runoff. In: M. De Boodt and D. Gabriels (eds.) *Assessment of Erosion*. John Wiley & Sons, Chichester, pp. 427-439.
- Poesen, J. and J. Savat. 1981. Detachment and transportation of loose sediment by raindrop splash: Part II, detachability and transportability measurements. *Catena* 8: 19-41.
- Proffitt, A.P.B. and C.W. Rose. 1991a. Soil erosion processes. I. The relative importance of rainfall detachment and runoff entrainment. *Aust. J. Soil Res.* 29: 671-683.
- Proffitt, A.P.B. and C.W. Rose. 1991b. Soil erosion processes. II. Settling velocity characteristics of eroded sediment. *Aust. J. Soil Res.* 29: 685-695.
- Proffitt, A.P.B., C.W. Rose, and P.B. Hairsine. 1991. Rainfall detachment and deposition: Experiment with low slope and significant water depths. *Soil Sci. Soc. Am. J.* 55: 325-332.
- Proffitt, A.P.B., C.W. Rose, and C.J. Lovell. 1993. Settling velocity characteristics of sediment detached from soil surface by raindrop impact. *Catena* 20: 27-40.
- Quansah, C. 1981. The effect of soil type, slope, rain intensity and their interactions on splash detachment and transport. *J. Soil Sci.* 32: 215-224.
- Renard, K.G., G.R. Foster, G.A. Weesies, D.K. KcCool, D.C. Yoder, and Coordinators. 1992. *Prediction of soil erosion by water: A guide to conservation planning with the revised universal soil loss equation (RUSLE)*. USDA, Agri. Handbook. Washington, DC.
- Roels, J.M. and Jonker, P.I., 1983. Probability sampling techniques for estimating soil erosion. *Soil Sci. Soc. Am. J.* 47: 1224-1228.
- Rose, C.W. 1961. Rainfall and soil structure. *Soil Sci.* 91: 49-54.
- Rose, C.W. 1985. Developments in soil erosion and deposition models. *Adv. Soil Sci.* 2: 1-63.
- Rose, C.W. 1993. Erosion and sedimentation. In: M. Bonell, M.M. Hufschmit, and J.S. Gladwell (eds.), *Hydrology and Water Management in the Humus Tropics*. Cambridge University Press, pp. 301-343.
- Savat, J. 1977. The hydraulics of sheet flow on a smooth surface and the effect of simulated rainfall. *Earth Surface Processes* 2: 125-140.
- Savat, J. 1980. Resistance to flow in rough supercritical sheet flow. *Earth Surface Processes* 5: 103-122.
- Sharma, P.P., S.C. Gupta, and G.R. Foster. 1993. Predicting soil detachment by raindrops. *Soil Sci. Soc. Am. J.* 57: 674-680.

- Sharma, P.P., S.C. Gupta, and G.R. Foster. 1995. Rainfall-induced soil detachment and sediment transport from interrill areas. *Soil Sci. Soc. Am. J.* 59: 727-734.
- Sharpley, A.N. 1980. The enrichment of soil phosphorous in runoff sediments. *J. Environ. Qual.* 9: 521-526.
- Sharpley, A.N. 1985. the selective erosion of plant nutrients in runoff. *Soil Sci. Soc. Am. J.* 49: 1527-1534.
- Stoltenberg, N. L. and J.L. White. 1953. Selective loss of plant nutrients by erosion. *Soil Sci. Soc. Am. Proc.* 17: 406-410.
- Sutherland, R.A., Y. Wan, A.D. Ziegler, C-T Lee, and S.A. El-Swaify. 1996. Splash and wash dynamics: An Experimental investigation using an Oxisol. *Geoderma* 69: 85-103.
- Swanson, N. P., A. R. Dedrick and H. E. Weakly. 1965. Soil particles and aggregates transported in runoff from simulated rainfall. *Trans. ASAE* 8: 437&440.
- Truman, C.C. and Bradford, J.M. 1993. Relationships between rainfall intensity and the interrill soil loss-slope steepness ratio as affected by antecedent water content. *Soil Sci.* 156: 405-413.
- Vaidyanathan, L.V. and O. Talibuden. 1968. Rate controlling processes in the release of soil phosphate. *J. Soil Sci.* 19: 342-252.
- Wan, Y., S.A. El-Swaify, and R.A. Sutherland. 1996. Partitioning interrill splash and wash dynamics: A novel laboratory approach. *Soil Technology* (In press).
- Watson, D.A. and J. M. Laflen. 1986. Soil strength, slope, and rainfall intensity effects on interrill erosion. *Trans. ASAE* 29: 98-102.
- Wischmeier, W.H. and D.D. Smith. 1978. Predicting rainfall erosion losses: A guide to conservation planning. USDA Agric. Handbook. No. 537. U.S. Gov. Printing Office. Washington, DC.
- Young, R.A. 1980. Characteristics of eroded sediment. *Trans. ASAE* 23: 1139-1142&1146.
- Young, R.A. and C.A. Onstad. 1978. Characteristics of rill and interrill eroded soil. *Trans. ASAE* 23: 1139-1142.
- Young, R.A., A.E. Olness, C.K. Mutchler, W.C. Moldenhauer. 1985. Chemical and physical enrichment of sediment from cropland. *Trans. ASAE* 29: 165-169.